DESIGN AND PERFORMANCE ANALYSIS OF A COUNTER ROTATING PROPELLER

A THESIS SUBMITTED TO
THE GRADUATE SCHOOL OF NATURAL AND APPLIED SCIENCES
OF
MIDDLE EAST TECHNICAL UNIVERSITY

BY

SERCAN ÖZTÜRK

IN PARTIAL FULFILLMENT OF THE REQUIREMENTS
FOR
THE DEGREE OF MASTER OF SCIENCE
IN
MECHANICAL ENGINEERING

DECEMBER 2022

Approval of the thesis:

DESIGN AND PERFORMANCE ANALYSIS OF A COUNTER ROTATING PROPELLER

submitted by **SERCAN ÖZTÜRK** in partial fulfillment of the requirements for the degree of **Master of Science** in **Mechanical Engineering, Middle East Technical University** by,

Prof. Dr. Halil Kalıpçılar
Dean, Graduate School of **Natural and Applied Sciences**   _____

Prof. Dr. M. A. Sahir Arıkan
Head of the Department, **Mechanical Engineering**   _____

Prof. Dr. M. Haluk Aksel
Supervisor, **Mechanical Engineering, METU**   _____

Examining Committee Members:

Asst. Prof. Dr. Özgür Uğraş Baran
Mechanical Engineering, METU   _____

Prof. Dr. M. Haluk Aksel
Mechanical Engineering, METU   _____

Asst. Prof. Dr. Ali Karakuş
Mechanical Engineering, METU   _____

Asst. Prof. Dr. Hediye Atik
Aerospace Engineering, Atılım University   _____

Asst. Prof. Dr. Onur Baş
Mechanical Engineering, TED University   _____

Date: 02.12.2022

I hereby declare that all information in this document has been obtained and presented in accordance with academic rules and ethical conduct. I also declare that, as required by these rules and conduct, I have fully cited and referenced all material and results that are not original to this work.

Name, Last name: Sercan Öztürk

Signature   :

ABSTRACT

DESIGN AND PERFORMANCE ANALYSIS OF A COUNTER ROTATING PROPELLER

Öztürk, Sercan
Master of Science, Mechanical Engineering
Supervisor: Prof. Dr. M. Haluk Aksel

December 2022, 112 pages

Whether it is a large container ship or a submarine operating at depths of hundreds of meters, propellers are in action to advance in the water. Counter-rotating propeller, abbreviated as CRP, is a combined propulsor where the propellers, called forward and aft, are placed one behind another and rotate in opposite directions. The main advantages of a CRP are increased efficiency due to less fuel consumption than a single propeller and torque cancellation phenomena by rotations in opposite directions. In the present study, design and performance analyses of a CRP are conducted for the bare hull geometry of DARPA Suboff. OpenProp which is an open-source computational tool for the design and analysis of propellers written in the MATLAB programming language is used as the parametric analysis and design tool. ANSYS Fluent is used for performance evaluations. The methodology for design and numerical analyses is set with a propeller called DTMB4119 and validated with an experimental data.

Keywords: Counter-rotating Propeller, OpenProp, DTMB4119, Design, Performance analysis

ÖZ

BİR TERS DÖNÜŞLÜ PERVANENİN TASARIMI VE PERFORMANS ANALİZİ

Öztürk, Sercan
Yüksek Lisans, Makina Mühendisliği
Tez Yöneticisi: Prof. Dr. Mehmet Haluk Aksel

Aralık 2022, 112 sayfa

İster büyük bir konteyner gemisi, isterse yüzlerce metre derinlikte çalışan bir denizaltı olsun, pervaneler suda ilerlemek için ana itki sistemi olarak kullanılmaktadır. CRP olarak kısaltılan ters dönüşlü pervane, ön ve arka olarak adlandırılan pervanelerin birbiri ardına yerleştirildiği ve zıt yönlerde döndüğü kombine bir pervane çiftidir. Ters dönüşlü pervanelerin avantajları, tek bir pervaneye göre daha az yakıt tüketimi nedeniyle artan verimlilik ve zıt yönlerde dönüşlerle tork iptali olgusudur. Bu çalışmada, DARPA Suboff'unun çıplak gövde geometrisi için bir CRP'nin tasarım ve performans analizleri yapılmıştır. Parametrik analiz ve tasarım aracı olarak MATLAB programlama dilinde yazılmış açık kaynak kodlu bir hesaplama aracı olan OpenProp kullanılmıştır. Performans değerlendirmeleri için ANSYS Fluent kullanılmaktadır. Tasarım ve sayısal analizler için metodoloji, DTMB4119 adlı pervane ile belirlenmiştir ve deneysel verilerle doğrulanmıştır.

Anahtar Kelimeler: Ters dönüşlü pervane, OpenProp, DTMB4119, Tasarım, Performans Analizi

To my loved ones

ACKNOWLEDGMENTS

TABLE OF CONTENTS

LIST OF TABLES

TABLES

LIST OF FIGURES

FIGURES

LIST OF ABBREVIATIONS

ABBREVIATIONS

1D	1 Dimensional
2D	2 Dimensional
3D	3 Dimensional
CAD	Computer Aided Design
CFD	Computational Fluid Dynamics
CRP	Counter Rotating Propeller
DARPA	Defense Advanced Research Projects Agency
DNS	Direct Numerical Simulation
DTMB	David Taylor Model Test Basin
FVM	Finite Volume Method
GUI	Graphical User Interface
LES	Large Eddy Simulation
MIT	Massachusetts Institute of Technology
MRF	Multiple Reference Frame
NACA	National Advisory Committee for Aeronautics
RANS	Reynolds Averaged Navier Stokes
SST	Shear Stress Transport

LIST OF SYMBOLS

SYMBOLS

a	Distance of leading edge to generator line at r, m
A_E/A_O	Blade area ratio
b	Distance of leading edge to maximum thickness location at r, m
c	Chord, m
c	Constant pressure specific heat, J/kg·K
C_D	Drag coefficient
C_L	Lift coefficient
C_{L_0}	Design lift coefficient
C_{L_I}	Ideal lift coefficient
D	Diameter, m
$\hat{e}_a$	Axial direction
$\hat{e}_t$	Tangential direction
$\hat{e}_r$	Spanwise direction
$\vec{F_l}$	Kutta-Joukowski lift force, N
$\vec{F_v}$	Viscous drag force, N
$\vec{f}$	Body force per unit mass, m/s^2
$\vec{g}$	Gravitational acceleration, m/s^2
J	Advance Coefficient

K_T	Thrust coefficient
K_Q	Torque coefficient
n	Rotation speed, rps
p	Pressure, Pa
P_{OUT}	Output power, kW
P_{IN}	Input power, kW
Q	Torque, N·m
q	Heat flux, W/m^2
Q	Heat generation per volume, $J/K \cdot m^3$
r	Radius, m
r_c	Control radius, m
r_h	Hub radius, m
t	Thrust deduction
T	Temperature, K
T	Thrust, N
T_s	Specified thrust, N
u	Velocity component in x-direction, m/s
$\overrightarrow{u_a^*}$	Axial induced velocity, m/s
$\overrightarrow{u_t^*}$	Tangential induced velocity, m/s
v	Velocity component in y-direction, m/s
$\overrightarrow{V_a}$	Axial inflow velocity, m/s

$\overrightarrow{V_t}$	Tangential inflow velocity, m/s
$\overrightarrow{V^*}$	Resultant velocity, m/s
V_s	Ship speed, m/s
w	Velocity component in z-direction, m/s
w	Rotation speed, rad/s
Z	Number of blades
Greek Symbols	
α	Angle of attack
α_I	Ideal angle of attack
β	Geometric pitch angle
β_i	Hydrodynamic pitch angle
θ	Blade angle
Γ	Circulation
ρ	Density
η_0	Efficiency
μ	Dynamic viscosity
$\bar{\bar{\sigma}}$	Cauchy (total) stress tensor
Φ	Viscous dissipation
$\bar{\bar{\varepsilon}}$	Strain rate tensor
λ	Second coefficient of viscosity
$\bar{\bar{I}}$	Identity (unit) tensor
w_T	Taylor wake fraction

CHAPTER 1

INTRODUCTION

Propulsion system of marine vehicles consists of propellers for long centuries. Whether it is large container ships or submarines operating at depths of hundreds of meters, propellers are in action to advance in the water. Working principle of propellers simply depends on the principle of Newton's Third Law. Propellers accelerate the fluid ahead of themselves to the back. This work done on the fluid provides a reaction in the opposite direction that enables the vehicle move forward.

Rotation of propellers is established by the propeller shaft laying between the center of the propeller and the engine [1]. Basic nomenclature for a propeller is presented in Figure 1.1. Propellers consist of blades at equal intervals of angle where all blades are connected to the center of the propeller, known as a boss or a hub. The edge connecting the blade to the hub is called root whereas blade tip is the furthest edge from the propeller shaft. Leading edge is the first cutting edge through the fluid in the direction of revolution. Trailing edge is the following edge opposite to the leading edge. Propeller back is called for the face which meets with the fluid first and propeller face is the face which is visible when looking at a propeller from the aft side.
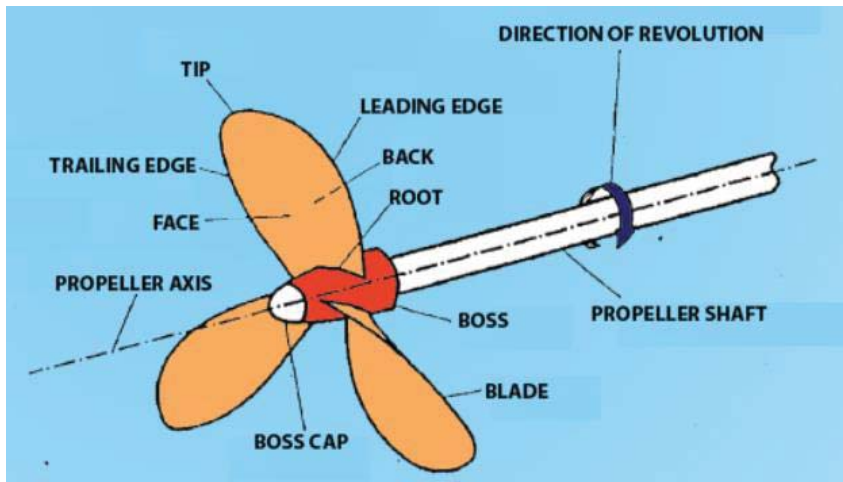
Figure 1.1. Propeller Nomenclature [2]

1.1   Literature Review

Increasing the propulsive efficiency has always been a subject for developers in marine industry. Several configurations for propellers have been tried for this purpose. One of the candidates is the concept of counter-rotating propeller or contra-rotating propellers, abbreviated as CRP. CRP is a combined propulsor where the propellers, called forward and aft, are placed one behind another and rotate in opposite directions.

Figure 1.2. Counter-rotating Propeller for a Ship [3]

Counter-rotating propellers have some advantages over a single propeller. Rotation of a single propeller creates a pressure difference in the flow between the faces of a propeller. This pressure difference produces thrust. At the same time, a rotational flow region is left behind the propeller due to the rotation as shown in Figure 1.3.

The generated rotational flow does not contribute to the obtained thrust. Therefore, it is an energy loss for a propulsion system [4]. By placing another propeller behind the forward one, rotational flow left from the forward propeller is recovered partially, hence more efficient propulsion systems with less fuel consumption can be obtained. Another advantage of a CRP is that torque-cancellation appears by two opposite rotations of separate propellers. This advantage is more significant for small volume vehicles such as submarines, torpedoes or autonomous underwater vehicles where rolling shall be avoided for stabilization. Although the advantages explained above, most of the propulsion systems in marine vehicles still consists of a single propeller. Complex shafting and gearing requirements are the main drawbacks to use a counter-rotating propeller. These mechanical drawbacks also bring larger installation and maintenance costs than a conventional screw propeller. Additionally, there has not been a standardized method to characterize the complex flow region between the forward and aft propellers in a CRP set.
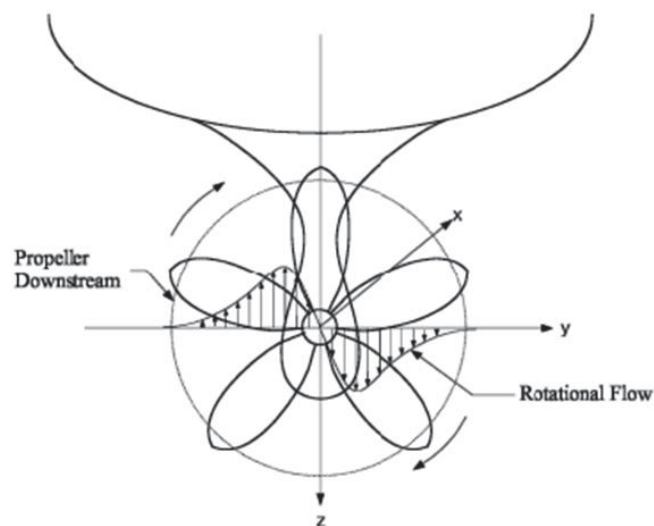
Figure 1.3. Tangential Slipstream Velocity Distribution for a Propeller Rotating in Clockwise Direction [4]

Design of a CRP is obviously more complicated than a single propeller due to complex flow region between the forward and aft propellers. Also, verification by experiments in tow-tanks or wind tunnels requires more advanced instrumentations than a single propeller. Therefore, numerous studies are being conducted by Computational Fluid Dynamics (CFD) to identify the flow characteristics of the non-uniform region between the propellers. To predict the steady and unsteady hydrodynamic performance of CRPs, panel method is applied by Liu [5]. Kinnas et al. [6] coupled a potential flow method and a Reynolds Averaged Navier Stokes (RANS) solver to determine CRP characteristics. Zhang et al. [7] and Wang et al. [8] evaluated CFD models for performance simulations of CRPs depending on the geometric differences and calculation settings. Brizzolara [9], Grassi et al. [10] and XIN et al. [11] considered the induced velocities between forward and aft propellers due to mutual interaction by lifting-line or lifting-surface theory and also, predicted the CRP performance by unsteady potential flow method and CFD simulations.

In below sections, a summary of historical development of marine propellers is presented first. Then, some tabulated data or series on propeller geometries are introduced. Numerical analyses by ANSYS Fluent are carried out to determine the characteristics of single propellers and CRPs. Therefore, governing equations and turbulence modelling for CFD are identified. Finally, objective and description of the current study is clarified.

1.1.1 Development of Marine Propellers

Seaborne transportation is as old as the human race itself [4]. Human force was the main drive for marine transportation in BC centuries. As innovations started to appear, propulsive systems like propellers are started to be used for transportation. In this section, history of development of propellers is explained starting with the concept of screw propeller.

1.1.1.1 Screw Propeller

The concept of screw propeller has started with Egyptians where they use screw-like devices in agriculture. The transformation of screw propeller concept to a marine propeller occurred around the mid-17th century when steam engines were introduced. Today's marine propellers have started to take their shape by Smith and Ericson who acquired patents in 1836 [12], also by George Rennie's conoidal screw known as a Conoidal propeller, patented in 1840 [13]. There have still been improvements on screw propeller based marine propellers to more reliable designs with better efficiencies and cavitation characteristics.

1.1.1.2 Counter-Rotating Propeller

Higher efficiency obtained with a concept of counter-rotating propellers has long been known by the patent by Ericson [12]. However, concentric shafts rotating in opposite directions made the concept technically unfeasible until late 1980's [14]. By the end of World War II., contra-rotating aircraft propellers came into service. Lower asymmetrical torque, higher efficiency and smaller propeller disks were discovered truly at that time [15]. However, still the complexity in shafting and gearing mechanisms resulted in delay from popular usage until late-20th and early-21st centuries.

1.1.2 Tabulated Propeller Series

Propellers consist of identical blades. The number of blades generally varies starting from two up to seven. Therefore, design of a propeller includes design of a blade in the core. Blade design requires inputs for chord and thickness profiles. There are many tabulated series to be used for preliminary design for fixed-pitch, non-ducted propellers which are Wageningen B-screw series or Troost series, Japanese AU-series and Gawn series [16], [17], [18].

Wageningen B-screw series are the most common and extensively used propeller series. They were introduced by Troost in the late 1940s [19]. Addition of other number of bladed propellers was also done by Troost in early 1950s [20], [21]. Geometric properties of B-series propellers for different number of blades is presented in Table 1.1.

Table 1.1. Geometric Properties of B-series propellers [22]

r/R	Parameters of four-bladed to seven-bladed propellers			Parameters of three-bladed propellers			$t/D = A_r - B_r Z$	
	$c/D *$ $Z/(A_E/A_O)$	a/c	b/c	$c/D *$ $Z/(A_E/A_O)$	a/c	b/c	A_r	B_r
0.2	1.662	0.617	0.350	1.633	0.616	0.350	0.0526	0.0040
0.3	1.882	0.613	0.350	1.832	0.611	0.350	0.0464	0.0035
0.4	2.050	0.601	0.351	2.000	0.599	0.350	0.0402	0.0030
0.5	2.152	0.586	0.355	2.120	0.583	0.355	0.0340	0.0025
0.6	2.187	0.561	0.389	2.186	0.558	0.389	0.0278	0.0020
0.7	2.144	0.524	0.443	2.168	0.526	0.442	0.0217	0.0015
0.8	1.970	0.463	0.479	2.127	0.481	0.478	0.0154	0.0010
0.9	1.582	0.351	0.500	1.657	0.400	0.500	0.0092	0.0005
1.00	0.000	0.000	0.000	0.000	0.000	0.000	0.000	0.000

In Table 1.1, Z denotes the number of blades. "c" and "t" refer to chord and maximum thickness, respectively, at that radial location. A_r and B_r are the constants for thickness calculation in radial sections. Chord distribution is determined via the ratio of A_E/A_O which is called the expanded area ratio, i.e. the ratio of total blade area to area of the circle covered by a blade tip. "a" and "b" parameters differ for each radial section, a is the distance of leading edge to generator line at r whereas b is the distance of leading edge to maximum thickness location. Parameters for blade sections at radial locations are shown in Figure 1.4.
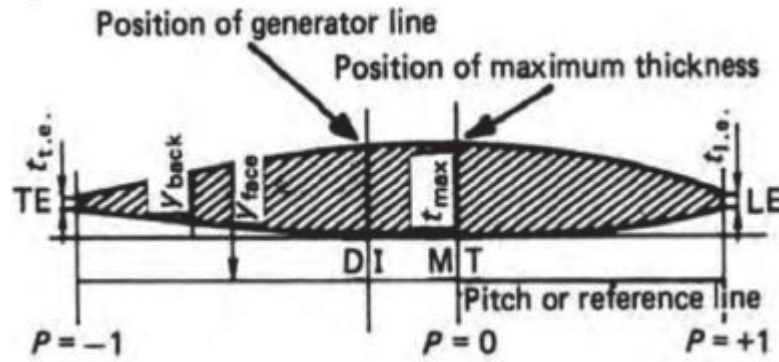
Figure 1.4. Geometric Properties of Blade Sections for B-series [22]

1.1.3 Governing Equations and Turbulence Modelling

Following fundamental laws are used to obtain the corresponding partial differential equations that are solved in a typical CFD study:

- Conservation of mass
- Conservation of linear momentum
- Conservation of energy

Conservation of mass, or continuity equation, states that the rate of change of mass in an infinitesimal control volume is equal to the rate of mass flux through the bonding surface of the same control volume. Differential form of the continuity equation is:

$$\frac{D\rho}{Dt} + \rho\left(\nabla \cdot \vec{V}\right) = 0 \qquad (1.1)$$

Equation (1.1) is said to be written in non-conservative form.

Conservation of linear momentum, also called Newton's 2nd law, states that the rate of change of linear momentum in infinitesimal control volume is equal to the rate in which linear momentum is entering or leaving through the bonding surface of the same control volume, plus the net external force acting on the control volume. The shortest differential form the linear momentum conservation equation is:

$$\rho \frac{D\vec{V}}{Dt} = \nabla \cdot \bar{\bar{\sigma}} + \rho \vec{f} \qquad (1.2)$$

where Cauchy (total) stress tensor, $\bar{\bar{\sigma}}$, includes the viscous and pressure stresses and, $\vec{f}$ is the body force per unit mass. When the only component contributing to $\vec{f}$ is the weight, the term drops to gravitational acceleration vector $\vec{g}$.

The shortest differential form of the conservation of energy equation, also called 1st Law of Thermodynamics, is:

$$\rho c \frac{DT}{Dt} = -\nabla \cdot \vec{q} + Q + \Phi \qquad (1.3)$$

Where c is the constant pressure specific heat, T is the temperature, q is the heat flux vector, Q is the heat generation per volume and Φ is the viscous dissipation representing the work done against viscous forces.

Conservation of energy equation is generally included in flow problems where isothermal conditions do not exist and temperature field is one of the primary concerns. In our cases, flow parameters of velocity and pressure are primary concerns. Therefore, it is not necessary to solve Equation (1.3) in CFD calculations and viscosity of the fluid is taken as constant at a preset isothermal temperature.

For incompressible flows,

$$\nabla \cdot \vec{V} = 0 \qquad (1.4)$$

For Newtonian fluids, viscous stress tensor which is a component of Cauchy stress tensor ($\bar{\bar{\sigma}}$) appearing in the Equation (1.2) can be written as:

$$\bar{\bar{\tau}} = 2\mu\bar{\bar{\varepsilon}} - \lambda(\nabla \cdot \vec{V})\bar{\bar{I}} \qquad (1.5)$$

where μ is the dynamic viscosity, $\bar{\bar{\varepsilon}}$ is the strain rate tensor, λ is the second coefficient of viscosity and $\bar{\bar{I}}$ is the identity (unit) tensor. The strain rate tensor is:

$$\bar{\bar{\varepsilon}} = \frac{1}{2}\left(\nabla\vec{V} + \left(\nabla\vec{V}\right)^T\right) \qquad (1.6)$$

By substituting the Equations (1.4), (1.5) and (1.6) into $\bar{\bar{\sigma}}$:

$$\bar{\bar{\sigma}} = -p\bar{\bar{I}} + \bar{\bar{\tau}} = -p\bar{\bar{I}} + 2\mu\bar{\bar{\mathcal{E}}} - \lambda(\nabla \cdot \vec{V})\bar{\bar{I}} = -p\bar{\bar{I}} + \mu\left(\nabla\vec{V} + (\nabla\vec{V})^T\right) \quad (1.7)$$

where p is the pressure.

The material derivatives appearing in Equations (1.1) and (1.2) can be decomposed into local and convective derivatives as follows [23]:

$$\frac{D\rho}{Dt} = \frac{\partial\rho}{\partial t} + (\vec{V} \cdot \nabla)\rho \quad (1.8)$$

$$\frac{D\vec{V}}{Dt} = \frac{\partial\vec{V}}{\partial t} + (\vec{V} \cdot \nabla)\vec{V} \quad (1.9)$$

Then, Equation (1.1) becomes equal to the Equation (1.4) and Equation (1.2) can be expressed as follows for incompressible flow of a Newtonian fluid:

$$\rho\left(\frac{\partial\vec{V}}{\partial t} + (\vec{V} \cdot \nabla)\vec{V}\right) = -\nabla p + \nabla \cdot \left[\mu\left(\nabla\vec{V} + (\nabla\vec{V})^T\right)\right] + \rho\vec{f} \quad (1.10)$$

As it is expressed before, viscosity of the fluid is taken constant for our cases. Therefore, it is possible to express:

$$\nabla \cdot \left[\mu\left(\nabla\vec{V} + (\nabla\vec{V})^T\right)\right] = \mu\nabla^2\vec{V} \quad (1.11)$$

Substituting Equation (1.11) into (1.10) gives the final form of governing equations for Newtonian, incompressible and isothermal flow with the Equation (1.4):

$$\rho\left(\frac{\partial\vec{V}}{\partial t} + (\vec{V} \cdot \nabla)\vec{V}\right) = -\nabla p + \mu\nabla^2\vec{V} + \rho\vec{f} \quad (1.12)$$

Equations (1.4) and (1.12) can be written in Cartesian coordinate system as follows:

$$\frac{\partial u}{\partial x} + \frac{\partial v}{\partial y} + \frac{\partial w}{\partial z} = 0 \quad (1.13)$$

$$\rho\left(\frac{\partial u}{\partial t} + u\frac{\partial u}{\partial x} + v\frac{\partial u}{\partial y} + w\frac{\partial u}{\partial z}\right) = -\frac{\partial p}{\partial x} + \mu\left(\frac{\partial^2 u}{\partial x^2} + \frac{\partial^2 u}{\partial y^2} + \frac{\partial^2 u}{\partial z^2}\right) + \rho f_x \quad (1.14a)$$

$$\rho\left(\frac{\partial v}{\partial t} + u\frac{\partial v}{\partial x} + v\frac{\partial v}{\partial y} + w\frac{\partial v}{\partial z}\right) = -\frac{\partial p}{\partial y} + \mu\left(\frac{\partial^2 v}{\partial x^2} + \frac{\partial^2 v}{\partial y^2} + \frac{\partial^2 v}{\partial z^2}\right) + \rho f_y \quad (1.14b)$$

$$\rho\left(\frac{\partial w}{\partial t} + u\frac{\partial w}{\partial x} + v\frac{\partial w}{\partial y} + w\frac{\partial w}{\partial z}\right) = -\frac{\partial p}{\partial z} + \mu\left(\frac{\partial^2 w}{\partial x^2} + \frac{\partial^2 w}{\partial y^2} + \frac{\partial^2 w}{\partial z^2}\right) + \rho f_x \quad (1.14c)$$

Equations (1.13) and (1.14) form a system of equations where there exist 4 unknowns for 4 equations. These unknowns are three components of velocity in each axis and the pressure. These equations are solved in a coupled-way to determine the velocity and pressure fields.

When numerical simulations are conducted around ships, submerged vehicles or propellers, the flow is in turbulent regime for many cases [24]. Turbulent flows have a wide range of time and length scales where Navier-Stokes equations alone are not capable of predicting the flow parameters completely during a numerical study. Turbulence includes eddies, swirls and flow instabilities. One way of capturing these infinitesimal fluctuations arising from turbulence is direct implementation of fluctuating values to Navier-Stokes equations called Direct Numerical Simulation (DNS); but, it requires very fine computational grids along with very small time steps. Since extreme resources of hardware and software are needed to use DNS, it is very costly and not used in industrial applications commonly. The most common methods are Reynolds Averaged Navier Stokes (RANS) and Large Eddy Simulation (LES). LES method has an approach of resolving large length scaled fluctuations and ignoring small length scales. This method is considered as suitable where wall interaction is not one of the primary concerns which is very important for any object in a viscous fluid. Still, it requires a considerable hardware and software which is not suitable for an everyday practice. Therefore, most of the studies in literature are based on RANS solvers. RANS type modelling is based on time averaging of flow parameters. Flow variables such as velocity and pressure are decomposed into mean and fluctuating parts where mean components are solved and effects of fluctuating parts are estimated based on the solutions of extra equations. RANS requires the least computational demand when compared with Direct Numerical Simulation and

Large Eddy Simulation; however, this advantage comes with disadvantages of increased modelling uncertainty and reduced accuracy.

RANS approaches are mainly divided into five [25]. In turbomachinery flows, two-equation models are preferred where two additional equations are solved as transport equations with Navier-Stokes equations. These models are SST (Shear Stress Transport) k-ω and k-ϵ. These additional equations are solved for k-ω or k-ϵ depending on the two-equation model. The terms 'k', 'ω' and 'ϵ' define turbulent kinetic energy and rate of dissipation of that turbulent kinetic energy.

1.1.4   Propeller Performance Characteristics

In operating conditions, a propeller creates the required thrust in a non-uniform wake region behind a ship, boat, submarine or a torpedo. Compared to a propeller size, these large bodies disturb the uniform flow ahead of the body and leaves a non-uniform flow parameters for a propeller. However, propeller performance is characterized by open-water tests where the propeller is fed by a uniform flow regime. Even in open-water tests, equipment used for experimental measurements disturbs the flow and create a wake region for the tested propeller. However, their characteristics are measured beforehand and their effects are subtracted from the main results.

In open-water conditions, performance of a propeller is characterized by some non-dimensional parameters. These parameters are advance coefficient, thrust coefficient, torque coefficient and efficiency. By knowing these parameters; all information about the propeller including propeller diameter, rotation speed, power absorption and created thrust can be determined. The equations for these non-dimensional parameters are given in Equations (1.15), (1.16), (1.17) and (1.18).

Advance Coefficient:

$$J = \frac{V}{nD} \tag{1.15}$$

Thrust Coefficient:

$$K_T = \frac{T}{\varrho n^2 D^4} \qquad (1.16)$$

Torque Coefficient:

$$K_Q = \frac{Q}{\varrho n^2 D^5} \qquad (1.17)$$

Efficiency:

$$\eta_0 = \frac{J K_T}{2\pi K_Q} \qquad (1.18)$$

In the Equations (1.15), (1.16), (1.17) and (1.18), *V* is the advance speed in m/s, *n* is the revolution speed in rps and *D* stands for the propeller diameter in m. *T*, *Q* and ϱ refer to the thrust, torque and flow density, respectively.
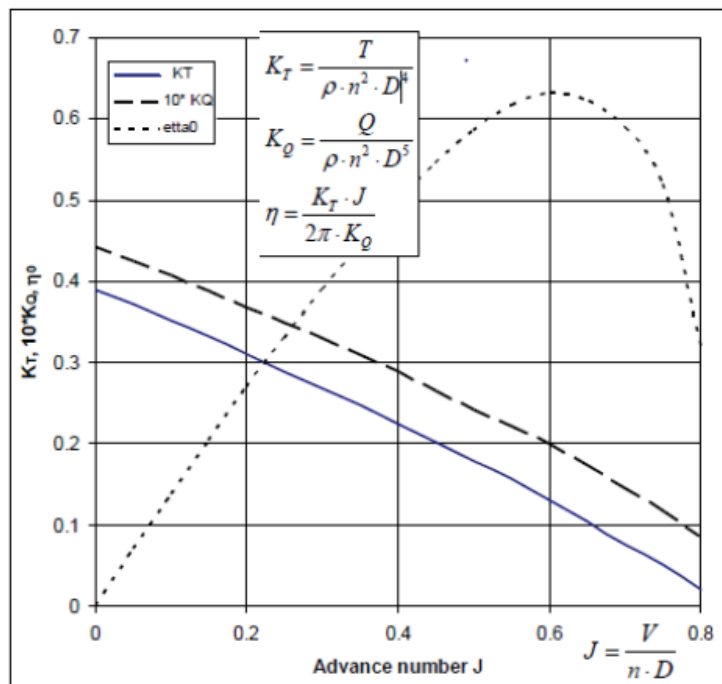
Figure 1.5. Open-Water Characteristics Plot of a Propeller [26]

1.2   Objective and Description of the Current Study

In this thesis, a counter-rotating propeller is going to be designed for a submersible vehicle. In Chapter 2, OpenProp is introduced which is going to be used as a design tool for propellers in this study. Its theory along with the modules of "Parametric Study" and "Single Design" are mentioned. After the introduction of OpenProp, design procedure is explained with a single propeller to verify the design capability of OpenProp. The chosen propeller is known as the DTMB4119 propeller whose geometry and experimental results are present in the literature. In Chapter 3, the designed propeller by OpenProp based on the same inputs for both blade geometry and performance requirements of DTMB4119 propeller is analyzed numerically in ANSYS Fluent. By comparing the results with the experimental ones, verification of design procedure in OpenProp and methodology for performance analyses are completed. Besides the design capability of OpenProp, performance estimation of OpenProp is evaluated with a different blade geometry based on the same performance requirements of DTMB4119 propeller in Chapter 3 to see that whether OpenProp alone is sufficient for a complete design including the performance estimation or not. In Chapter 4, a propeller is designed by following the design procedure of OpenProp based on the speed and thrust requirements of the DTMB4119 propeller by an iterative approach to reach the final design. For this purpose; a methodology is developed including the modules of "Parametric Study" and "Single Design" of OpenProp, and also numerical analysis. In Chapter 5, after the methodology for design and performance analysis is set in Chapter 4 and Chapter 3, respectively, bare hull DARPA Suboff geometry is selected as the submersible vehicle that a counter-rotating propeller drives. Viscous flow analyses are conducted on the body to compare the results with the experimental one. When the speed and thrust requirements of the counter-rotating propeller are identified; thrust distribution and geometric dimensioning are done on forward and aft propellers. After that, forward propeller is designed based on the methodology developed in Chapter 4. Once the forward propeller is designed, the methodology is repeated for the aft

propeller. Since the aft propeller is located behind the forward propeller, wake region of the forward propeller is used in the geometric design and performance analyses of the aft propeller. Finally, the designed propellers are mounted on the DARPA Suboff for performance evaluations. Results are obtained in Chapter 5. Discussion is also presented in Chapter 5. Finally, conclusion with future work suggestions is pointed out in Chapter 6.

CHAPTER 2

OPENPROP

In this chapter, OpenProp is introduced first which is going to be used as a design tool for propellers in this study. After that, design procedure of OpenProp is explained on a single propeller whose geometry and experimental performance results are published in the study by Jessup [27]. The chosen propeller is known as David Taylor Model Test Basin 4119, abbreviated as DTMB4119. Performance analysis of the propeller, which is the output of OpenProp based on the geometry of DTMB4119 propeller is conducted in Chapter 3.

2.1 OpenProp

OpenProp is an open-source computational tool for the design and analysis of propellers and turbines written in the MATLAB programming language [28]. OpenProp is designed to be a GUI-based user-friendly tool for both inexperienced and professional designers. Development of the code has begun with Kerwin's MIT propeller design course notes in 2001 [29]. The first MATLAB version this code included GUI for parametric and preliminary design [30]. Geometry extraction routines and interface with the CAD program Rhino to generate 3D printable propeller are added later on [31]. By using a generalized optimizer routine implemented by Epps [32], design of ducted propellers is added to the code [33].

OpenProp uses vortex-lattice lifting-line theory for propeller blades with constant diameter helical vortices to represent the blade wake. The computational model includes a wake alignment procedure to represent the moderate blade loading. The model also has an analysis capability to estimate the performance in off-design

stages. Information flow chart of OpenProp is given in Figure 2.1. The input data is defined by the user either through the GUI menu or by running a short script [32]. The optimizer module is responsible for the optimum propeller design based on the specified inputs. After the design is finalized, analyzer module is able to determine the performance of off-design operating states and crafter module determines the 3D geometry for manufacturing of the propeller.
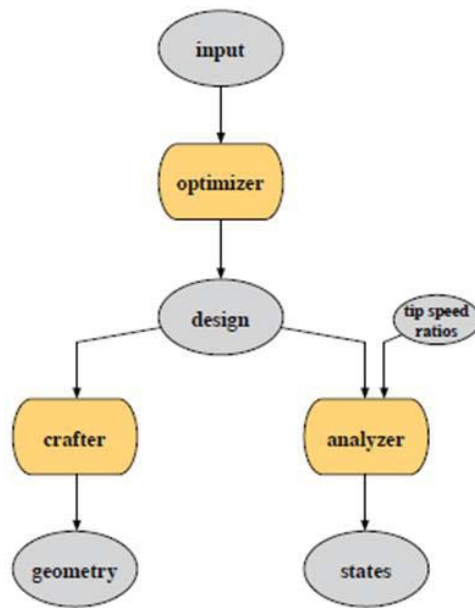
Figure 2.1. OpenProp Information Flow Chart [32]

2.1.1 Theory and Validation

The theory behind OpenProp is based on the studies by Kerwin [29], Coney [34] and Carlton [35]. Propeller blade is represented by discrete lifting lines, which is related with lifting-line theory. Trailing vorticities along the blade sections are aligned to the local flow velocity, which is a vector sum of free-stream flow and induced velocity. Vortex-lattice method is used to compute the induced velocities. Loads are computed by integrating the 2D loads over the span of the blade via discrete sections. With the specified flow and blade 2D section properties, the goal of the propeller

optimization module is to determine the optimum circulation distribution along the span of the blade, which yields the best efficiency.
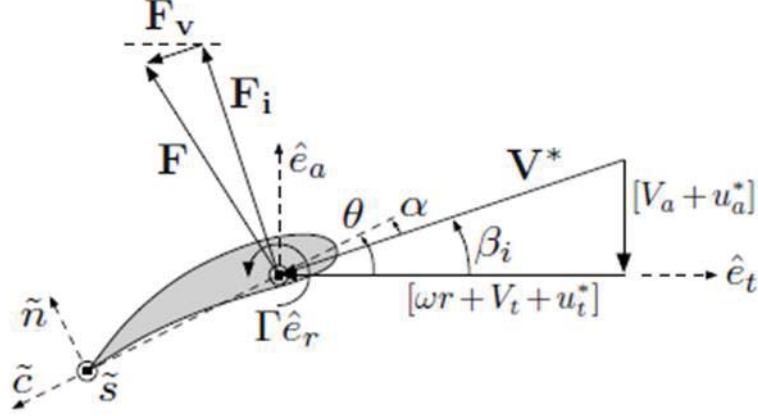
Figure 2.2. Propeller Velocity and Force Triangles, as Viewed from the Tip towards the Root of the Blade [32]

Figure 2.2. shows the velocity and force components on a 2D foil section in axial and tangential directions. Axial direction is denoted by $\hat{e}_a$ in which the thrust force acts whereas $\hat{e}_t$ shows the tangential direction. Tangential velocity of the inflow at radius r is $-wr\hat{e}_t$ due to angular velocity $w\hat{e}_a$ of the propeller shaft. There are 4 remaining velocity components which are axial inflow velocity of $\vec{V_a} = -V_a\hat{e}_a$, tangential inflow velocity $\vec{V_t} = -V_t\hat{e}_t$, induced axial velocity $\vec{u_a^*} = -u_a^*\hat{e}_a$ and induced tangential velocity of $\vec{u_t^*} = -u_a^*\hat{e}_t$. By these notations, total resultant inflow velocity becomes $\vec{V^*}$ whose magnitude and pitch angle are given in Equations (2.1) and (2.2).

$$V^* = \sqrt{(V_a + u_a^*)^2 + (wr + V_t + u_t^*)} \qquad (2.1)$$

$$\beta_i = \tan^{-1}\left[\frac{V_a + u_a^*}{wr + V_t + u_t^*}\right] \qquad (2.2)$$

Θ shows the blade pitch angle that is the sum of angle of attack, α, and flow angle β_i. Circulation is defined by $\Gamma\hat{e}_r$ where $\hat{e}_r$ represents the spanwise direction. For the force components, Kutta-Joukowski lift force is $\vec{F_l} = \rho\vec{V^*}(\Gamma\hat{e}_r)$ and viscous drag

force is $\vec{F_v}$ aligned with the flow. The total thrust and torque on the propeller is calculated via Equations (2.3) and (2.4).

$$T = Z \int_{r_h}^{R} [F_i cos\, \beta_i - F_v sin\, \beta_i\,] dr(\hat{e}_a) \tag{2.3}$$

$$Q = \rho Z \int_{r_h}^{R} [F_i sin\, \beta_i + F_v cos\, \beta_i\,] r dr(-\hat{e}_a) \tag{2.4}$$

In Equations (2.3) and (2.4), Z is the number of blades. Viscous drag force is $F_v = \frac{1}{2}\rho(V^*)^2 C_D c$ where ρ is the density of fluid, C_D is the drag coefficient of the 2D foil, c is the foil chord length and finally, r_h and R refer to hub and tip radii, respectively.

To compute axial and tangential induced velocities, OpenProp uses a propeller vortex lattice model. In this model, a Z-bladed propeller is taken as a single radial lifting line consisting of M panels. A horseshoe vortex filament with a circulation of $\Gamma(i)$ surrounds the ith panel with panel endpoints $r_v(i)$ and $r_v(i + 1)$. The control points on the lifting line at radial locations are $r_c(m)$ where the counter m is between 1 and M. The induced velocities are computed at these points by taking the sum of each horseshoe vortex:

$$u_a^*(m) = \sum_{i=1}^{M} \Gamma(i)\overline{u_a^*}(m, i) \tag{2.5}$$

$$u_t^*(m) = \sum_{i=1}^{M} \Gamma(i)\overline{u_t^*}(m, i) \tag{2.6}$$

In Equations (2.5) and (2.6), $\overline{u_a^*}(m, i)$ and $\overline{u_t^*}(m, i)$ are the axial and tangential velocities induced at $r_c(m)$ by a unit-strength horseshoe vortex surrounding panel i.

Propeller optimization module works on the principles defined in [34], the code tries to find the set of M circulations of the vortex lattice panels that produce the least torque;

$$Q = \rho Z \sum_{m=1}^{M} \left\{ [V_a + u_a^*]\Gamma + \frac{1}{2}V^*C_D c[wr_c + V_t + u_t^*] \right\} r_c \Delta r_v \tag{2.7}$$

18

for a specified thrust, T_s;

$$T = \rho Z \sum_{m=1}^{M} \left\{ [wr_c + V_t + u_t^*]\Gamma - \frac{1}{2}V^*C_D c[V_a + u_a^*] \right\} \Delta r_v - Hflag$$

$$* \frac{\rho Z^2}{16\pi} \left[ln\left(\frac{r_h}{r_o}\right) + 3 \right] [\Gamma(1)]^2 = T_s \tag{2.8}$$

where *Hflag* component stands for hub or no hub model. It takes values of 1 and 0 for hub and no hub cases, respectively.

The circulation optimization is performed using an auxiliary function of $H = Q + \lambda_1(T - T_s)$ where λ_1 is the unknown Lagrange multiplier. $T = T_s$ is the design point where minimum torque Q appears. To find this minimum, first order derivatives with respect to $\Gamma(i)$ for each panel i between 1 and M are computed and equated to zero, i.e. $\frac{\partial H}{\partial \Gamma(i)} = 0$ for $i=1\ldots M$, along with the $\frac{\partial H}{\partial \lambda_1} = 0$. This computation results in $M+1$ equations. The resulting non-linear system of equations is solved iteratively until the convergence of optimized circulation distribution along with flow parameters.

After the design state of flow chart presented in Figure 2.1 is obtained, the 3D geometry is constructed from user-specified 2D profiles that are scaled and rotated according to the design lift coefficient (C_{L_0}), chord (c) and inflow angle (C_{L_0}) through the blade span. The section lift coefficient is given in terms of the geometry by:

$$C_L = 2\pi(\alpha - \alpha_I) + C_{L_I} \tag{2.9}$$

where α_I and C_{L_I} are the ideal angle of attack and lift coefficient, respectively. In the geometry module, the angle of attack of each blade section is set to the ideal angle of attack, i.e. $\alpha = \alpha_I$, to prevent leading edge flow separation and cavitation. By this substitution into the Equation (2.9), the lift coefficient is equated to the desired lift coefficient:

$$C_L = C_{L_I} \tag{2.10}$$

The blade pitch angle then becomes fixed at $\Theta = \alpha_I + \beta_{i_0}$ along the span. With this computed 2D blade section geometry, OpenProp is able to export 3D form of a propeller.

OpenProp was validated with U.S. Navy propeller 4119. Circulation distribution of OpenProp is compared with both experimental data from Black [36] and U.S. Navy code PBD.
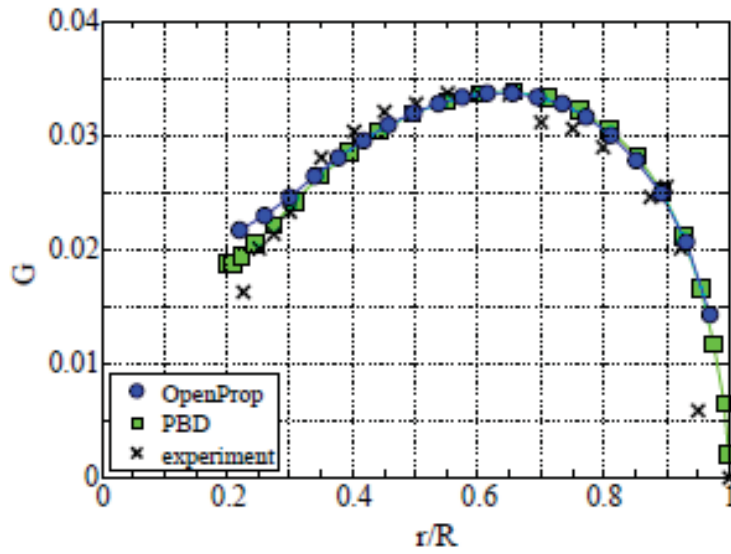
Figure 2.3. Comparison of Results for Circulation Distribution for U.S. Navy Propeller 4119 [32]

2.1.2   Parametric Analysis

OpenProp is able to do a parametric analysis based on three parameters: the number of blades, the propeller revolution speed and the propeller diameter. By defining the minimum-maximum values and increments for each parameter, OpenProp calculates and graphically represents efficiencies for different combinations. The formulation for efficiency is:

$$\eta_0 = \frac{P_{OUT}}{P_{IN}} = \frac{TV_s}{Q\omega} \tag{2.11}$$

20

where T and V_s represent thrust and ship speed, respectively. Their multiplication gives the output power from the propeller. Q and ω stand for torque and propeller revolution speed, their multiplication is equated to inlet power supplied by the motor shaft. By specifying the T, V_s and ω; OpenProp finds the optimum Q based on the Eqn. (2.7) and calculates the efficiency. Default GUI menu of parametric analysis is shown in Figure 2.4. Thrust, ship speed, hub diameter and fluid density shall be specified by user input. The parameters appearing in default menu is valid for U.S. Navy 4148 propeller, as a guide to users.
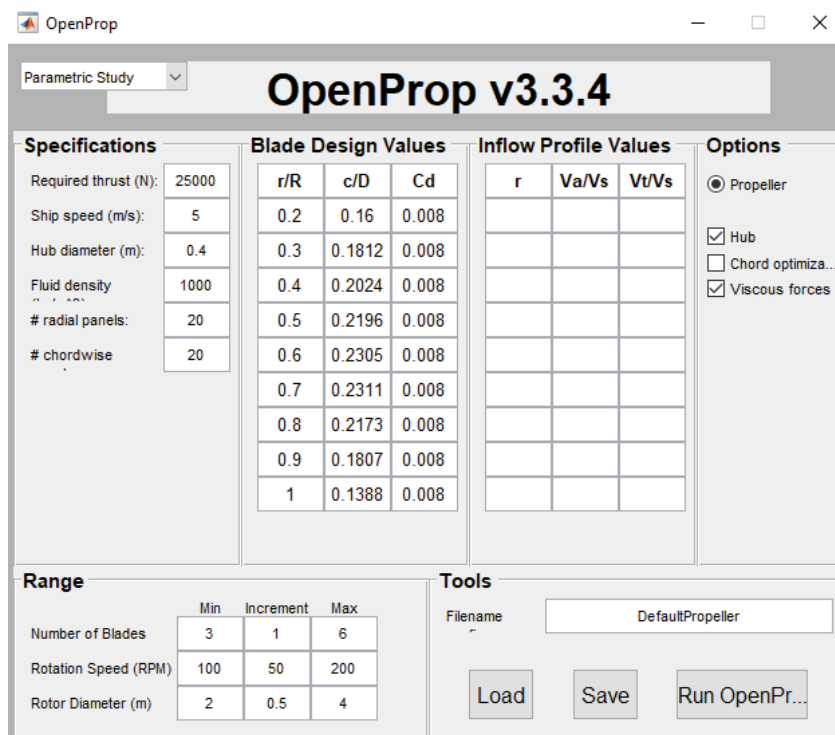
Figure 2.4. Default GUI Menu of "Parametric Study" in OpenProp

2.1.3   Single Design

With the "Parametric Study" of OpenProp; number of blades, propeller rotation speed and propeller diameter can be determined by comparing the corresponding efficiencies. "Single Design" module of OpenProp is used for detailed design. Default GUI menu of "Single Design" is shown in Figure 2.5. The specifications

appearing on left side of the menu is either entered by the user in "Parametric Study" or determined from the outputs of "Parametric Study".
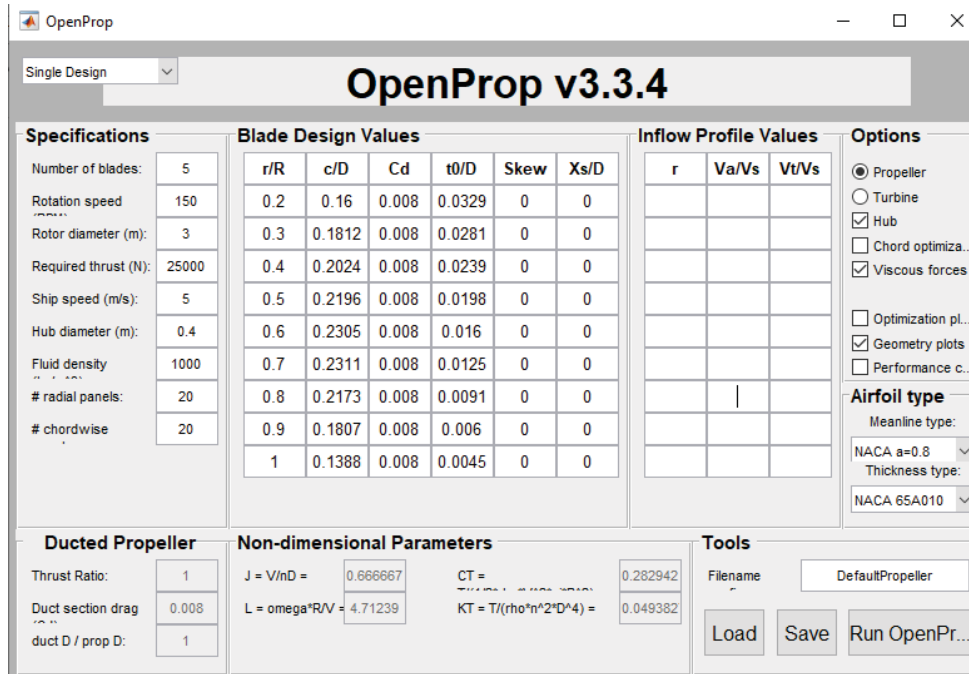
Figure 2.5. Default GUI Menu of "Single Design" in OpenProp

Chord and thickness distributions in the table of "Blade Design Values" shall be specified by the user. Skew or rake data can also be entered through the GUI menu. Inflow profile is taken as a uniform inlet profile if left blank; however, axial and tangential velocity distributions can be specified radially by the user. The available meanline types are NACA a=0.8, NACA a=0.8 (modified) and parabolic and, also available thickness forms are NACA 65A010, NACA 65A010 (modified), elliptical, parabolic and NACA 66 (DTRC modified). OpenProp can be easily modified to accommodate other well-known profiles or user-specific designed profiles.

2.2   Verification of OpenProp by the DTMB4119 Propeller

Before using OpenProp as a design tool in the next chapters, its capability for design shall be verified clearly. In addition to that, inputs and outputs of the design procedure shall be clarified. For this reason, a single propeller whose geometry is

reported in the experimental study is chosen to verify the design capability of OpenProp [27]. The chosen propeller is known as David Taylor Model Test Basin 4119, abbreviated as DTMB4119. Geometric and hydrofoil section parameters are presented in Table 2.1 and 2.2, respectively.

Table 2.1. Geometry of DTMB4119 Propeller

Diameter (m)	0.3048
Rotation	Right Hand
Number of Blades	3
Hub-Diameter Ratio	0.2
Skew (°)	0
Rake (°)	0
Section Thickness Form	NACA66 (DTRC Modified)
Section Meanline	a=0.8

Table 2.2. Section Profiles along DTMB4119 Propeller [27]

r/R	c/D	P/D	t/c	f/c
0.2	0.320	1.105	0.2055	0.01429
0.3	0.3625	1.102	0.1553	0.02318
0.4	0.4048	1.098	0.1180	0.02303
0.5	0.4392	1.093	0.09016	0.02182
0.6	0.4610	1.088	0.06960	0.02072
0.7	0.4622	1.084	0.05418	0.02003
0.8	0.4347	1.081	0.04206	0.01967
0.9	0.3613	1.079	0.03321	0.01817
0.95	0.2775	1.077	0.03228	0.01631
1.0	0.0	1.075	0.03160	0.01175

In Table 2.2, r denotes the radial location along the blade whereas R is radius of the propeller. "c" is used for chord. "p" is referred to a pitch, i.e. the distance travelled

in translational axis for one revolution of the blade. "*t*" and "*f*" are used to describe maximum thickness and camber along the sections.

In the experimental study, the propeller is tested at five different advance coefficients. Open-water results at five different advance ratios is given in Table 2.3.

Table 2.3. Experimental Results of DTMB4119 Propeller [27]

J	K_T	$10 * K_Q$	η_0
0.5	0.285	0.477	0.489
0.7	0.200	0.360	0.632
0.833	0.146	0.280	0.692
0.9	0.120	0.239	0.725
1.1	0.034	0.106	0.575

DTMB4119 propeller has a tip diameter of 304.8 mm whereas the hub diameter is one fifth of the tip diameter, which is equal to 60.96 mm. The design advance coefficient of the propeller, denoted as *J*, is 0.833. At this advance coefficient, incoming flow has a uniform speed of 2.54 m/s and the propeller rotates at 600 rpm in the experimental setup. With this experimental setup, resultant thrust and torque coefficients are 0.146 and 0.028 which correspond to a thrust of 129.16 N and a torque of 7.55 N.m.

"Single Design" menu of OpenProp requires inputs for "Specifications" to define number of blades, overall dimensions, rotation speed, performance requirements of thrust and speed shown as a red box in Figure 2.6; for "Blade Design values" such as chord and thickness distributions at the specified radial sections along a propeller shown as a blue box; for "Inflow Profile Values" to define the axial and tangential components of the incoming flow shown as a yellow box; and for "Airfoil Type" to define meanline and thickness types as a green box.

The parameters specified in Table 2.1 are entered as the inputs for the tabs of "Specifications" and "Airfoil Type". Default settings of OpenProp arrange the

incoming flow as a uniform axial inlet if left blank. For the tab of "Blade Design Values", the profile presented in Table 2.2 is copied into OpenProp. With these inputs presented in Figure 2.6, OpenProp is run.
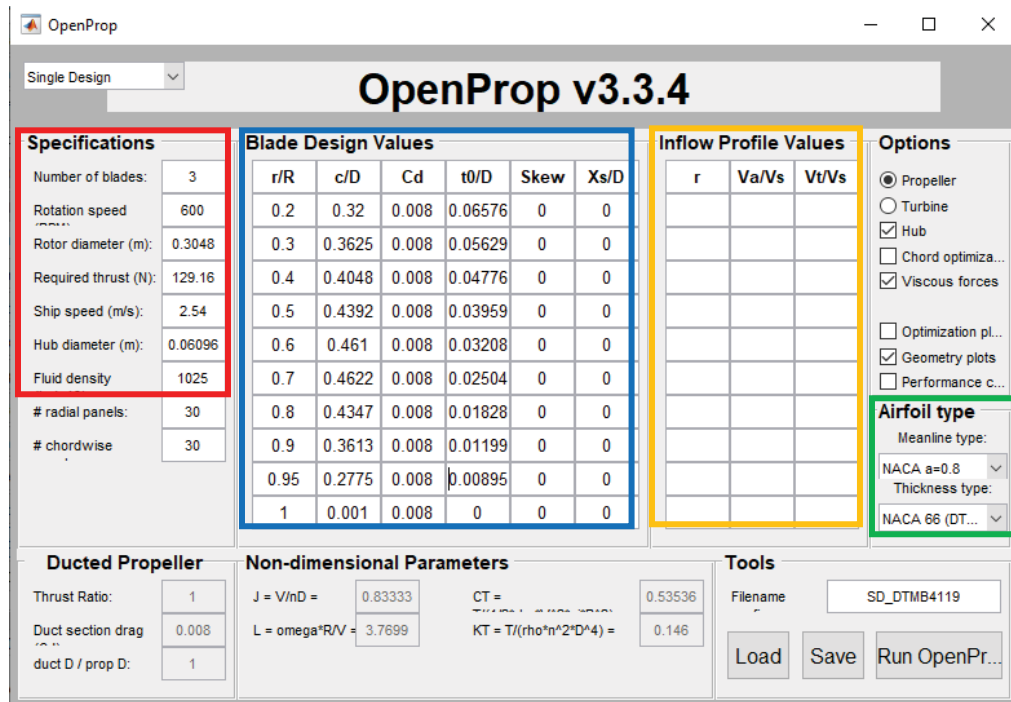
Figure 2.6. "Single Design" GUI of OpenProp with DTMB4119 Propeller Inputs

When the convergence is established, OpenProp is able to output the 3D view of the propeller.
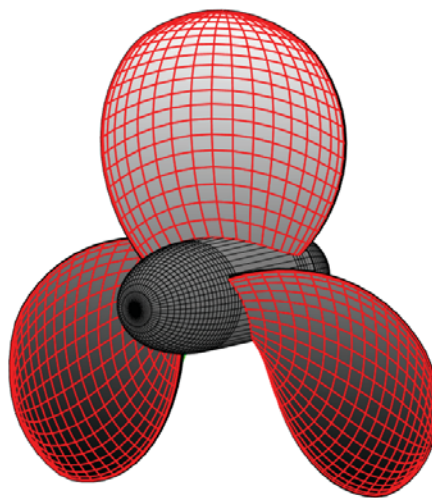
Figure 2.7. 3D Model View of DTMB4119 Propeller in OpenProp

Although the inputs for "Blade Design Values" include chord and thickness distributions at total 10 radial locations from $r/R = 0.2$ to $r/R = 1$, i.e., from hub to tip, OpenProp keeps these two-dimensional profiles as a base and determines the chord and thickness distributions in non-specified radial sections. In other words, the input of two-dimensional chord and thickness distributions is preserved throughout the design procedure without any change or optimization on the input profiles.

It bends the propeller in 3D space based on the given two-dimensional profiles to find the optimum circulation distribution, which supplies the specified thrust with a minimum torque output based on the calculated hydrodynamic pitch angle and angle of attack of each specified and non-specified radial sections. In other words, OpenProp finds the 3D twisted distribution of the propeller based on the given 2D profiles. By this way, it gives the 3D output of the propeller.

2D chord and thickness distributions of the design output are given in Figure 2.8 and Figure 2.9, respectively. The dotted regions are the ones that are already specified in the inputs. As explained before, the dotted regions are not changed or optimized throughout the design procedure.
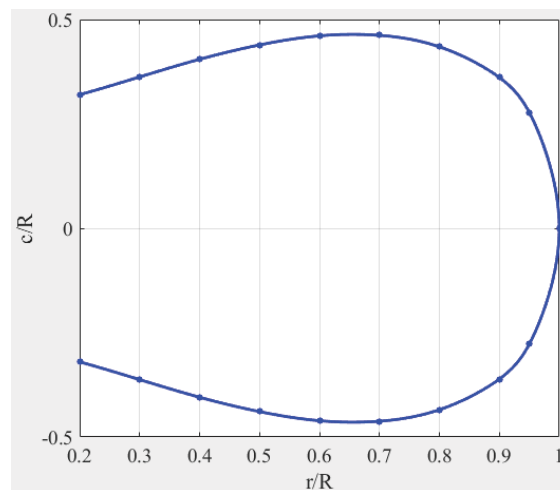
Figure 2.8. Chord Distribution along the DTMB4119 Propeller
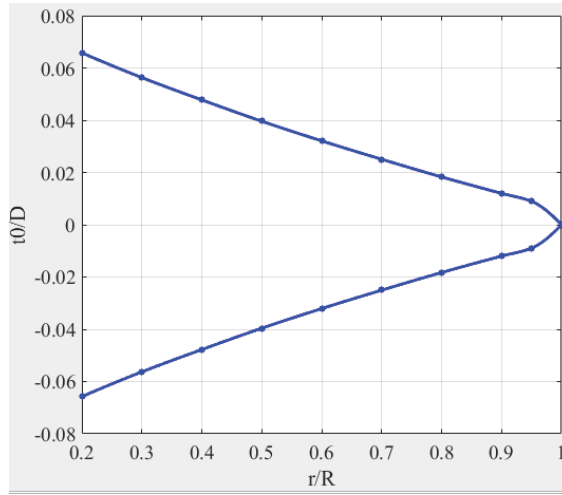
Figure 2.9. Thickness Distribution along the DTMB4119 Propeller

Water density, ship speed, revolution speed and required thrust are also given as inputs before the design procedure of OpenProp is started. These are the parameters to calculate the advance coefficient and thrust coefficient. Once the design procedure is finalized, OpenProp finds the torque output, which yields the torque coefficient. By knowing the thrust and torque coefficients, efficiency can be calculated. With these non-dimensional parameters, performance results of OpenProp and their comparison with experimental results are presented in Table 2.4. OpenProp can also estimate the performance at off-design stages, which means it estimates the performance at other advance coefficients. Figure 2.10 shows the comparison between the performance estimations of OpenProp and experimental results.

Table 2.4. Performance Results of OpenProp for DTMB4119 Propeller

	OpenProp	Experiment	True Error (%)
Advance Coefficient (J)	0.833	0.833	-
Thrust Coefficient (K_T)	0.146	0.146	-
Torque Coefficient (K_Q)	0.0275	0.028	1,79
Efficiency (η_0)	0.7041	0.692	1,75

27
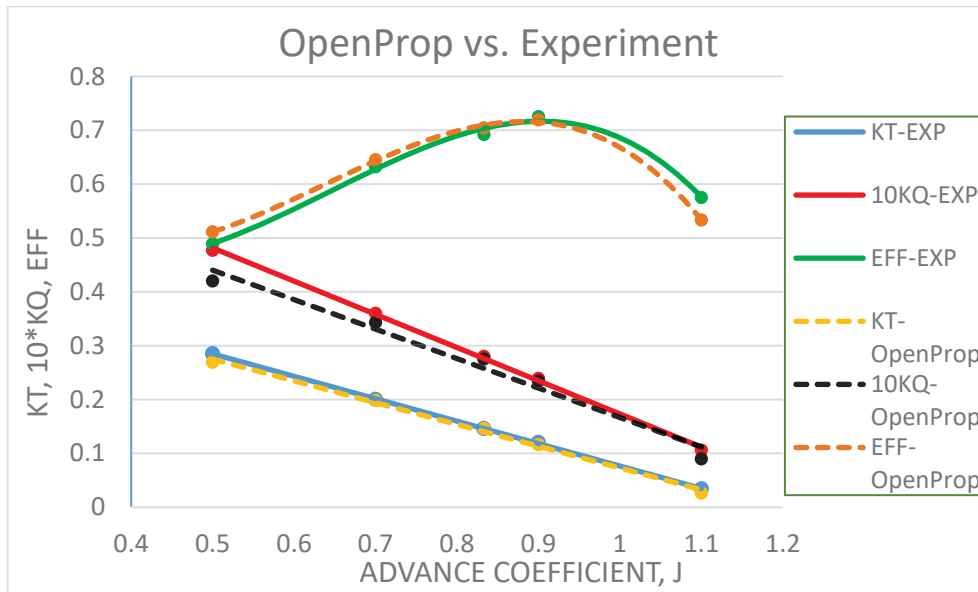
Figure 2.10. Comparison of Results between OpenProp and Experiment

As it is seen in Table 2.4 and Figure 2.10, the performance results of OpenProp are very close to the experimental ones. The results for the thrust coefficients are almost the same whereas OpenProp estimates the torque coefficients slightly lower than experimental ones. For the design advance coefficient of 0.833, the errors for torque coefficient and efficiency are very small in Table 2.4. At the off-design stages, the errors increase but they are still in the acceptable range.

However, during the design procedure of OpenProp, required thrust which is given as an input is not evaluated. OpenProp does not evaluate the design output whether it is going to supply the required thrust or not, it keeps the same thrust as specified by the user and reports the same thrust, which is already given before the design procedure is started, as an output in the end. To prove this, a propeller with narrower blades than the DTMB4119 propeller is tested. Everything is kept the same except the "Blade Design Values". The chord distribution is selected to be exactly 2 times narrower than the DTMB4119 propeller. Inputs are specified in "Single Design" menu of OpenProp as shown in Figure 2.11. 3D view of the propeller and chord distribution along the propeller is also presented.
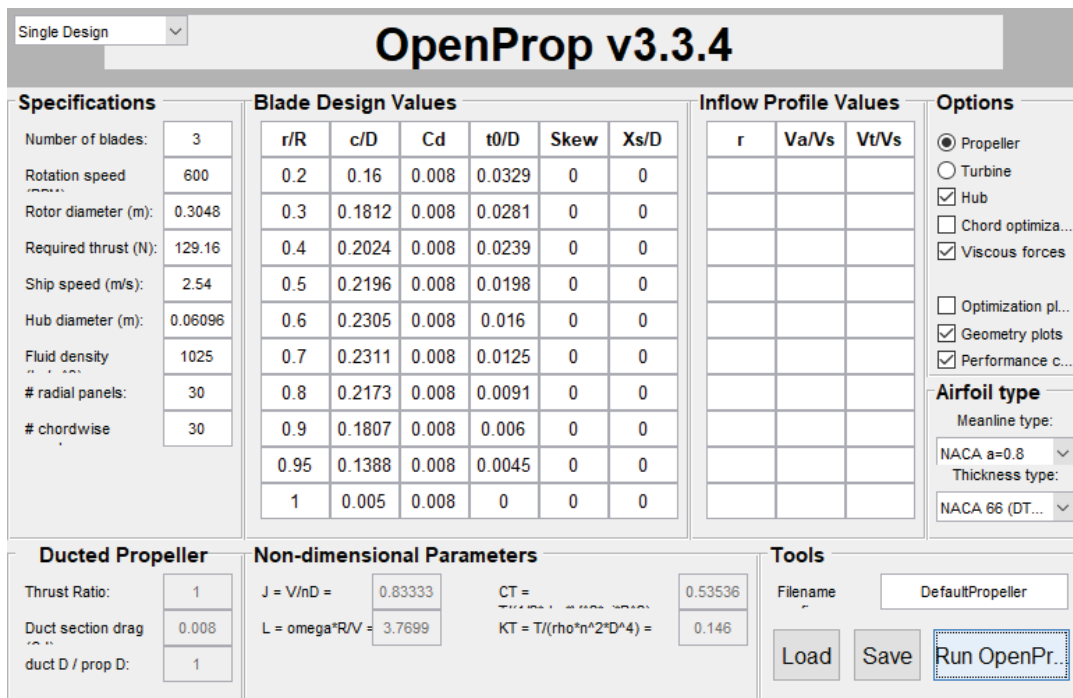
Figure 2.11. "Single Design" GUI of OpenProp with Narrower Bladed Propeller
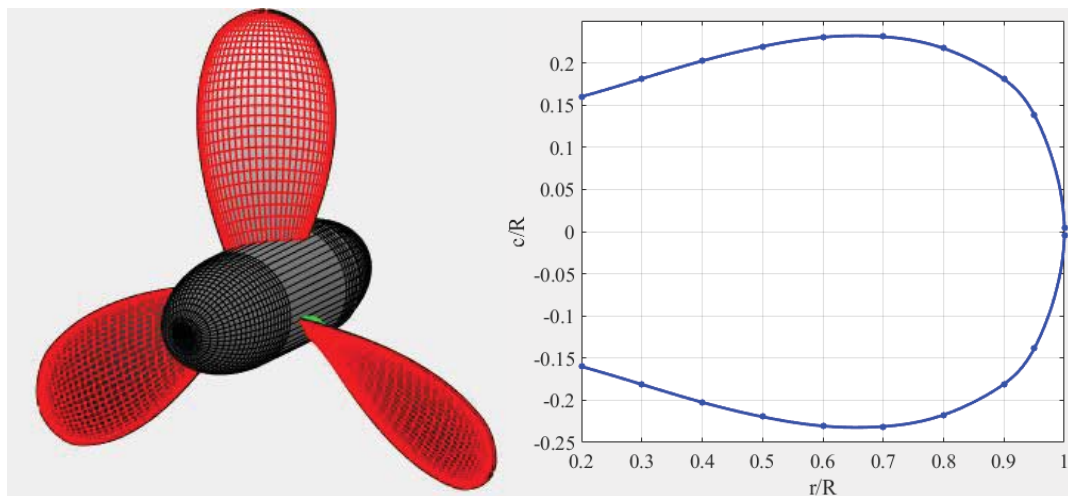
Figure 2.12. 3D Model View and Chord Distribution of the Narrower Blades

When the 3D model and chord distribution of the narrower bladed propeller are compared with Figure 2.7 and Figure 2.8, it is obvious that the DTMB4119 propeller has more blade area. Therefore, the performance results of OpenProp with narrower bladed propeller shall be different than the DTMB4119 propeller. The performance

results of DTMB4119 propeller and narrower bladed propeller designed by OpenProp are shown in Table 2.5.

Table 2.5. Performance Comparison of Two Different Designs in OpenProp

	OpenProp DTMB4119 Propeller	OpenProp Narrower Bladed Propeller	
Advance Coefficient (J)	0.833	0.833	
Thrust (N)	129.16	129.16	**No change**
Torque (N.m)	7.42	6.93	
Efficiency	0.70	0.75	
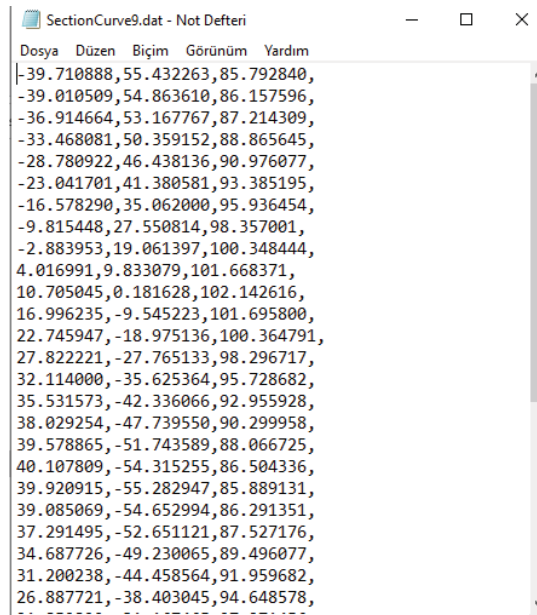
Although the blade profile for the narrower bladed propeller is two times smaller than the DTMB4119 case, the results show that it produces the same thrust. It shows the exact input of required thrust as if the designed propeller can create the specified thrust.

In the design methodology of OpenProp, a propeller is designed to achieve the required thrust if the code converges. However, convergence does not guarantee that the resultant thrust is close to the required thrust as it is seen with the narrower bladed propeller. The reason for this situation is that OpenProp finds the optimum circulation distribution by using an auxiliary function of $H = Q + \lambda_1(T - T_s)$ as explained in Section 2.1.1. In this function, minimum torque of Q appears on the design point where the resultant thrust of T is equated to the input thrust of T_s. For this reason, if the design point is achieved, then the resultant thrust is already equated to the input thrust. Therefore, the same thrust given as an input is shown in the output as a resultant thrust.

For this reason, performance evaluations of OpenProp may be misleading if the correct inputs are not selected. To prevent this situation, performance evaluations of

any propeller designed in OpenProp shall be carried out by Computational Fluid Dynamics (CFD) studies.

To complete the verification of design procedure in OpenProp, the designed propeller with the inputs of DTMB4119 propeller shall be investigated by CFD studies. For this purpose, the 3D geometry in OpenProp needs to be imported into a CFD environment. OpenProp is based on ".*m*" code which has a lot of subroutines. Some of the subroutines has been left to further developments one of which is exporting the coordinates for the points along the section foils. Some modifications are done on this subroutine to have a ".dat" file in which coordinates of points along a section foil is present as shown in Figure 2.13.

Figure 2.13. Coordinates of Points along a Section Foil for DTMB4119 Propeller

Then, the coordinates of points for each hydrofoil is exported to a file. After that, the hydrofoils are drawn in Siemens NX to complete the design of the propeller. Imported section curves are shown in Figure 2.14 and 3D model of the designed DTMB4119 propeller is shown in Figure 2.15.

Figure 2.14. Imported Section Curves to Siemens NX for DTMB4119 Propeller
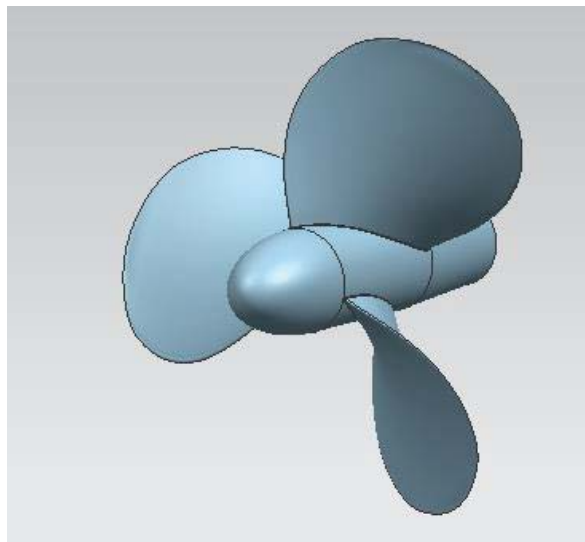
Figure 2.15. 3D Model of DTMB4119 Propeller

In Chapter 3, performance analysis of the designed propeller which is the output of OpenProp based on inputs of DTMB4119 propeller is carried out to complete the verification of design procedure in OpenProp.

CHAPTER 3

PERFORMANCE ANALYSIS OF DTMB4119 PROPELLER AND VERIFICATION OF OPENPROP

In this chapter, performance analyses of the designed propeller in Chapter 2 which is the output of OpenProp based on inputs of DTMB4119 propeller are carried out. The results of the numerical analyses and performance estimations of OpenProp are compared with the experimental results presented in Jessup's study [27] to complete the verification of design procedure in OpenProp. After that, the designed narrower bladed propeller in Chapter 2 is analyzed numerically to see that OpenProp may not be reliable tool for performance estimation without conducting CFD studies on the designed propellers.

ANSYS Fluent software is used for numerical analyses. To be able to perform an analysis, a solution domain shall be constructed to enclose the propeller in which fluid flow occurs. For turbomachinery flows, Multiple Reference Frame (MRF) methods are preferred [37]. In MRF, two or more regions can have relative translational or rotational motion with respect to each other. Frozen Rotor method which is one of the Multiple Reference Frame (MRF) methods is selected for the upcoming analyses. It is a steady-state analysis and faster than other methods in terms of convergence. Since the final results of the analyses are important for our case, steady-state solution with faster convergence is appropriate. In Frozen Rotor approach, the domain is divided into two regions, namely rotating domain and static domain. Rotating domain encloses the propeller and rotational version of flow equations are solved in this region whereas static region encloses the rotating domain and it is the region where solution boundaries are defined.

3.1 Performance Analysis of DTMB4119 Propeller

To reduce the computational time during meshing and solution, periodicity is used, i.e. one third of the whole model in Figure 2.15 is constructed as shown in Figure 3.1.
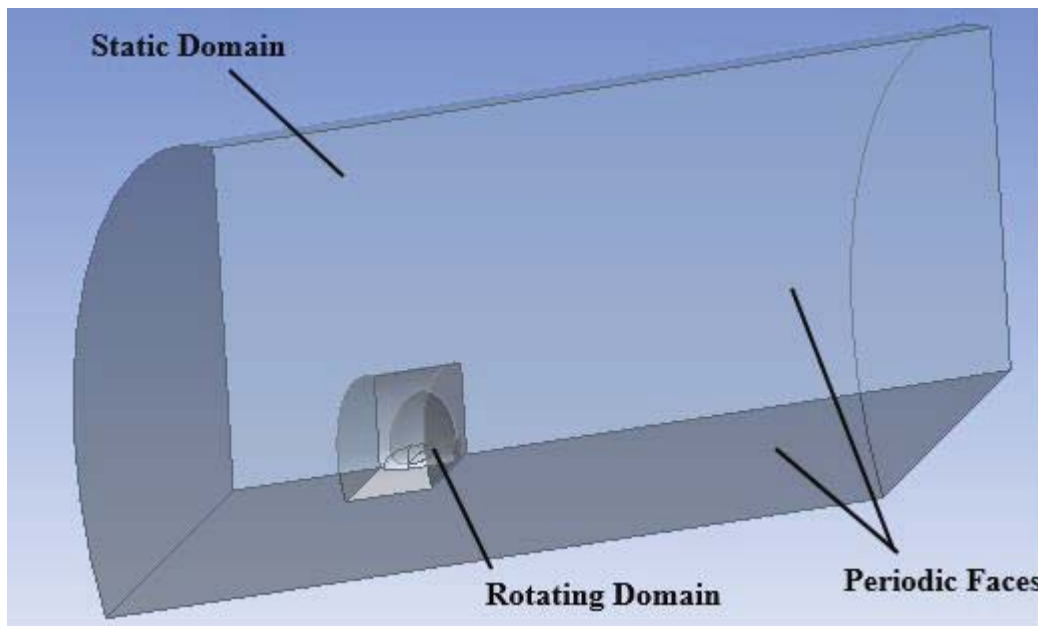
Figure 3.1. Solution Domain and Periodicity for DTMB4119 Propeller

Dimensions of rotating domain is set as $1.1R$ in radial direction and $2R$ in longitudinal direction where R denotes the radius of the propeller. The dimensions for solution domain including the static domain are given in Figure 3.2.
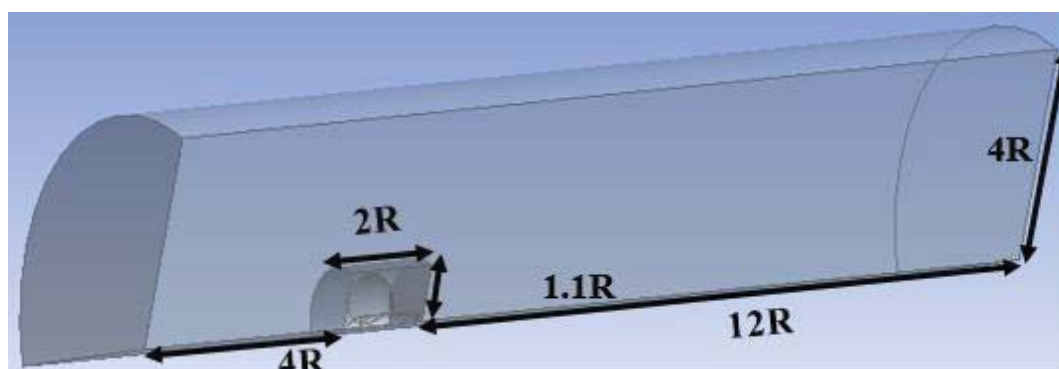
Figure 3.2. Solution Domain for DTMB4119 Propeller

Fluent uses Finite Volume Method (FVM) to discretize integral form Navier-Stokes and turbulence equations. Dimensional space is discretized into cells where each equation is solved in a coupled way. Therefore, it is very important to have a mesh with good quality to capture all flow variables accurately to achieve convergence. After determining the method and domain for solution, there shall be a mesh independence test, i.e. the solutions shall be free of the used mesh. The rotating domain shall have smaller element sizes than static region because it is expected to have large gradients in flow variables along this region. The cells in the interface between the static and rotating domains shall have closer sizes for convergence. Three different cases of mesh are considered, namely coarse, medium and fine meshes. From coarse to fine mesh, main improvements are as follows:

- Face and edge sizing get smaller both in rotating domain and static domain.
- The number of layers in the boundary layer increases whereas y^+ is fixed.

Mesh independence study has been carried out at the design advance coefficient of 0.833 of the DTMB4119 propeller. This non-dimensional value corresponds to uniform inlet velocity of 2.54 m/s with a water density of 1025 kg/m³ and revolution speed of 10 rps. Realizable k-ϵ model with standard wall functions is used for turbulence modelling and it is kept the same for all meshes. Overall results for mesh independence are presented in Table 3.1.

Table 3.1. Overall Results for Mesh Independence Study at J=0.833

	Number of Cells	K_T	$10 * K_Q$	K_T Exp.	$10 * K_Q$ Exp.	Error %K_T	Error %K_Q
Coarse mesh	1,672,389	0.1423	0.3109			2.53	11.04
Medium mesh	2,638,295	0.1442	0.2936	0.146	0.280	1.23	4.86
Fine mesh	3,284,982	0.1444	0.2941			1.10	5.04

As it is presented in Table 3.1, the thrust and torque coefficients obtained with medium and fine meshes do not differ significantly. In fact, they are very close to each other. This means that the solution is independent of the used mesh at the design advance coefficient of 0.833 of the DTMB4119 propeller. Therefore, medium mesh is selected for foregoing analyses. It has 2,638,295 cells. The medium mesh is presented in Figure 3.4. Mesh metrics obtained with the medium mesh is given in Table 3.2.

Table 3.2. Mesh Metrics for the Medium Mesh

First cell height in boundary layer	0.001m
Total number of layers in boundary layer	20
Minimum orthogonal quality	0.09
Maximum skewness	0.93

There are total 20 layers used to model the boundary layer. Turbulent viscosity ratio is plotted at a radial section close to the blade tip to see whether the created mesh is enough to capture the boundary layer. As it is seen in Figure 3.3, turbulence vanishes around the 7th and 8th cells in the boundary layer. Therefore, the created mesh is enough to capture the boundary layer.
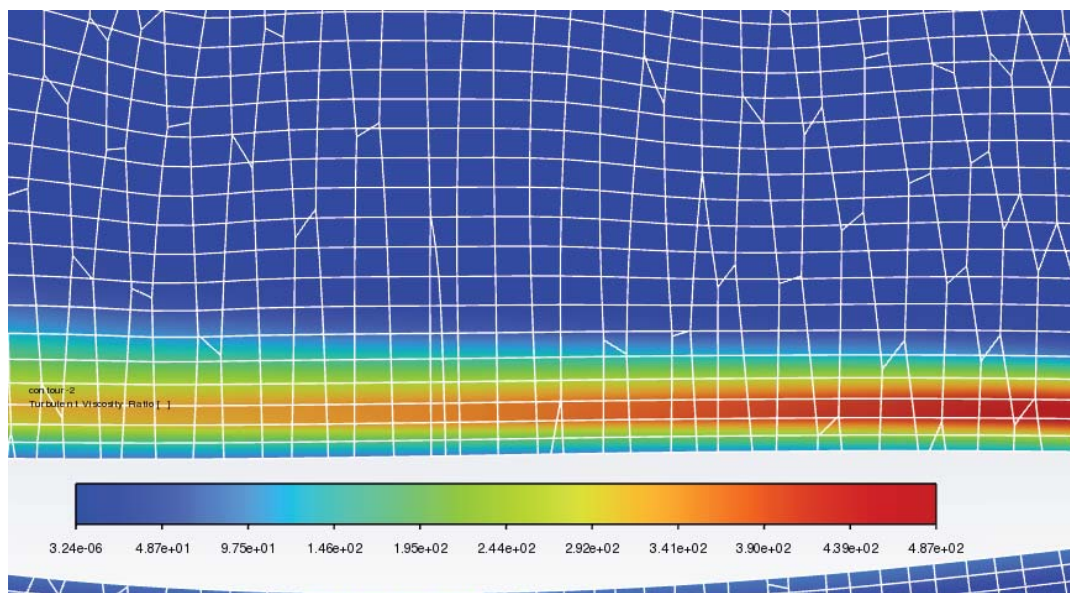
Figure 3.3. Mesh Capturing the Boundary Layer
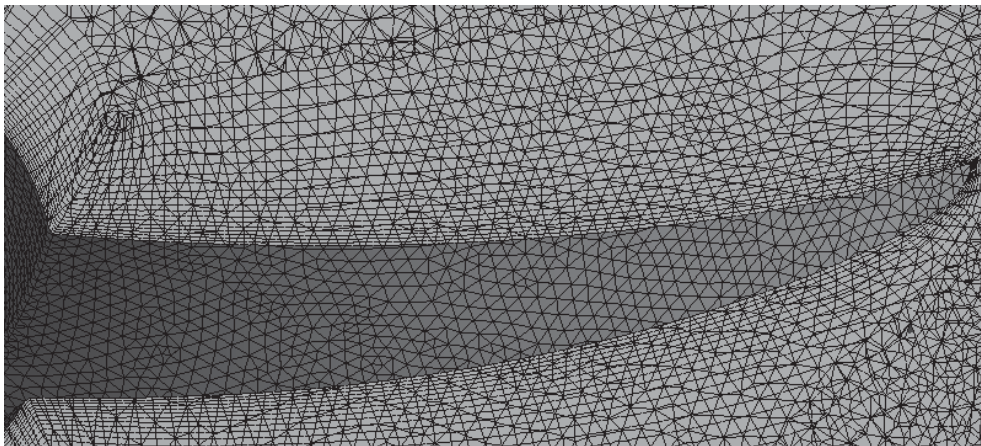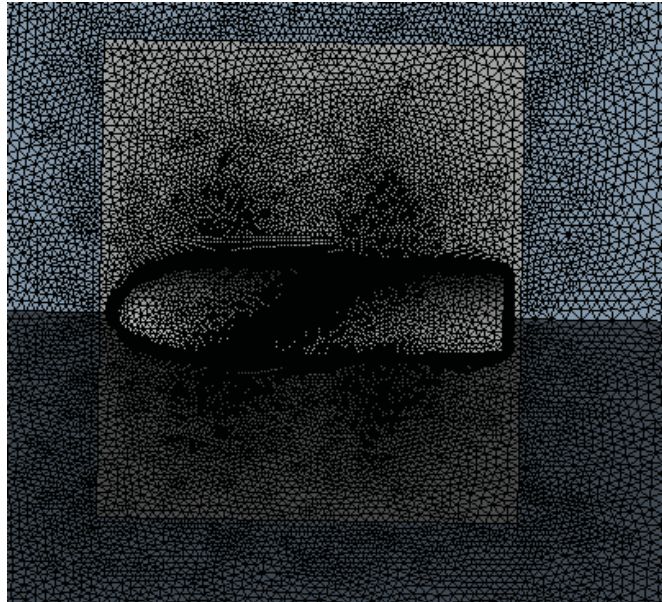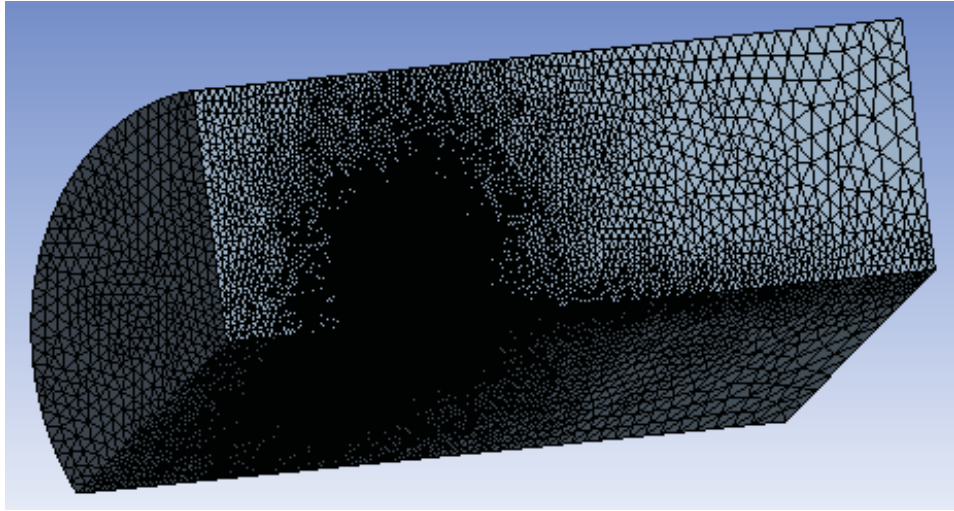
Figure 3.4. Mesh for the DTBM4119 Propeller

In the solution settings, boundary conditions are set as presented in Figure 3.5. Also, solver settings are given in Table 3.3.
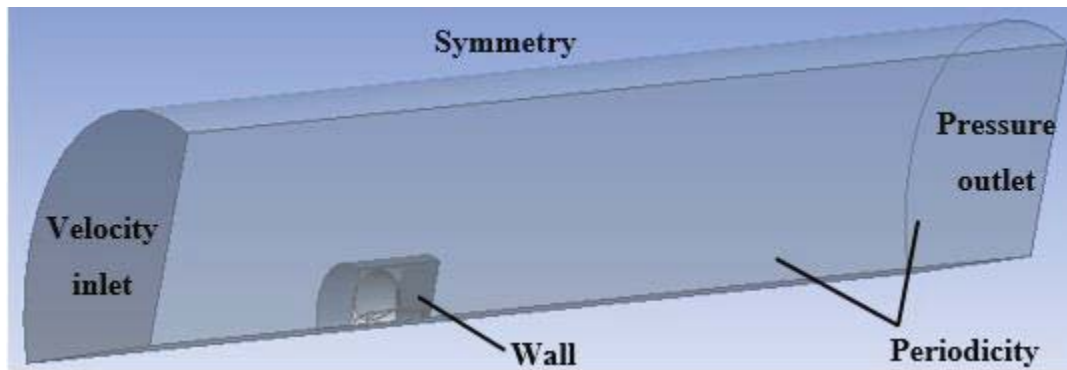
Figure 3.5. Boundary Conditions

Table 3.3. Solution Settings

Solver	Pressure based - Steady
Turbulence Modelling	Realizable k-ϵ
Near Wall Treatment	Standard Wall Functions
Inlet Speed (m/s)	2.54
Water Density (kg/m^3)	1025
Water Viscosity (kg/m.s)	0.001003
Pressure-Velocity Coupling	SIMPLE
Depth	250m

With these settings, the solution is obtained in 262 iterations. Convergence is obtained when the residual for continuity equation has reached 1e-5. Additionally, the thrust force created by the propeller is drawn throughout the solution to check whether the solution is converged or not. As it is presented in Figure 3.6, convergence is established.

38
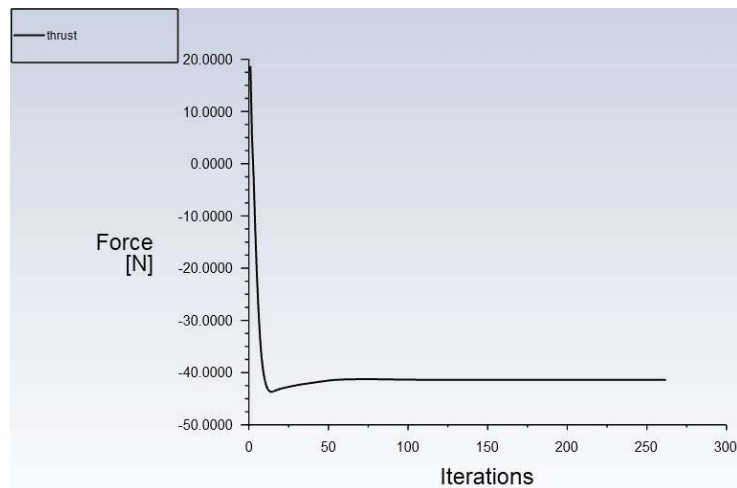
Figure 3.6. Convergence Plot of Thrust Force Created by the DTMB4119 Propeller

For turbulence modelling, y^+ defines the expression for first cell height over the boundary layer. Therefore, it is an important parameter to capture the boundary layer correctly. On the propeller surface, contour of y^+ is presented in Figure 3.7. In Figure 3.7, there seems to be small zones where y^+ is smaller than 30. These zones are especially on the leading edge of the propeller and they are very close to the hub where the flow speed is very low. Therefore, flow regime in this zone can be regarded as a laminar one where turbulence modelling is not required. However, y^+ value is between 30 and 300 in most of the regions. For this reason, the choice of k-ϵ model with standard wall functions for turbulence modelling seems suitable because it is recommended for applications where y^+ value is between 30 and 300 [38].
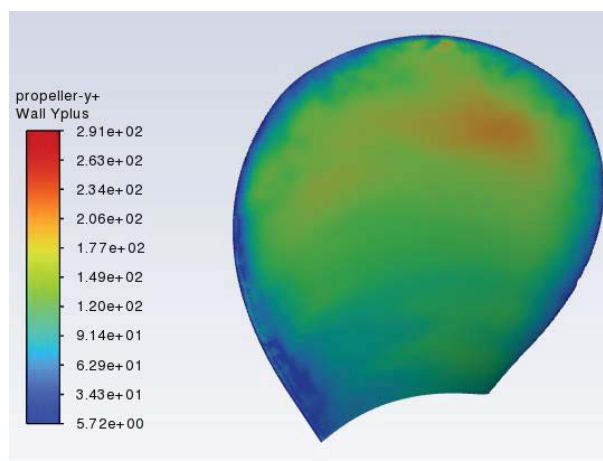
Figure 3.7. Variation of y^+ Values along the DTMB4119 Propeller

The propeller has two surfaces which are the one which accelerates the fluid called suction face and the other one follows the suction face that is called pressure face. Velocity of the flow increases along the leading edge of the propeller in the suction face where the pressure decreases accordingly. Absolute pressure contours for both surfaces are given in Figure 3.8. As it is seen the pressure is greater in pressure face which creates a pressure difference between the faces, and hence thrust is obtained.
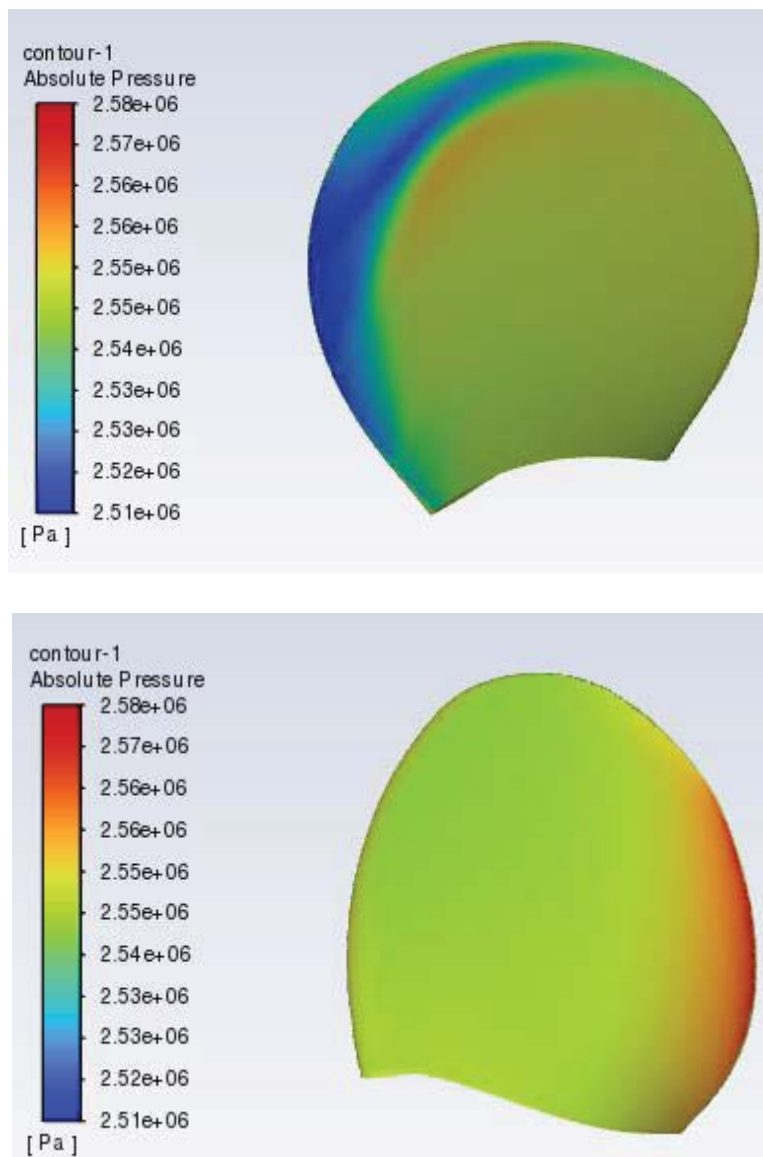
Figure 3.8. Absolute Pressure Contours over the Suction (Upper) and Pressure (Lower) Faces

The propeller is tested at five different advance coefficients as it is followed in the experiment as shown in Table 2.3. With the same solution domain, mesh and solution settings, numerical analyses are repeated at the specified advance coefficients. During the numerical analyses, rotational speed of the propeller is kept constant at 10 rps and velocity at the inlet face is changed according to the advance coefficient as it is followed in the experiment [27]. The graph showing all results with numerical analyses and experimental values is given in Figure 3.9.
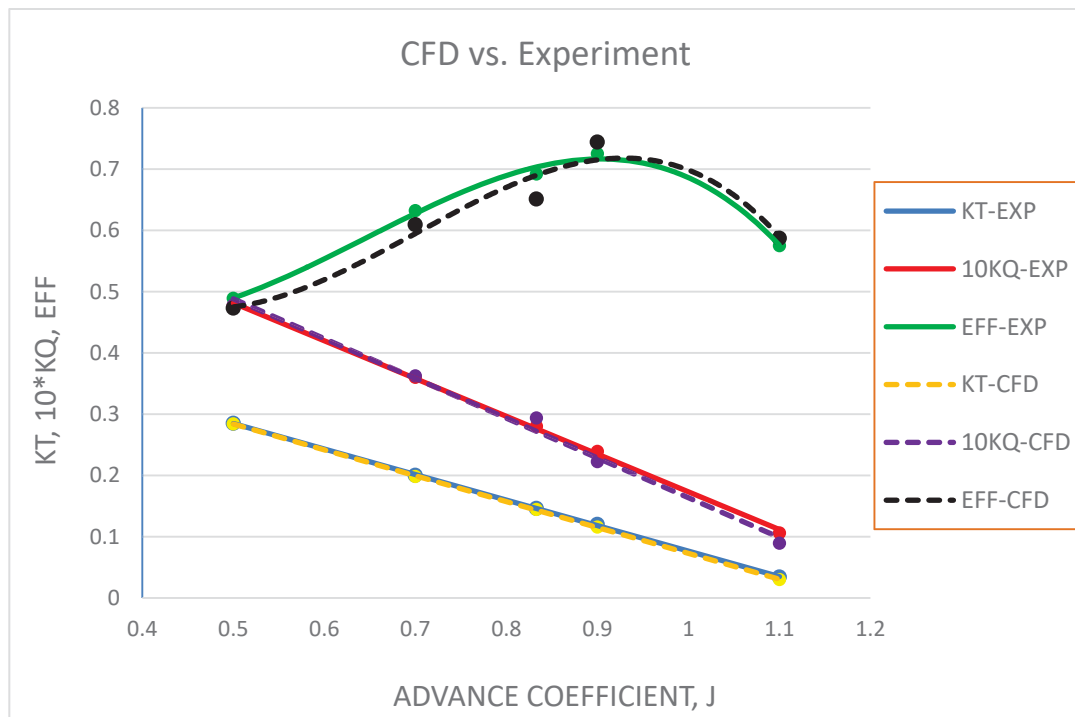
Figure 3.9. Overall Results Showing CFD vs. Experimental Results for DTMB4119 Propeller

It is seen that both thrust and torque coefficients obtained with numerical analyses are very close to experimental measured values. The true error rates for thrust and torque coefficients are at minimum for the lower advance coefficients. As the advance coefficients increase, the error rates start to increase. Also, the true error rates for K_Q are slightly bigger than K_T which directly effects the errors for the efficiency. Especially for the advance coefficient of 1.1 which is the maximum

advance coefficient in the investigated range, K_T and K_Q have their maximum errors as 12% and 15%, respectively. The reason for these maximums is that k-ϵ turbulence modelling and selected wall treatment method become less accurate at high advance coefficients due to high water velocity. However, the results of numerical analyses are still in good agreement with the experimental values in general. Therefore, the methodology followed in ANSYS Fluent can be taken as a base for further investigations both for single and counter-rotating propeller designs.

3.2 Verification of OpenProp

In Chapter 2, performance estimation of the designed propeller based on the inputs of DTMB4119 propeller is made by OpenProp at the design advance coefficient of 0.833 and also at other off-design coefficients. It is possible to compare performance results of both OpenProp and CFD to verify the design procedure of OpenProp.
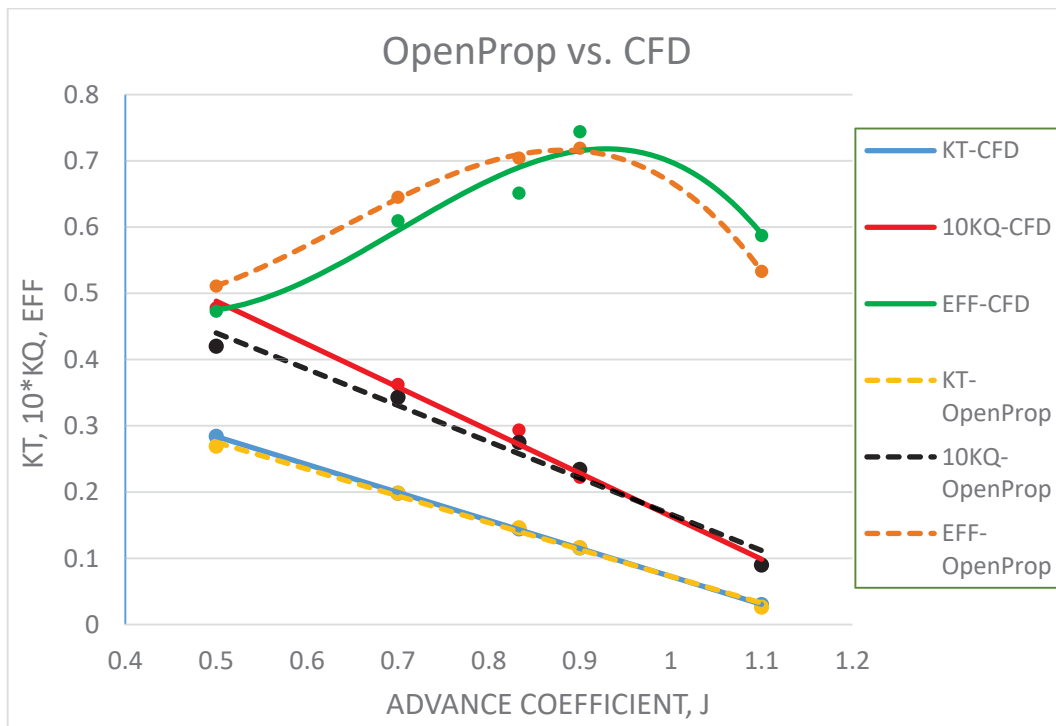
Figure 3.10. Overall Results Showing CFD vs. OpenProp for DTMB4119 Propeller

As it is seen in Figure 3.10, the results for thrust coefficients are nearly the same. OpenProp underestimates the torque coefficient as already stated in Figure 2.10 where the results of OpenProp and experiment are compared. This directly influences the results for the efficiency, but the trends for both CFD and OpenProp are very similar to each other. Also, the graph showing the results for the experiment, OpenProp and numerical analyses is presented in Figure 3.11.
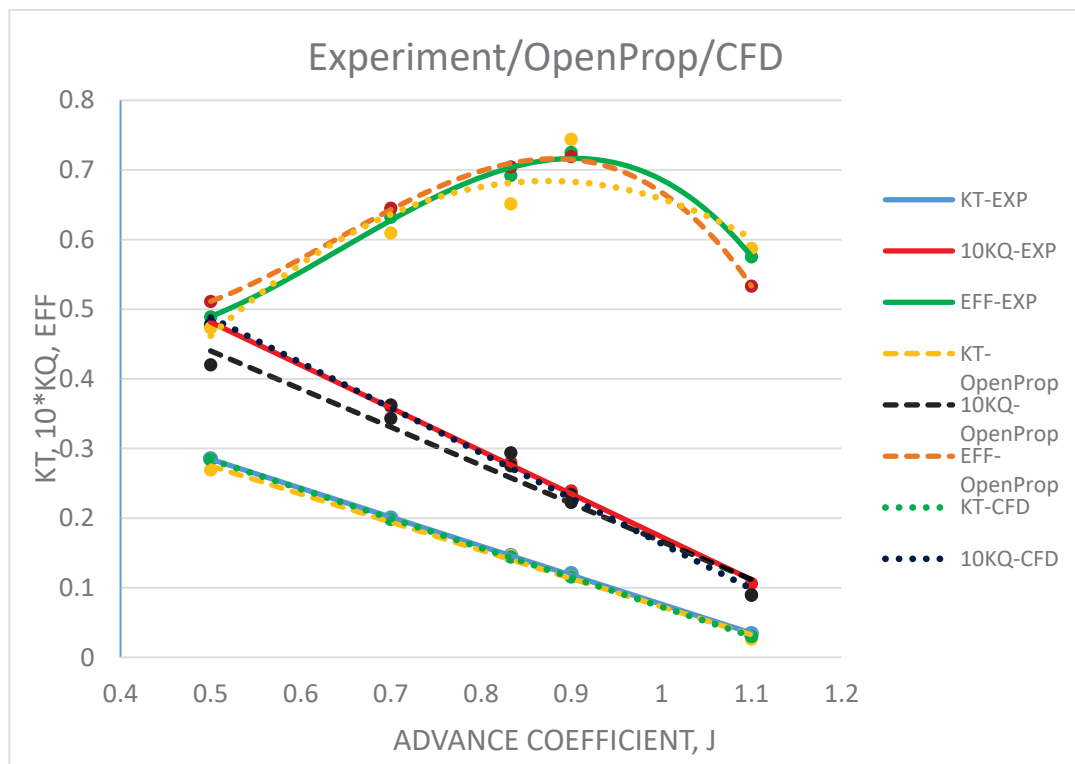
Figure 3.11. Comparison of Results for the Experiment, OpenProp and CFD

The thrust coefficients are almost identical for each method at five advance coefficients. OpenProp underestimates the torque coefficient slightly lower than the results of the experiment and numerical analyses. For this reason, the trend for the efficiency of OpenProp shows smaller results than the others around the design advance coefficient; however, the results are very close to each other in general. Therefore, it is quite possible to conclude that the design procedure of OpenProp is verified. This tool can be used as a geometric design tool in the upcoming chapters.

3.3   Performance Analysis of the Narrower Bladed Propeller

In Chapter 2, it is stated that OpenProp does not evaluate the thrust output of the designed propeller. It shows the input of required thrust as if the designed propeller can create that thrust. To see that, a narrower bladed propeller is designed by OpenProp which has exactly two times smaller chord distribution than the chord distribution of DTMB4119 propeller with the same performance requirements of ship speed and required thrust. OpenProp has reported the input thrust as an output. Now, it is possible to see the actual thrust that the narrower bladed propeller can supply. For this purpose, the 3D geometry is extracted from OpenProp and it is imported into Fluent. The same steps in Section 3.1 is followed to create the solution domain and the mesh. The results are obtained as presented in the Table 3.4.

Table 3.4. Comparison of Results for the Narrower Bladed Propeller

Narrower Bladed Prop.	OpenProp	CFD	True Error (%)
Advance Coefficient (J)	0.833	0.833	-
Thrust Coefficient (K_T)	0.146	0.102	43.1
Torque Coefficient (K_Q)	0.0257	0.0190	35.3

According to the result obtained with numerical analysis, two times narrower bladed propeller has a thrust coefficient of 0.102 which corresponds to a 90.2 N thrust at advance coefficient of 0.833. This results in an error of 43.1%. The situation is similar for the torque coefficient, the error is 35.3% based on the results of OpenProp.

This was not an issue in case of DTMB4119 propeller since the blade geometry with the experimental results were known. For DTMB4119 case, OpenProp manages to come up with a design and estimates the performance very close the experimental ones. This case is shown to verify the design procedure of OpenProp. If the inputs of OpenProp are chosen correctly, then it works in a correct way both in design and

performance estimation. However, in further chapters, the only inputs are going to be speed and required thrust where the main objective is to reach the final blade geometry by an iterative approach that can supply the required thrust at the specified speed. If performance estimations of OpenProp are used, it is going to be reported that the required thrust is achieved for all different blade geometries and revolution speeds. Therefore, it is not possible to be sure about the performance estimation of OpenProp without knowing the actual result obtained by CFD.

To conclude, in the upcoming chapters, the verified design procedure of OpenProp is going to be followed for geometric design of propellers whereas performance evaluations of designed propellers are going to be conducted by CFD studies until the correct inputs required for OpenProp are identified by CFD.

CHAPTER 4

METHODOLOGY

DTMB4119 propeller creates 129.16 N thrust at a speed of 2.54 m/s at the design advance coefficient of 0.833. In a progress of propeller design, required thrust at a certain speed is a key parameter to start the design while geometry of the propeller is unknown. In this chapter; "Parametric Study" and "Single Design" modules of OpenProp and performance analyses by ANSYS Fluent are carried out to meet the performance requirements of the DTMB4119 propeller starting with an unknown geometry. In other words, alternative design of the DTMB4119 propeller is conducted.

4.1   Parametric Design

OpenProp has a module of "Parametric Study" in which required thrust, ship speed and hub diameter are given as inputs to the "Specifications" in the upper left corner. Parametric design is carried out on number of blades, rotation speed and rotor diameter in terms of efficiency. By this way; number of blades, general dimensioning and working conditions of the propeller can be analyzed parametrically as explained in Section 2.1.2.

The GUI menu of "Parametric Study" with the requirements of DTMB4119 propeller is presented in Figure 4.1. The range is defined in the bottom as 3 - 5 for number of blades, 400 – 1000 rpm with 100 rpm increments for rotation speed, 0.300m - 0.310 m for propeller diameter. The reason for selecting the range of propeller diameter small is that the maximum diameter for a propeller is restricted by the wake region created by the body that the propeller drives. Since unnecessarily

large propeller increases the exposed drag and decreases the efficiency, maximum propeller diameter is generally set to 85% of the wake diameter [39]. Since there is not any object forward to the propeller at this point, the region around the propeller diameter of 0.3048m is considered to narrow the design space.
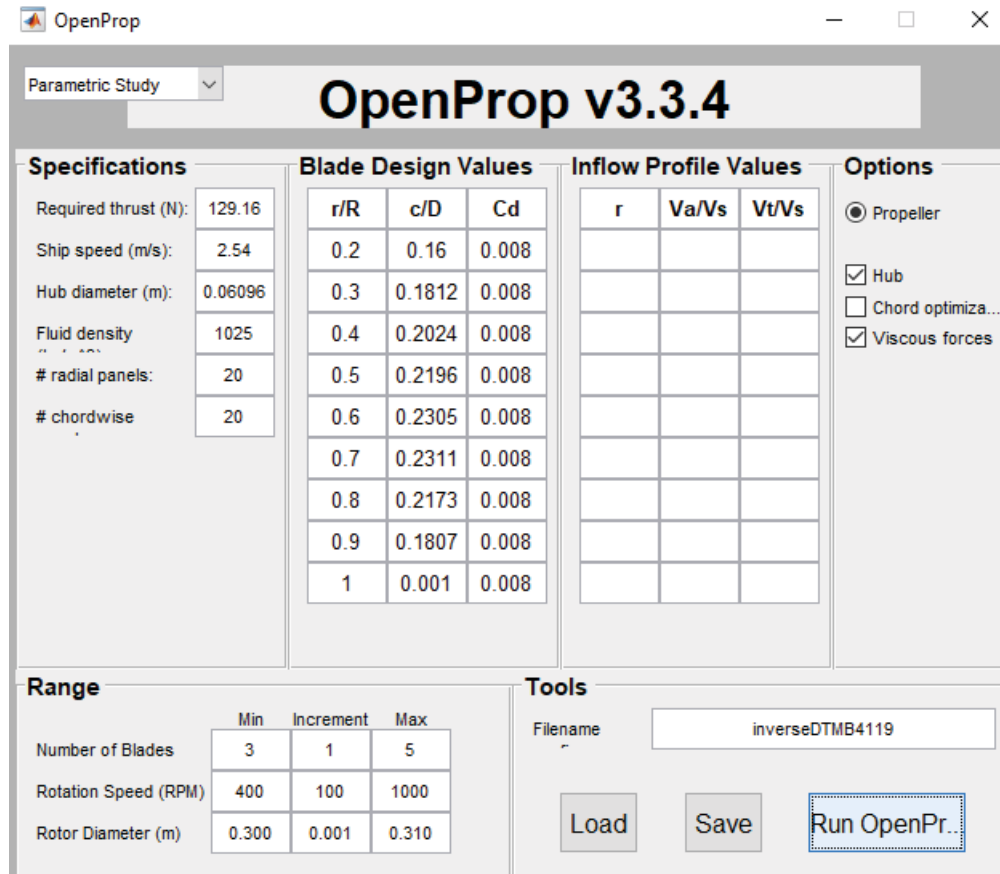
Figure 4.1. GUI Menu of "Parametric Study" for the Alternative Design

The results are given in Figure 4.2. OpenProp estimates the efficiency based on number of blades and propeller diameter for each specified rotation speed. From the results, first implication is that as the propeller diameter increases, since the range is kept small, the efficiencies stay almost the same. A closer look which is given in Figure 4.3 is needed to identify the best match of number blades and rotation speed in terms of efficiency.
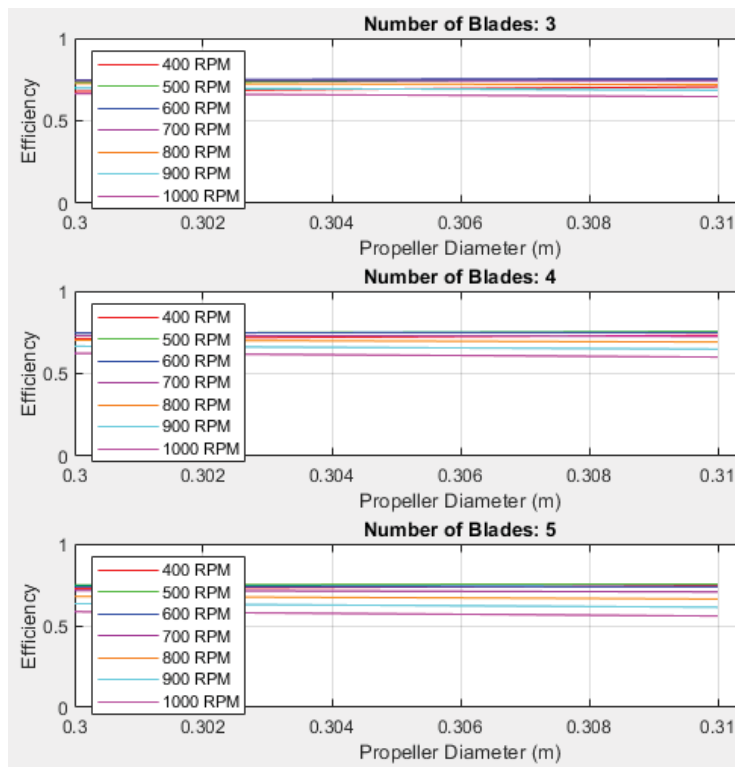
Figure 4.2. Results of "Parametric Study" for the Alternative Design
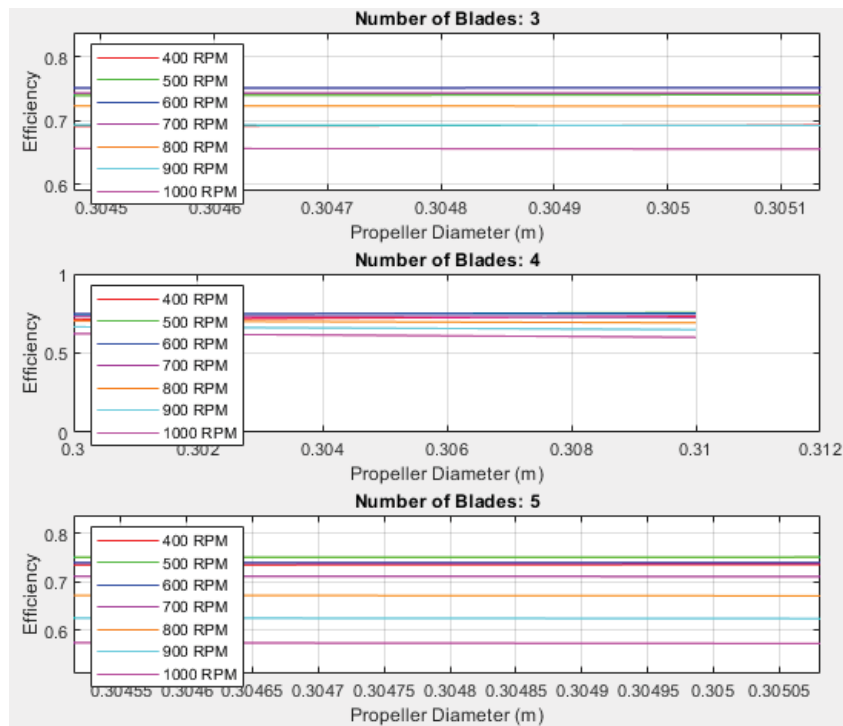
Figure 4.3. Results of "Parametric Study" around the Diameter of 304.8mm

Figure 4.3 shows that; the highest efficiencies are obtained around the rotation speeds of 600 rpm and 700 rpm for a 3-bladed propeller, however; the efficiencies for different number of blades and rotational speeds are very close each other. Since the original DTMB4119 propeller has 3 blades and the efficiencies between 3 and 5 blades do not differ significantly, 5 bladed propeller is selected for the upcoming sections to come up with a propeller different than the DTMB4119 propeller. The results of the "Parametric Study" based on the inputs specified in Figure 4.1 are presented in Table 4.1.

Table 4.1. Results of "Parametric Study" for the Alternative Design

	Number of Blades	Propeller Diameter (m)	Revolution Speed (rpm)
Parametric Study	5	0.3048	600-700

4.2 Single Design

At this point, the parameters appearing on the tab of "Specifications" such as number of blades, rotation speed, rotor diameter, required thrust, ship speed and hub diameter are all known. To narrow the design space more, meanline type of NACA a=0.8 and thickness type of NACA65010 is selected. The only and essential unknown is the "Blade Design Values".

For the inputs of chord and thickness distributions required in "Blade Design Values", tabulated data of B-series propellers is used. According to the tabulated data presented in Table 1.1, chord distribution is dependent on number of blades, Z, and expanded area ratio, abbreviated as EAR, whereas thickness distribution is only dependent on number of blades. Since it is decided to have five blades in the propeller based on the results of "Parametric Study", the thickness distribution is fixed along the propeller. Different chord distributions can be obtained by changing the expanded area ratio. Therefore, chord distribution is the iterative parameter in

this approach. Additionally, revolution speeds can vary in the determined range if the changes in *EAR* are not sufficient to reach the objectives. The methodology can be summarized as shown in Figure 4.4.
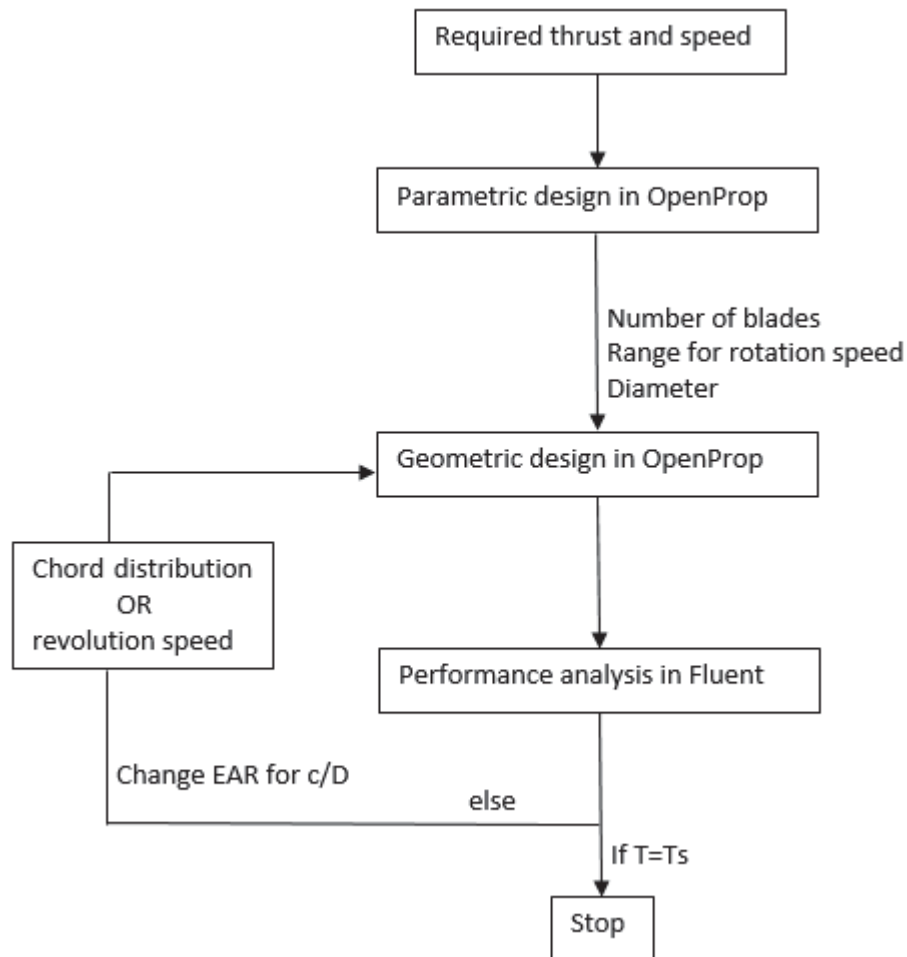
Figure 4.4. Flow Chard of the Methodology

To be able to reach 129.16 N of thrust at 2.54 m/s, the bottom loop in Figure 4.4 is cycled for different chord distributions depending on *EAR* and range for the revolution speed. The iterations are reported in Table 4.2. In each iteration, OpenProp is used as the geometric design tool whereas performance analyses are conducted in Fluent. The methodology developed for solution domain, mesh and solution settings in Section 3.1 is repeated for each design. If the obtained thrust in the end of a numerical analysis has a large error with the objective thrust, "*else*" path

shown in Figure 4.4 is followed to change the chord distribution or revolution speed. To start the iterations, propellers with low and high *EAR* are selected first to detect the region where the objective thrust is present.

Table 4.2. Iterations for the Alternative Design of the DTMB4119 Propeller

Iteration Number	Expanded Area Ratio (*EAR*)	Revolution Speed (rpm)	Resultant Thrust (N)	Resultant Torque (N.m)	Eff.
1	0.4	600	91.66	5.47	0.68
2	0.9	600	96.12	6.04	0.64
3	0.6	600	92.45	5.58	0.67
4	0.4	700	187.47	9.89	0.66
5	0.9	700	200.53	10.96	0.63
6	0.6	700	193.13	10.38	0.64
7	0.5	700	194.08	10.30	0.65
8	0.4	650	137.44	7.61	0.67
9	**0.4**	**640**	**128.34**	**7.11**	**0.68**

The objective is reached at the 9th iteration where the expanded area ratio is 0.4. The propeller supplies a net thrust of 128.34 N with a torque output of 7.11 N.m where the objective thrust is 129.16 N. Efficiency is calculated to be 0.68.

There can be made some important observations in Table 4.2. First of all, increasing *EAR* of the propeller at the constant revolution speed may not be direct sign of the net increased thrust. More blade area causes more pressure drag on the blade. Additionally, since the blades are closer to each other for increased *EAR*, the flow speed is increased due flow contraction which causes more viscous drag. The increased thrust is used to cancel out these drags and the net thrust stays almost the same in iteration numbers 1, 2 and 3. Therefore, revolution speed is increased in the determined range after the 3rd iteration and *EAR* of 0.5 added to iterations. In the iterations of 4, 5, 6 and 7; all propellers are able to supply the required thrust. However, as the *EAR* increases the torque output of a propeller increases. Since the

rate of change of torque is greater than the net thrust, the efficiencies decrease with increasing *EAR*. For this reason, *EAR* of 0.4 is chosen in iteration numbers of 8 and 9.

The GUI menu of "Single Design" for the 9th iteration is given in Figure 4.5. 3D model of the propeller and the created mesh based on the settings studied in Section 3.1 are also presented. Since the propeller has 5 blades, periodicity of 72° is used in numerical analysis. The created mesh has 2,156,721 cells.
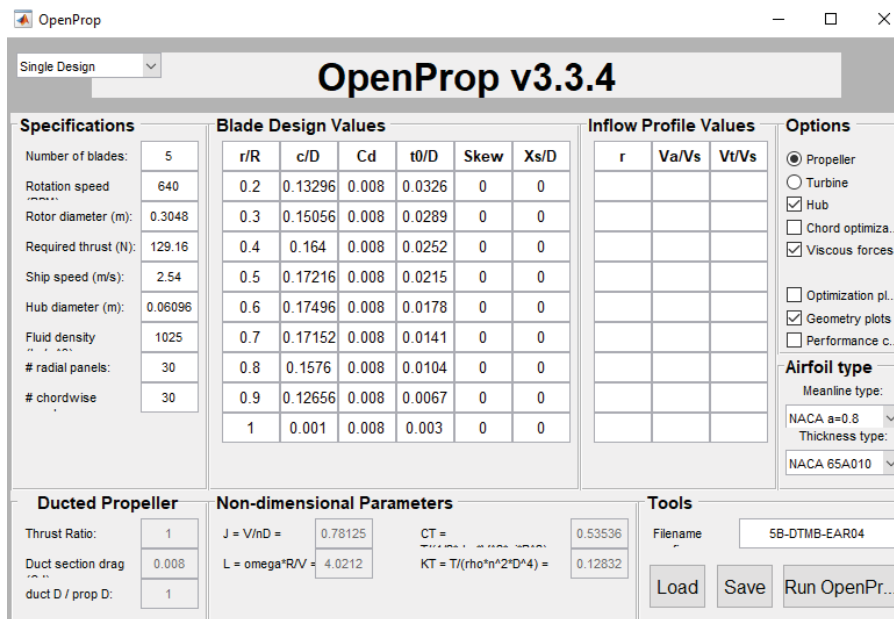
Figure 4.5. "Single Design" GUI of OpenProp with Alternative Design Inputs
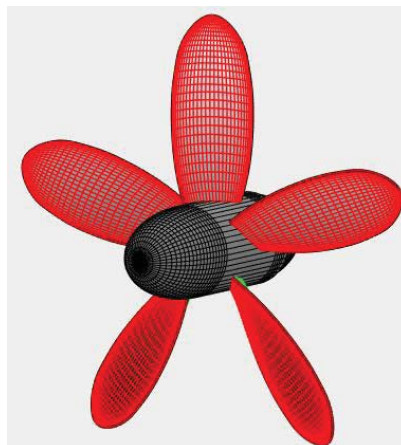
Figure 4.6. 3D Model View of Alternative Design in OpenProp

53
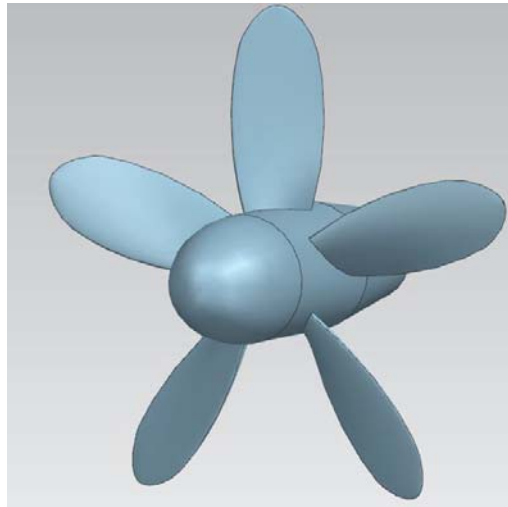
Figure 4.7. 3D Model of the Alternative Design
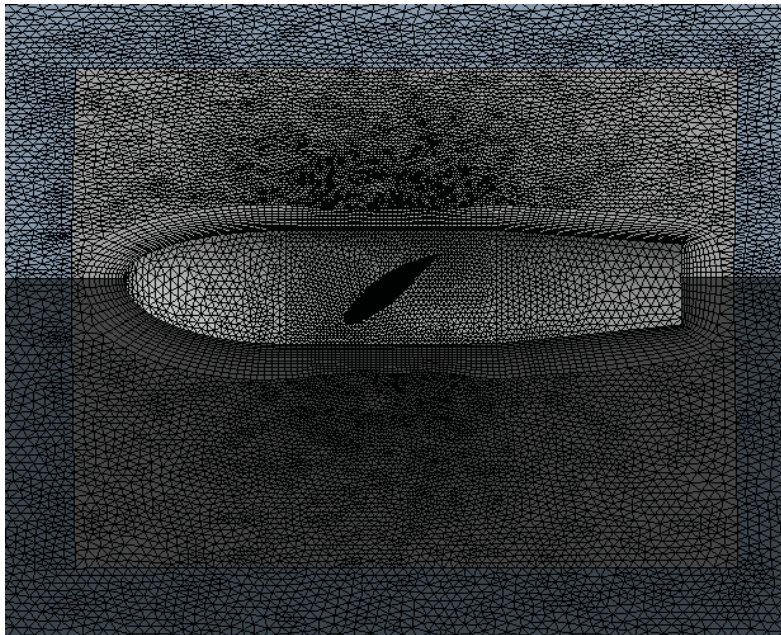
Figure 4.8. Created Mesh for the Alternative Design

In the end of Chapter 3, it is stated that OpenProp shows the input of required thrust as an output. Therefore, it is not advisable to rely on the performance estimations of OpenProp if the correct inputs are not known. Now, based on the performance results of the propeller obtained in the 9th iteration, correct inputs are identified. Therefore, results of OpenProp and numerical analysis can be compared as shown in Table 4.3.

Table 4.3. Comparison of Results for the Alternative Design

Alternative Design	CFD	OpenProp	True Error (%)
Advance Coefficient (J)	0.781	0.781	-
Thrust Coefficient (K_T)	0.1307	0.1315	0.61
10*Torque Coefficient ($10 * K_Q$)	0.2375	0.2295	3.4
Efficiency	0.684	0.713	4.2

Since the correct inputs for the blade design values and revolution speed are identified, the errors for thrust coefficient, torque coefficient and efficiency between the results of numerical analysis and OpenProp are very small in Table 4.3. The errors for thrust and torque coefficients are 0.61% and 3.4%, respectively. They both result in the 4.2% error for the efficiency.

To conclude, starting with requirements of thrust and speed at the design advance coefficient of DTMB4119 propeller, the developed iterative methodology shown in Figure 4.4 is used to design a propeller that supplies the required thrust at a specified speed. Therefore, developed methodology is verified and can be used in upcoming chapters where the forward and aft propellers are designed for a counter-rotating propeller configuration.

CHAPTER 5

DESIGN AND PERFORMANCE ANALYSIS OF A CRP

In this chapter, design and performance analyses of a CRP are carried out. The chapter starts with the selection and viscous flow analysis of a submerged body. After that, performance requirements are determined which starts the section of "Parametric Study" and "Single Design" for both forward and aft propellers. Both propellers are designed based on the methodology developed in Chapter 4. During the design of the aft propeller, the wake region left from the forward propeller is used both in geometric design in OpenProp and performance analyses in Fluent. Finally, designed propellers are located on the submerged body and performance analyses of the whole model is carried out.

5.1   Submerged Body

After setting the design and analysis methodology for a propeller, design of a counter-rotating propeller can be carried out. As explained before, velocity and required thrust are the needed parameters for initiation of a design process. For this reason, a torpedo or a submarine shall be modelled and studied numerically to determine the exposed drag. Since there are experimental results [40] and lots of numerical investigations [41], [42], [43]; bare hull form of the Defense Advanced Research Projects Agency Suboff, abbreviated as DARPA Suboff, is selected as the submerged body. In the content of DARPA Suboff Project, an axisymmetric body, fairwater and several appendages are manufactured and tested at a tow tank for future advanced submarine designs [44]. The geometry is described by equations in [44] whereas the experimental procedure and results are presented in [40]. The bare hull

geometry is tested at 6 model speeds and resistance values are recorded shown in Table 5.2.
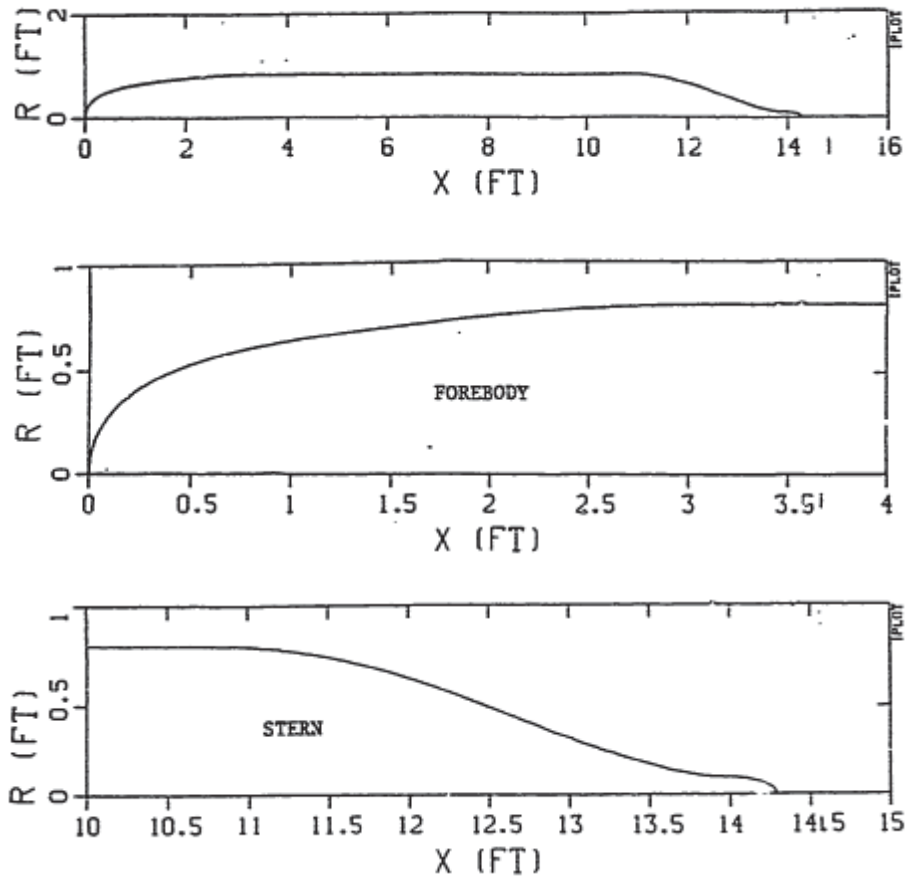
Figure 5.1. Bare Hull Profile of DARPA Suboff [44]

Table 5.1. Main Dimensions of Bare Hull DARPA Suboff

Description	Symbol	Magnitude (mm)
Forebody Length	-	1016
Parallel Middle Body Length	-	2229
Stern Length	-	1111
Overall Length	L	4356
Maximum Hull Diameter	-	508

Table 5.2. Bare Hull Tow Tank Results of DARPA Suboff [40]

Model Configuration	Model Speed (knots)	Model Speed (m/s)	Model Resistance (N)
Bare Hull	5.92	3.05	87.40
	10.00	5.14	242.2
	11.84	6.09	332.9
	13.92	7.16	451.5
	16.00	8.23	576.9
	17.99	9.25	697.0

The body is exposed to 697 N of drag force at 17.99 knots which corresponds to an advance speed of 9.25 m/s. Since the most compelling situation for a counter-rotating propeller occurs at the highest speed, these results are taken as the initial requirements for a counter-rotating propeller. Therefore, a numerical analysis is carried out based on the speed of 9.25 m/s to determine the resultant drag and compare with the experimental result at a depth of 250 m.

Based on the defined equations in [44], the geometry is modelled 3D in Siemens NX as presented in Figure 5.2. Flow domain is set as given in Figure 5.3 to eliminate boundary effects where L stands for the overall length of the Suboff. Half of the model is used in numerical analyses to decrease computational time. Inlet boundary condition is set to 9.25 m/s uniform inlet velocity. Outlet is specified as 0-gauge pressure outlet. Top, bottom and side walls are set to "Wall" type boundary condition where no-slip is applied. Finally, symmetry type boundary condition is specified on the half plane.
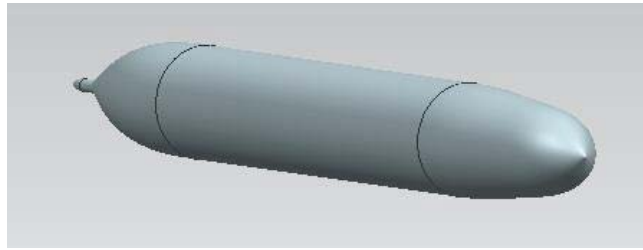
Figure 5.2. Bare Hull Model of DARPA Suboff
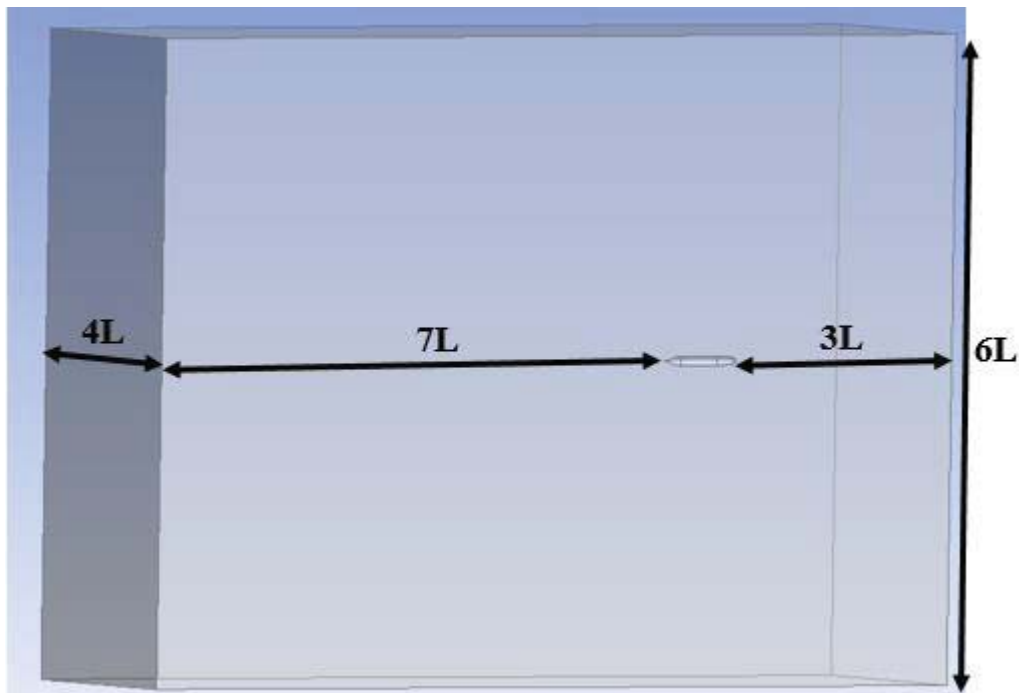
Figure 5.3. Solution Domain for DARPA Suboff

Since bare hull is a streamlined geometry, the drag force created by the flow is expected to be viscous-dominant. Therefore, boundary layer resolution shall be fine enough to capture the viscous effects properly. Also, mesh independence study shall be carried out to ensure that the resultant drag is free from the used mesh. Three meshes are constructed, namely coarse, medium and fine, as shown in Table 5.3 along with the corresponding drag forces and true errors. In the solver settings, steady-state analysis is carried out. Realizable k-ϵ model with standard wall functions is used for turbulence modelling and it is kept the same for all meshes. From coarse

to fine meshes, number of layers in the boundary layer is increased and also sizing for faces and edges are refined whereas the y^+ value is kept constant.

Table 5.3. Mesh Independence Study of Bare Hull DARPA Suboff

MESH	Cell Count	Drag Force (N)	True Drag (N)	True Error (%)
Coarse	2,318,141	629.04		9.75
Medium	3,687,897	664.85	697	4.61
Fine	4,989,116	665.49		4.52

As it is presented in Table 5.3, the drag forces obtained with medium and fine meshes do not differ significantly. In fact, they are very close to each other. This means that the solution is obtained independently from the used mesh. Therefore, medium mesh is selected for foregoing analyses. It has 3,687,897 cells. The mesh is presented in Figure 5.5. Variation of y^+ along the bare hull is also presented in Figure 5.4. Area weighted average of y^+ is 135.7. The choice of realizable k-ϵ model with standard wall functions for turbulence modelling seems suitable because it is recommended for applications where y^+ value is between 30 and 300 [38].
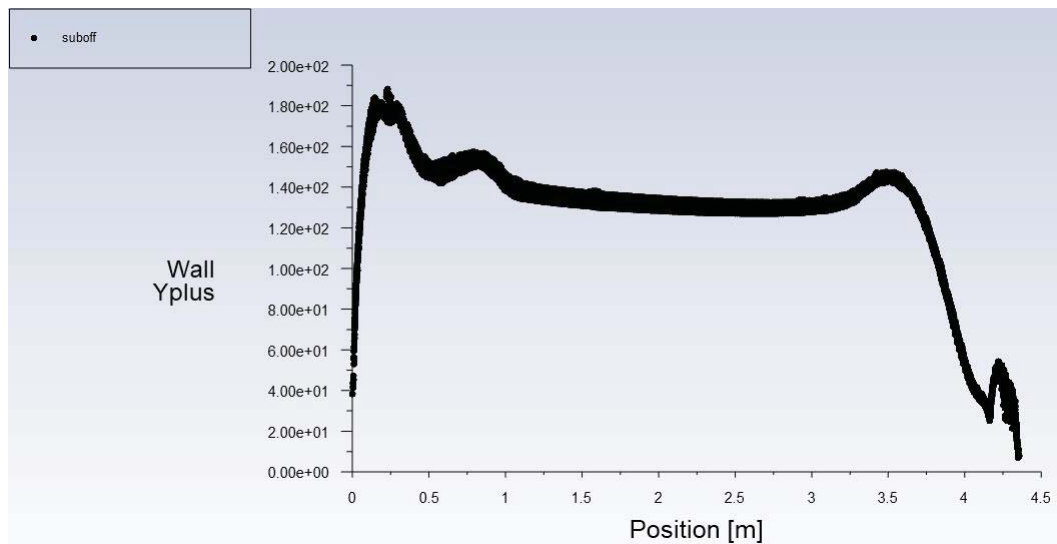
Figure 5.4. Variation of y^+ Values along the Bare Hull DARPA Suboff
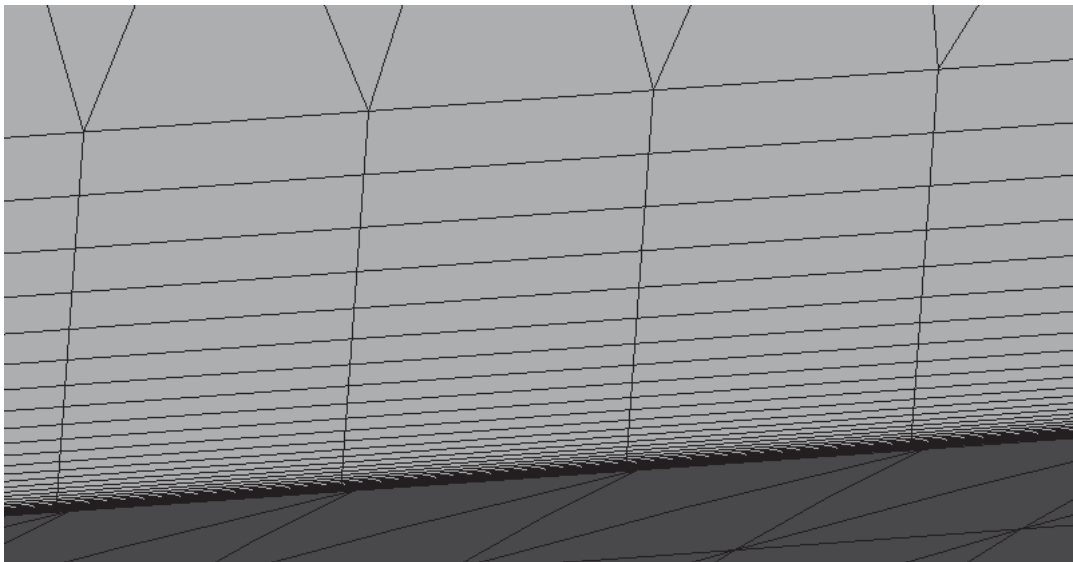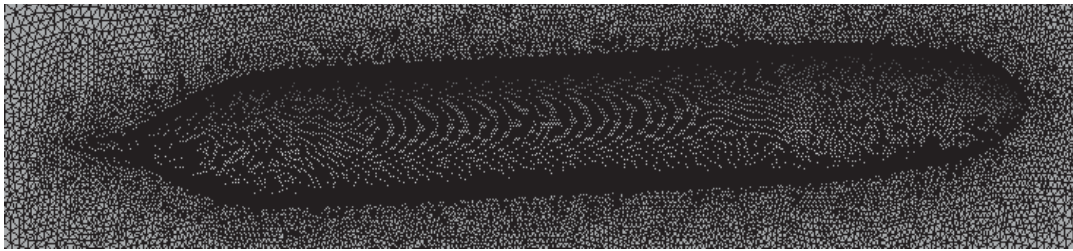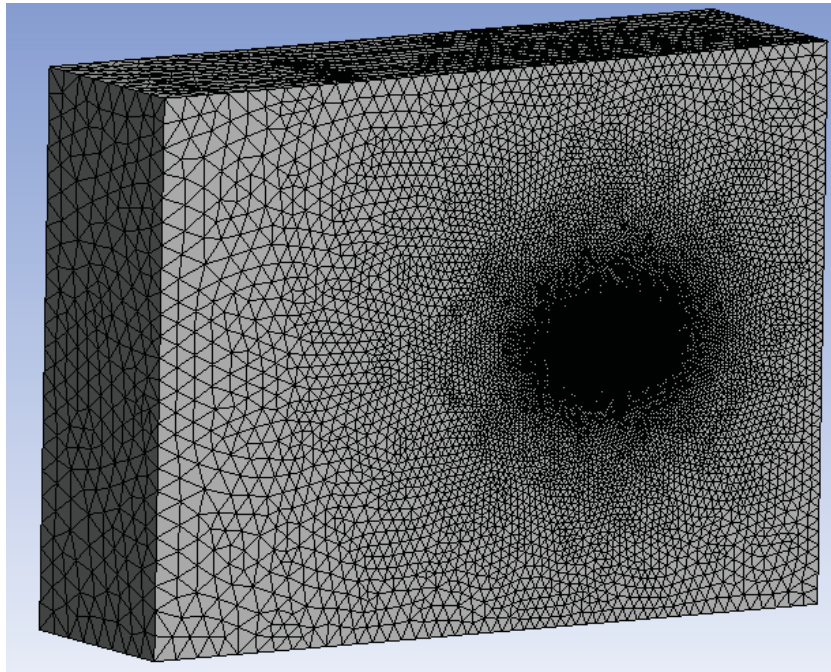
Figure 5.5. Mesh for the Bare Hull DARPA Suboff

Residual plot of the numerical analysis is presented in Figure 5.6. Also, the drag force created on the Suboff body is recorded throughout the solution. As it is seen in Figure 5.7, the convergence is established.
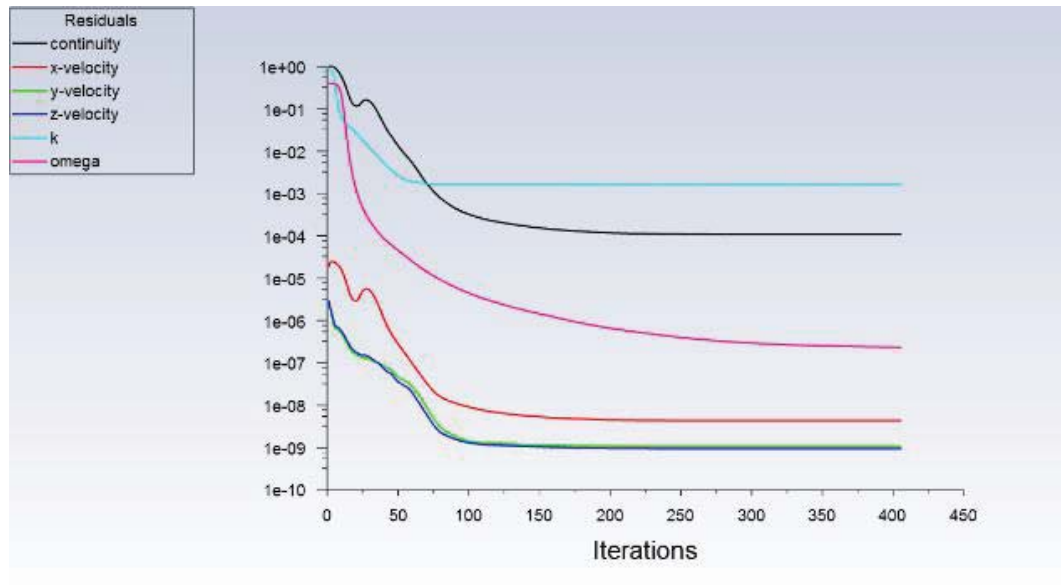
Figure 5.6. Residual Plot of the Numerical Analysis for Bare Hull DARPA Suboff
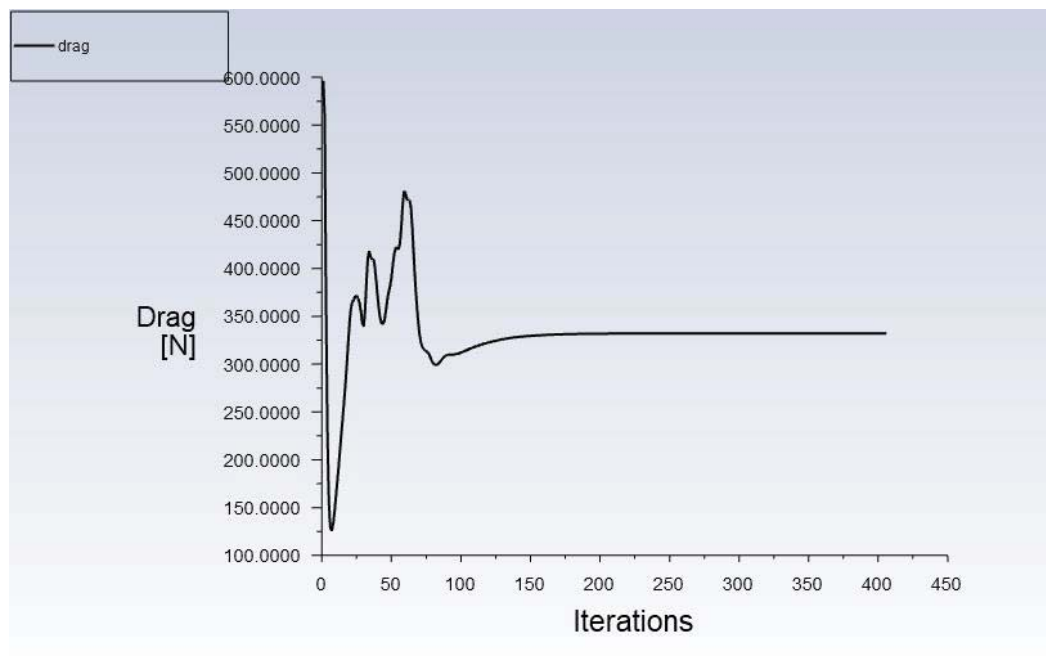
Figure 5.7. Plot of the Drag Force on the Bare Hull DARPA Suboff at 9.25 m/s

Velocity and pressure contours are presented in Figure 5.8 and 5.9.
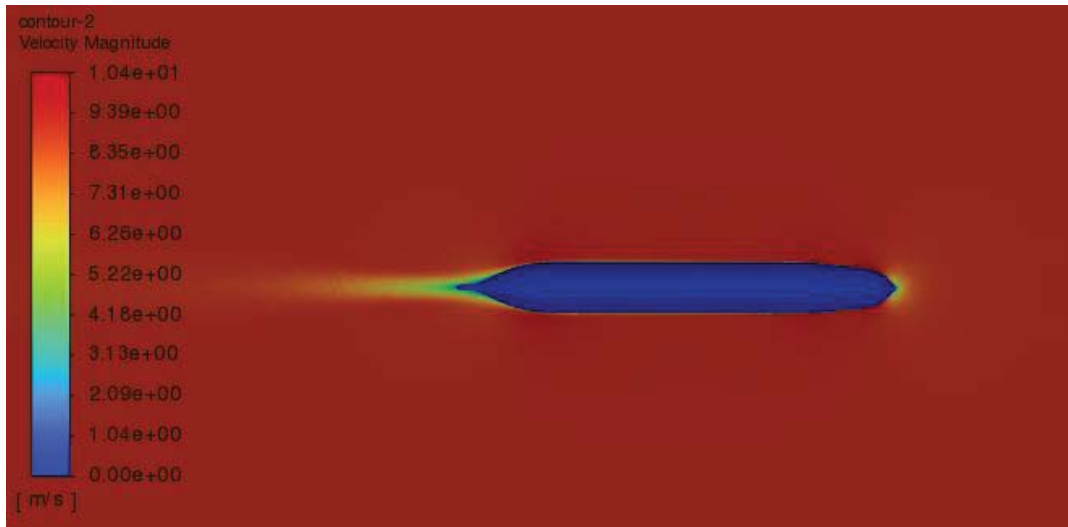
Figure 5.8. Velocity Contour of the Bare Hull DARPA Suboff at 9.25 m/s
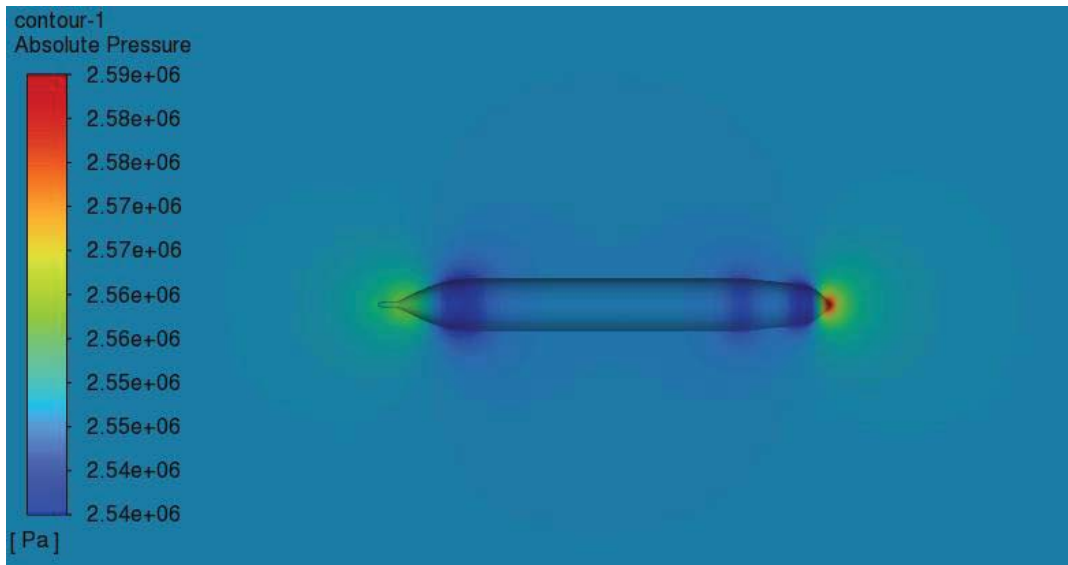
Figure 5.9. Absolute Pressure Contour of the Bare Hull DARPA Suboff at 9.25 m/s

As it is seen in the contours, the flow comes to stop at the nose of the body where the absolute pressure is maximum. This is called the stagnation point in the flow where the flow comes to stop. After this point, water near to the submerged body starts to flow in the boundary layer. The flow gets accelerated after the nose in the curvature of the body. The flow reaches its maximum speed again around middle

section of the body where the pressure is slightly lower than the end sections. Its speed starts to decrease through the stern of the body as the adverse pressure gradient is present. After this region, due to stream-wise contraction, the flow starts to accelerate and pressure decreases accordingly.

5.2   Thrust Distribution

As it is found in the previous section, the bare hull of DARPA Suboff is exposed to a drag force of 664.85 N without a CRP while advancing with a speed of 9.25 m/s. There is an additional drag force exposed on forward and aft propellers which shall be considered. For this purpose, 20% of the initial drag value is added for a CRP set. Then, thrust requirement of a vehicle becomes 800 N. This is the required thrust which shall be supplied by a CRP. Different than a propulsion system with a single screw, thrust distribution is needed between forward and aft propellers in a CRP set [45]. Since the forward propeller is going to have a greater diameter, it is expected to supply a larger thrust than the aft one. However, in a CRP configuration, one of the primary concerns is counteracting the torque created by the forward propeller via the opposite rotation of the aft one. If most of the thrust load is supplied by the forward propeller, effect of torque-cancellation may be small. Therefore, thrust distribution shown in Table 5.4 is selected for further investigations.

Table 5.4. Thrust Distributions of Forward and Aft Propellers

Thrust Distribution	Thrust Load (%)	Required Thrust (N)
Forward Propeller	55	440
Aft Propeller	45	360

5.3   Hub and Propeller Diameters

Maximum hull diameter of the body is 508 mm previously shown in Table 5.1. As explained in the Section 4.1, maximum diameter restriction of the propellers is 85%

of the maximum hull diameter which turns out to be 430 mm. For preliminary design purposes, diameters are set to 390 mm and 300 mm for forward and aft propellers, respectively. In addition to that, hub diameters are 110 mm and 59.6 mm for forward and aft propellers. A length of 250 mm is considered to locate the propellers in longitudinal direction. Diameters for forward and aft propellers are shown in Figure 5.10 along with the reserved length in the stern of the body.
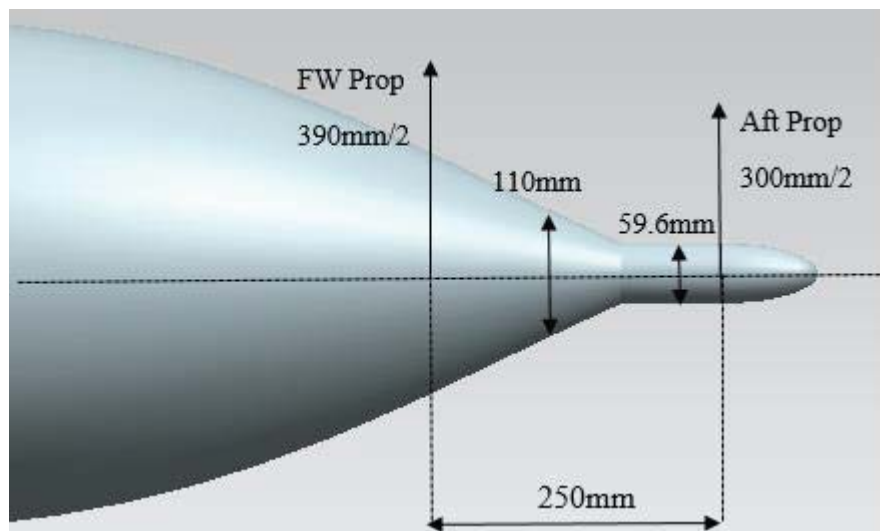
Figure 5.10. Longitudinal and Radial Dimensions for Forward and Aft Propellers

5.4 Forward Propeller

After deciding on the dimensions of the propellers, number of blades and rotation speed of the forward propeller shall be determined to continue through the phase of "Single Design" in OpenProp and performance analyses. For this purpose, "Parametric Study" module of OpenProp is used to determine the number of blades and the range for rotation speed. After that, design procedure shown in Figure 4.4 is applied to obtain the forward propeller by an iterative approach to reach the objective thrust at the specified advance speed of 9.25 m/s.

5.4.1   Parametric Study for Forward Propeller

Figure 5.11 shows the input GUI menu of "Parametric Study" in OpenProp for the forward propeller operating at 55% load. Load requirement corresponds to a thrust of 440 N as shown in Table 5.4. Ship speed is taken as 9.25 m/s whereas hub diameter is set to 110 mm. The range is 3-6 for number of blades and 1000 - 2000 rpm for rotation speed with 200 rpm increments. Propeller diameter is taken between 380 mm - 400 mm with 10 mm increments.

OpenProp v3.3.4 (Parametric Study)

Specifications

Required thrust (N):	440
Ship speed (m/s):	9.25
Hub diameter (m):	0.110
Fluid density	1000
# radial panels:	20
# chordwise	20

Blade Design Values

r/R	c/D	Cd
0.2	0.1662	0.008
0.3	0.1882	0.008
0.4	0.205	0.008
0.5	0.2152	0.008
0.6	0.2187	0.008
0.7	0.2144	0.008
0.8	0.197	0.008
0.9	0.1582	0.008
1	0.001	0.008

Inflow Profile Values

r	Va/Vs	Vt/Vs

Options
- ◉ Propeller
- ☑ Hub
- ☐ Chord optimiza...
- ☑ Viscous forces

Range

	Min	Increment	Max
Number of Blades	3	1	6
Rotation Speed (RPM)	1000	200	2000
Rotor Diameter (m)	0.38	0.01	0.40

Tools

Filename: ForwardProp

Load   Save   Run OpenPr...

Figure 5.11. Input GUI Menu of Parametric Study for the Forward Propeller
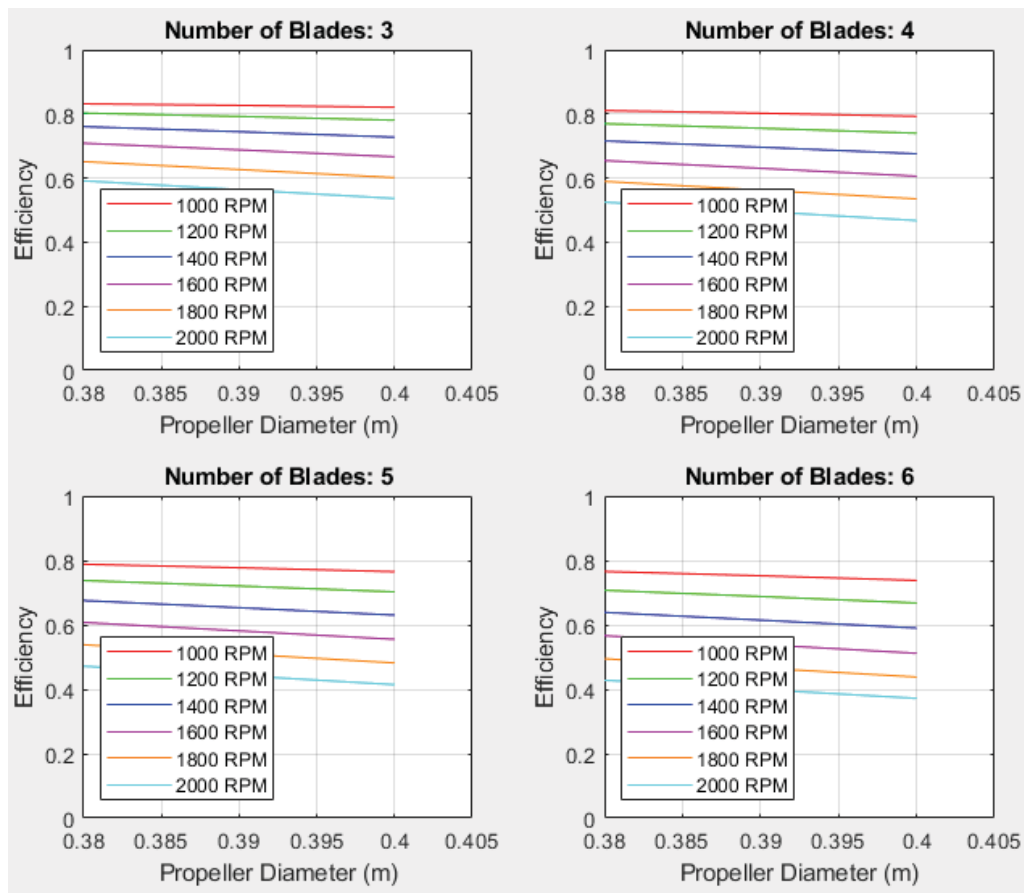
Figure 5.12. Results of "Parametric Study" for the Forward Propeller

Following conclusions can be drawn from the results of "Parametric Study" for the forward propeller:

- The efficiencies decrease slightly as the diameters increase. The efficiency for a diameter of 390 mm do not differ significantly in the investigated range. Therefore, propeller diameter of 390 mm can be used in further stages.

- The efficiencies are higher for blade numbers of 3, 4 and 5 when compared with the 6 blades for all revolution speeds. Since the forward propeller is required to supply more thrust than the aft one, selection of 5 blades for the forward propeller is reasonable.

- Increasing the revolution speed has a direct effect on decreasing the efficiency as indicated by the Equation (2.11). Also, it has an effect on increasing the torque which does the same decreasing effect on efficiency. The required revolution speeds are going to be determined in performance analysis stages; however, lower revolution speeds seem to supply the required thrust with a good efficiency. Therefore, it is reasonable to start performance analyses by setting revolution speeds between 1000 - 1200 rpm.

5.4.2   Design and Performance Analysis of Forward Propeller

Based on the methodology developed in Section 4.2, design and performance analysis of the forward propeller can be carried out. All parameters required in "Single Design" menu of OpenProp is known based on the dimensioning of the forward propeller in Section 5.3 and results of "Parametric Study" except the "Blade Design Values" which consists of the inputs for chord and thickness distribution.

For the inputs of chord and thickness distributions, tabulated data of B-series propellers is used as in Section 4.2. Since the thickness distribution is only dependent on the number of blades and forward propeller has five blades, it is also known. Different chord distributions can be obtained by changing the expanded area ratio.

The iterative methodology developed in Section 4.2 is repeated for different chord distributions and revolution speeds in the determined range as shown in Table 5.5. The revolution speed is set to 1200 rpm in the 1st iteration. For each iteration, geometric design is carried out in OpenProp based on the determined chord distribution and revolution speed. After that the coordinates for points in each hydrofoil is exported to a file to obtain the 3D geometry in Siemens NX. Finally, performance evaluations are carried out in ANSYS Fluent.

Table 5.5. Iterations for the Forward Propeller

Iteration Number	Expanded Area Ratio (EAR)	Revolution Speed (rpm)	Resultant Thrust (N)	Resultant Torque (N.m)	Eff. (%)
1	0.3	1200	1141.58	111.07	0.757
2	0.9	1200	1402.93	141.74	0.729
3	0.3	1000	239.58	31.21	0.678
4	0.9	1000	206.71	30.83	0.592
5	0.5	1000	230.05	29.54	0.688
6	0.3	1100	665.77	69.89	0.765
7	0.9	1100	770.61	83.57	0.741
8	0.5	1100	707.18	74.39	0.763
9	0.7	1100	751.21	80.13	0.753
10	0.3	1050	445.72	50.27	0.746
11	0.9	1050	490.35	57.02	0.723
12	0.7	1050	478.63	54.31	0.741
13	0.55	1050	465.18	52.51	0.745
14	**0.5**	**1050**	**455.79**	**51.33**	**0.747**
15	**0.5**	**1045**	**431.32**	**49.08**	**0.743**

In the first two iterations, propellers with low and high *EAR* are tested at 1200 rpm. There is a significant increase in the thrust obtained with *EAR* of 0.9 when compared with the *EAR* of 0.3. But, the results for these propellers are above the objective thrust of 440 *N*. After that, since the range for rotational speed is chosen to be between 1000 and 1200 rpm, the rotational speed is decreased to 1000 rpm and *EAR* of 0.5 is added to the iterations. This time, the thrust levels are lower than the objective thrust. Also, increasing the *EAR* is not sufficient to increase the thrust. Then, rotational speed is increased to 1100 rpm and *EAR* of 0.7 is added to the iterations. Propellers with higher *EAR* have higher thrust outputs, but they are again more than the objective. Therefore, the rotational speed is decreased to 1050 rpm.

Total five propellers with different expanded area ratios are considered at 1050 rpm. The highest efficiency is obtained in the 14th iteration with the propeller which has an *EAR* of 0.5. The created thrust is very close to the objective thrust of 440 N. Another iteration consisting of design and performance analysis at 1045 rpm is carried out to determine the range where the objective thrust is present. According to the results in the 14th and 15th iterations, forward propeller with an *EAR* of 0.5 is able to supply 440 N of thrust between 1045 and 1050 rpm.

The GUI menu of "Single Design" for the 14th iteration is given in Figure 5.13. 3D models of the propeller are also presented.

OpenProp v3.3.4

Single Design

Specifications

Number of blades:	5
Rotation speed (RPM)	1050
Rotor diameter (m):	0.39
Required thrust (N):	440
Ship speed (m/s):	9.25
Hub diameter (m):	0.11
Fluid density	1000
# radial panels:	30
# chordwise	30

Blade Design Values

r/R	c/D	Cd	t0/D	Skew	Xs/D
0.2	0.1662	0.008	0.0326	0	0
0.3	0.1882	0.008	0.0289	0	0
0.4	0.205	0.008	0.0252	0	0
0.5	0.2152	0.008	0.0215	0	0
0.6	0.2187	0.008	0.0178	0	0
0.7	0.2144	0.008	0.0141	0	0
0.8	0.197	0.008	0.0104	0	0
0.9	0.1582	0.008	0.0067	0	0
1	0.001	0.008	0.003	0	0

Inflow Profile Values

r	Va/Vs	Vt/Vs

Options

- ◉ Propeller
- ○ Turbine
- ☑ Hub
- ☐ Chord optimiza...
- ☑ Viscous forces
- ☐ Optimization pl...
- ☑ Geometry plots
- ☑ Performance c...

Airfoil type

Meanline type:

NACA a=0.8

Thickness type:

NACA 65A010

Ducted Propeller

Thrust Ratio:	1
Duct section drag	0.008
duct D / prop D:	1

Non-dimensional Parameters

| J = V/nD = | 1.3553 |
| L = omega*R/V = | 2.318 |

CT = 0.086095

KT = T/(rho*n^2*D^4) = 0.062104

Tools

Filename: 5B-FW-440N-EAR05

Load Save Run OpenPr...

Figure 5.13. "Single Design" GUI of OpenProp with Forward Propeller Inputs

71
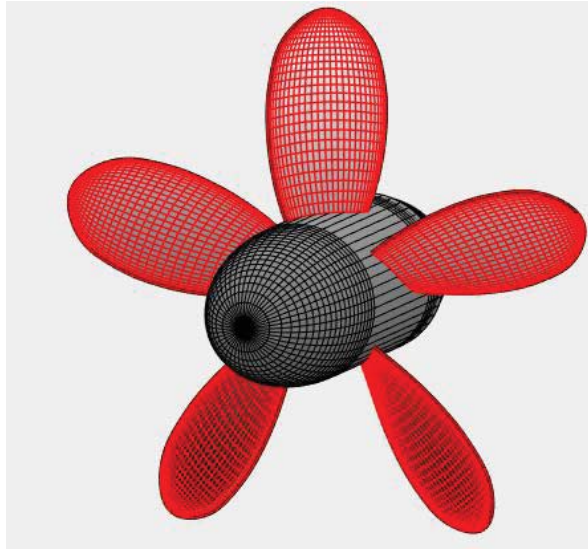
Figure 5.14. 3D Model View of the Forward Propeller in OpenProp
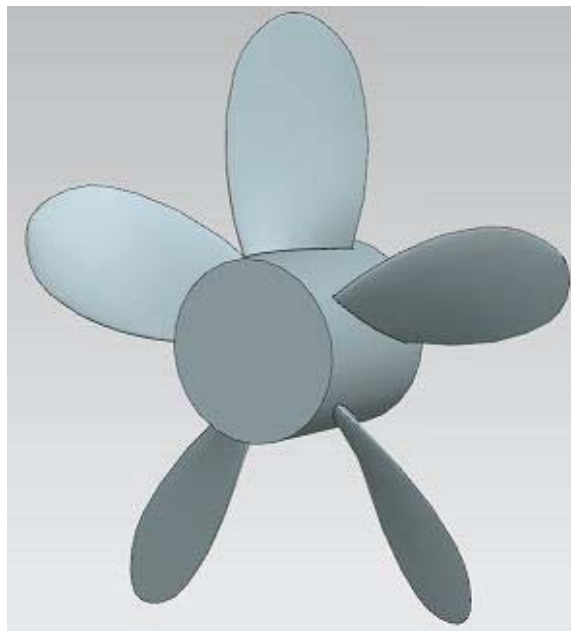
Figure 5.15. 3D Model of the Forward Propeller

Since the propeller has 5 blades, periodicity of 72° is used in solution domain. Upstream, downstream and side lengths of the solution domain used in Section 3.1 is re-arranged based on the radius of 195 mm. Mesh is also created based on the settings studied in Section 3.1. The created mesh has 2,467,266 cells. It is shown in Figure 5.17.
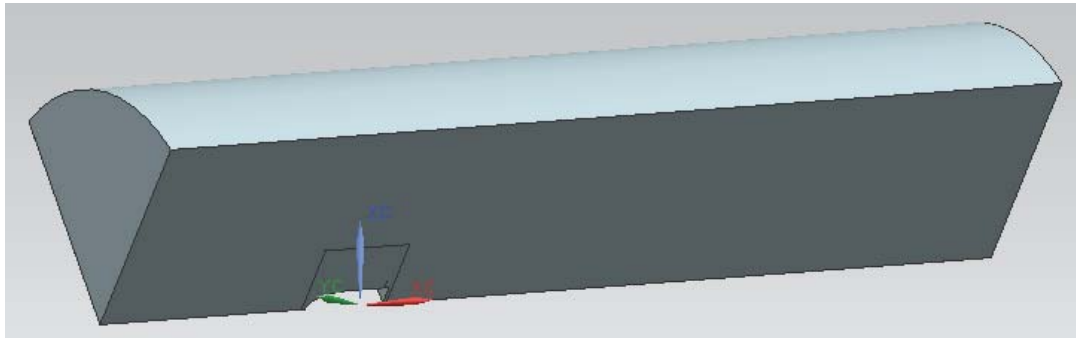
Figure 5.16. Solution Domain with 72° Periodicity for the Forward Propeller
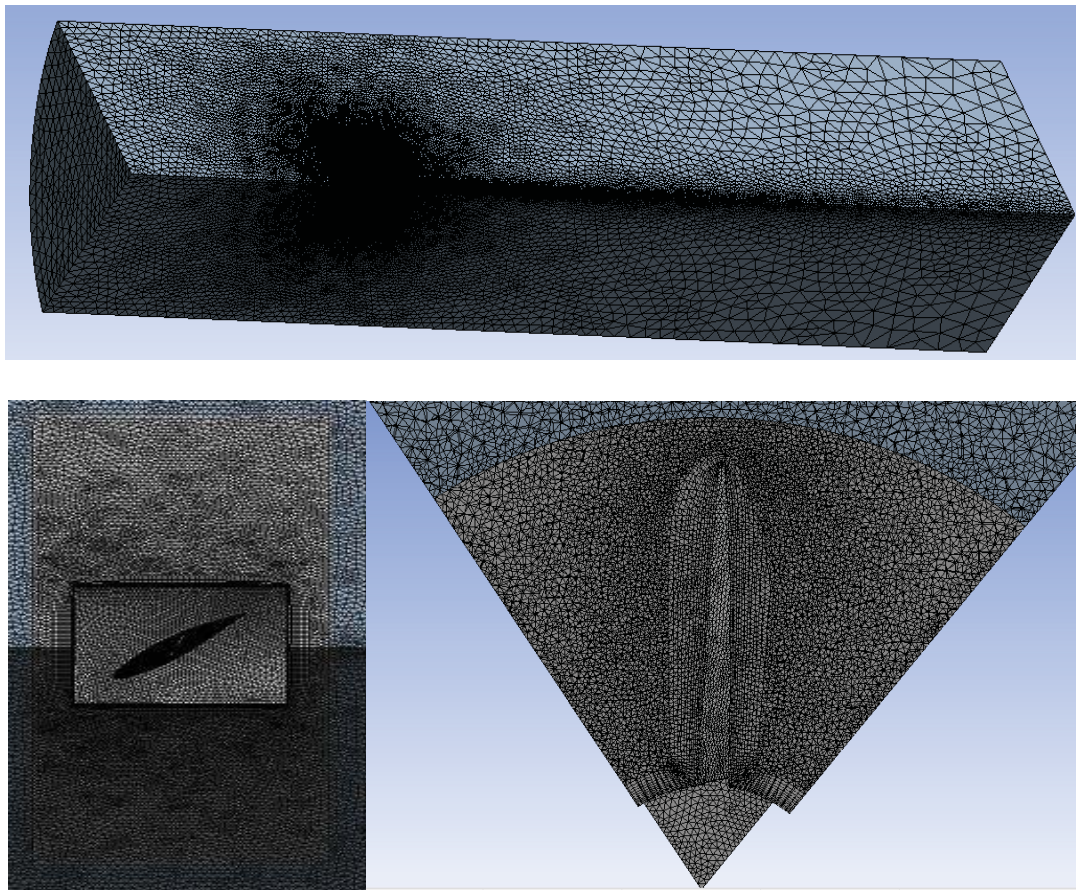
Figure 5.17. Mesh for the Forward Propeller

Boundary conditions and solution settings are kept the same as Section 3.1 except the inlet velocity. It is set to uniform inlet of 9.25 m/s. The solution is obtained in 331 iterations. Convergence is obtained when the residual for continuity equation has reached 1e-5. Additionally, the thrust force created by the propeller is drawn throughout the solution to check whether the solution is converged or not. As it is presented in Figure 5.19, convergence is established.
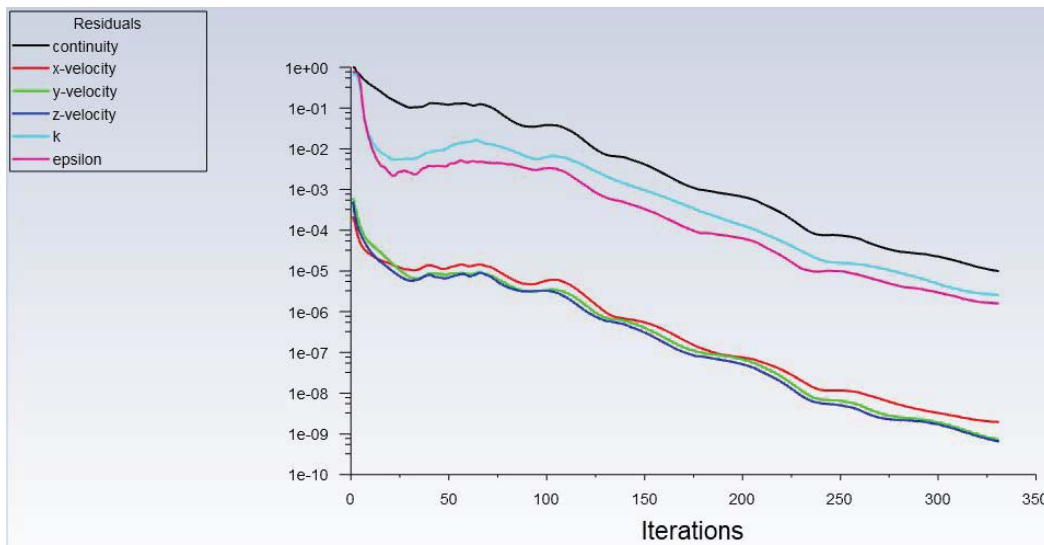
Figure 5.18. Residual Plot of the Numerical Analysis for the Forward Propeller
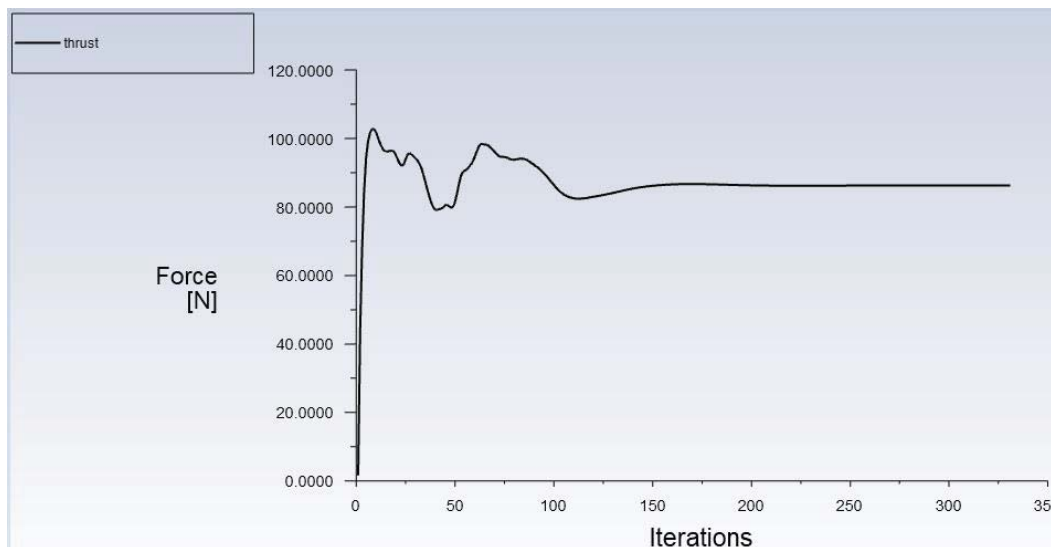
Figure 5.19. Convergence Plot of the Thrust Created by the Forward Propeller

74

Since the correct inputs for OpenProp are identified by CFD studies, it is possible to summarize the results of numerical analyses and OpenProp for the designed forward propeller as shown in Table 5.6.

Table 5.6. Comparison of Results for the Forward Propeller

Forward Prop	Numerical Analysis			OpenProp		
Revolution (rpm)	Thrust (N)	Torque (N.m)	Eff (%)	Thrust (N)	Torque (N.m)	Eff (%)
1050	455.79	51.33	0.747	440	49.51	0.744
1045	431.32	49.08	0.743	440	48.57	0.766

The results of OpenProp for 1045 rpm and 1050 rpm are very close to the results obtained in the numerical analyses. The true error rates for the torque values are 1.04% and 3.55% for 1045 rpm and 1050 rpm, respectively. The errors in torque directly influence the efficiency. Also, since OpenProp does not evaluate the thrust input, it shows the same input of 440 N in both results. This is also source of error for the efficiencies in the results of OpenProp.

To conclude, revolution speeds around 1045 rpm supply the required thrust of 440 N in open water conditions. Upstream pressure and velocity fields will be different for cases where the forward propeller is located in open-water conditions or behind Suboff. This change results in different thrust and torque outputs from the propeller which is investigated in the performance analyses of whole model including the DARPA Suboff and CRP in Section 5.6. However, open-water performance analysis of propellers separately is advantageous for further whole model investigations to determine the starting point for the revolution speed.

5.5   Aft Propeller

In this section, similar procedure followed in the case for the forward propeller is repeated except the "Inflow Profile Values". Aft propeller is located behind the forward propeller in a CRP configuration. Therefore, it operates in the wake region of the forward propeller. This shall be considered in the geometric design stage in OpenProp and, also in the performance analysis. For this reason, table of "Inflow Profile Values" appearing in "Parametric Study" and "Single Design" modules of OpenProp is used. Additionally, velocity profile obtained in the wake of the forward propeller is fed through the inlet of the aft propeller in performance analyses. Design procedure for the aft propeller can be summarized as shown in Figure 5.20.
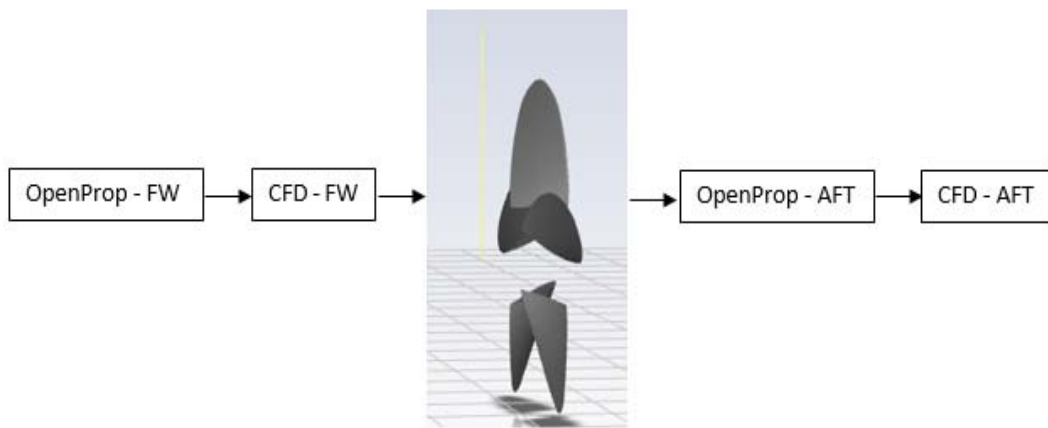
Figure 5.20. Design Methodology for the Aft Propeller

Table of "Inflow Profile Values" requires inputs for axial and tangential velocities scaled by the advance velocity in different radial dimensions. To obtain these velocities, 15th iteration in Table 5.5 is repeated for the full model. A line is drawn at the exit of the rotating domain for the forward propeller in the downstream side shown as a yellow line in Figure 5.20. Axial and tangential velocities are drawn and exported on this line.
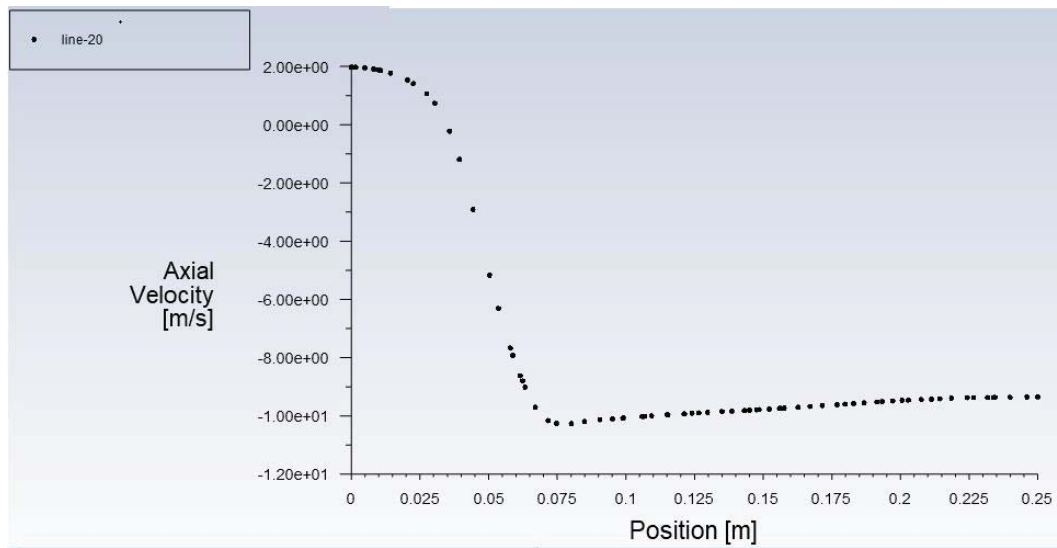
Figure 5.21. Axial Velocity Profile at the Wake of the Forward Propeller
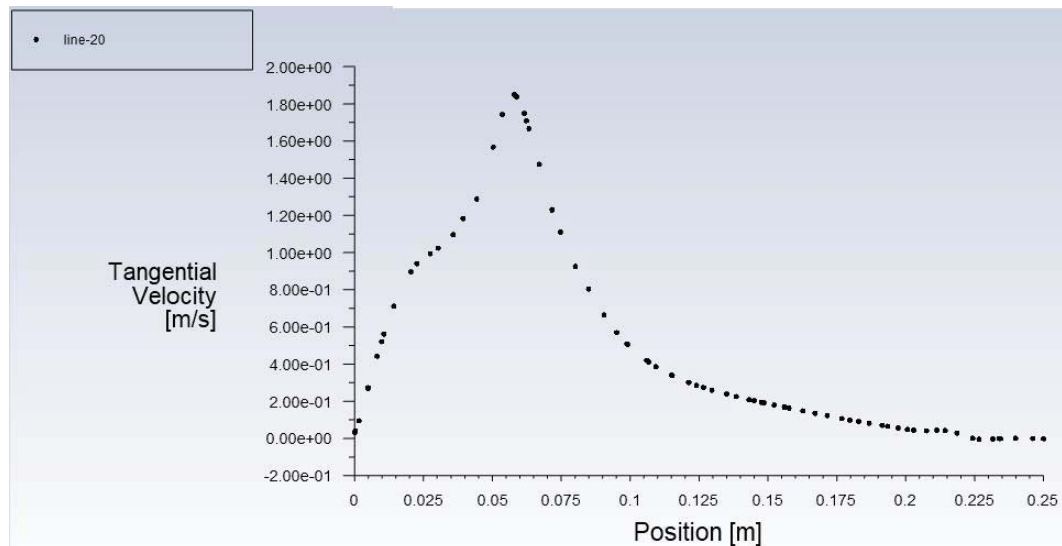
Figure 5.22. Tangential Velocity Profile at the Wake of the Forward Propeller

From the profiles in Figure 5.21 and 5.22, it is possible to identify the required axial and tangential velocities in the table of "Inflow Profile Values". Therefore, "Parametric Study" module of OpenProp can be started to determine the number of blades and the range for rotation speed. After that, design procedure shown in Figure 4.4 is applied to design the aft propeller by an iterative approach to reach the objective thrust of 360 N. For performance analysis, a plane is drawn at the exit of the rotating domain for the forward propeller in the downstream side to export the

velocity profile and import it during the performance analyses of the aft propellers. The location of the plane is shown in Figure 5.23. Contour showing the velocity magnitude at this plane is presented in Figure 5.24.
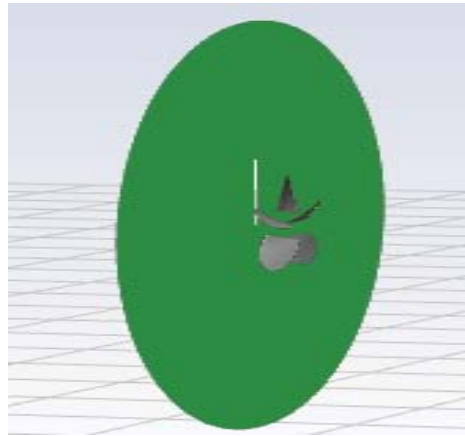
Figure 5.23. Location of the Profile Plane at the Wake of the Forward Propeller
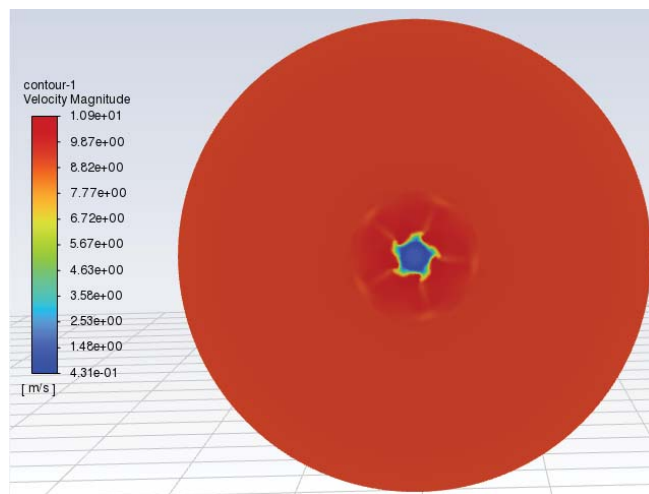
Figure 5.24. Velocity Magnitude Contour at the Wake of the Forward Propeller

5.5.1   Parametric Study for Aft Propeller

Figure 5.26 shows the input GUI menu of "Parametric Study" in OpenProp for the aft propeller operating at 45% load. Load requirement corresponds to a thrust of 360 N as shown in Table 5.4. Ship speed is taken as 9.25 m/s whereas hub diameter is set to 59.6 mm. Axial and tangential velocities scaled by the ship velocity are given as

inputs at 10 different radial locations. The range is 3 - 6 for number of blades and 1000 – 2000 rpm for rotation speed with 200 rpm increments. Propeller diameter is taken between 280 mm – 320 mm with 10 mm increments.

Specifications		Blade Design Values			Inflow Profile Values			Options
		r/R	c/D	Cd	r	Va/Vs	Vt/Vs	● Propeller
Required thrust (N):	360	0.2	0.16	0.008	0.02996	-0.095	0.0786	
Ship speed (m/s):	9.25	0.3	0.1812	0.008	0.04867	0.2649	0.0643	☑ Hub
Hub diameter (m):	0.0596	0.4	0.2024	0.008	0.06096	0.8452	0.1456	☐ Chord optimiza... ☑ Viscous forces
Fluid density	1000	0.5	0.2196	0.008	0.07436	1.098	0.0929	
# radial panels:	20	0.6	0.2305	0.008	0.08885	1.1034	0.0684	
# chordwise	20	0.7	0.2311	0.008	0.10484	1.0894	0.0387	
		0.8	0.2173	0.008	0.12143	1.0781	0.0273	
		0.9	0.1807	0.008	0.13602	1.0705	0.0216	
		1	0.001	0.008	0.14773	1.0625	0.0183	

Range

	Min	Increment	Max
Number of Blades	3	1	6
Rotation Speed (RPM)	1000	200	2000
Rotor Diameter (m)	0.28	0.01	0.32

Tools

Filename: AftProp

Load   Save   Run OpenPr...

Figure 5.25. Input GUI Menu of Parametric Study for the Aft Propeller

Figure 5.26. Results of "Parametric Study" for the Aft Propeller

Following conclusions can be drawn from the results of "Parametric Study" for the aft propeller:

- The efficiencies decrease slightly as the diameters increase. The efficiency for a diameter of 300 mm do not differ significantly in the investigated range. Therefore, propeller diameter of 300 mm can be used in further stages.
- The efficiencies are higher for 3 blades when compared with the 4, 5 and 6 blades for all revolution speeds. Therefore, selection of 3 blades for the aft propeller is reasonable.
- As the revolution speeds increase, the efficiencies decrease as expected. The required revolution speeds are going to be determined in performance analysis stages; however, lower revolution speeds seem to supply the required thrust with a good efficiency. Therefore, it is reasonable to start performance analyses by setting revolution speeds between 1000 - 1200 rpm.

80

5.5.2 Design and Performance Analysis of Aft Propeller

Based on the methodology developed in Section 4.2 and similar to the case followed in the forward propeller in Section 5.4, design and performance analysis of the aft propeller can be carried out. Since the tabulated data of B-series propellers is used for blade design and the aft propeller is decided to have three blades, the thickness distribution is known. Then, the iterative parameter becomes the expanded area ratio along with the revolution speed in the determined range of 1000 – 1200 rpm.

The iterative methodology developed in Section 4.2 is repeated for different chord distributions and revolution speeds in the determined range as shown in Table 5.7. The revolution speed is set to 1200 rpm in the 1st iteration. For each iteration, geometric design is carried out in OpenProp based on the determined chord distribution and revolution speed. After that the coordinates for points in each hydrofoil is exported to a file to obtain the 3D geometry in Siemens NX. Finally, performance evaluations are carried out in ANSYS Fluent. During the performance analyses, exported velocity profile consisting of x, y and z velocities shown in Figure 5.24 is used as the inlet profile.

Table 5.7. Iterations for the Aft Propeller

Iteration Number	Expanded Area Ratio (EAR)	Revolution Speed (rpm)	Resultant Thrust (N)	Resultant Torque (N.m)	Eff.
1	0.3	1200	489.80	49.21	0.733
2	0.9	1200	556.58	60.71	0.675
3	0.3	1100	285.03	31.20	0.734
4	0.9	1100	239.22	31.34	0.613
5	0.5	1100	268.62	31.89	0.676
6	0.3	1150	379.16	40.49	0.719
7	0.9	1150	383.68	45.12	0.653
8	0.5	1150	388.27	41.54	0.718
9	0.7	1150	388.89	42.51	0.703
10	0.6	1150	394.13	42.03	0.720
11	**0.6**	**1145**	**369.84**	**40.16**	**0.710**

In the first two iterations, propellers with low and high *EAR* are tested at 1200 rpm. There is a significant increase in the thrust obtained with *EAR* of 0.9 when compared with the *EAR* of 0.3. But, the results for these propellers are above the objective thrust of 360 N. After that, since the range for rotational speed is chosen to be between 1000 and 1200 rpm, the rotational speed is decreased to 1100 rpm and *EAR* of 0.5 is added to the iterations. This time, the thrust levels are lower than the objective thrust. Also, increasing the *EAR* is not sufficient to increase the thrust. Then, rotational speed is increased to 1150 rpm. Two different propellers with *EAR* of 0.6 and 0.7 are added to the iterations. Total five propellers with different expanded area ratios are considered at 1150 rpm. The highest efficiency is obtained in the 10th iteration with the propeller which has an *EAR* of 0.6. The created thrust is very close to the objective thrust of 360 N. Another iteration consisting of design and performance analysis at 1145 rpm is carried out. According to the results in the

11th iteration, aft propeller with an *EAR* of 0.6 is able to supply 360 N of thrust around 1145 rpm.

The GUI menu of "Single Design" for the 11th iteration is given in Figure 5.27. 3D models of the propeller are also presented.

OpenProp v3.3.4

Single Design

Specifications

Number of blades:	3
Rotation speed (RPM)	1145
Rotor diameter (m):	0.3
Required thrust (N):	360
Ship speed (m/s):	9.25
Hub diameter (m):	0.0596
Fluid density	1000
# radial panels:	30
# chordwise	30

Blade Design Values

r/R	c/D	Cd	t0/D	Skew	Xs/D
0.2	0.3266	0.008	0.0406	0	0
0.3	0.3664	0.008	0.0359	0	0
0.4	0.4	0.008	0.0312	0	0
0.5	0.424	0.008	0.0265	0	0
0.6	0.4372	0.008	0.0218	0	0
0.7	0.4336	0.008	0.0171	0	0
0.8	0.4254	0.008	0.0124	0	0
0.9	0.3314	0.008	0.0077	0	0
1	0.001	0.008	0.003	0	0

Inflow Profile Values

r	Va/Vs	Vt/Vs
0.02996	-0.095	0.0786
0.04867	0.2649	0.0643
0.06096	0.8452	0.1456
0.07436	1.098	0.0929
0.08885	1.1034	0.0684
0.10484	1.0894	0.0387
0.12143	1.0781	0.0273
0.13602	1.0705	0.0216
0.14773	1.0625	0.0183

Options

- ⦿ Propeller
- ○ Turbine
- ☑ Hub
- ☐ Chord optimiza...
- ☑ Viscous forces

- ☐ Optimization pl...
- ☑ Geometry plots
- ☐ Performance c...

Airfoil type

Meanline type:
NACA a=0.8
Thickness type:
NACA 65A010

Ducted Propeller

Thrust Ratio:	1
Duct section drag	0.008
duct D / prop D:	1

Non-dimensional Parameters

J = V/nD = 1.6157
L = omega*R/V = 1.9444
CT = 0.11905
KT = T/(rho*n^2*D^4) = 0.12204

Tools

Filename: 3B-AFT-360N-EAR06

Load Save Run OpenPr...

Figure 5.27. "Single Design" GUI of OpenProp with Aft Propeller Inputs
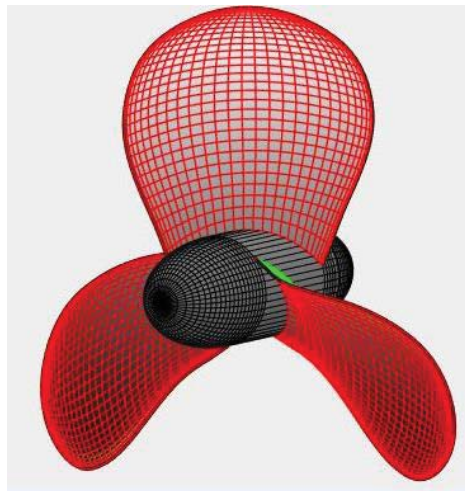
Figure 5.28. 3D Model View of the Aft Propeller in OpenProp
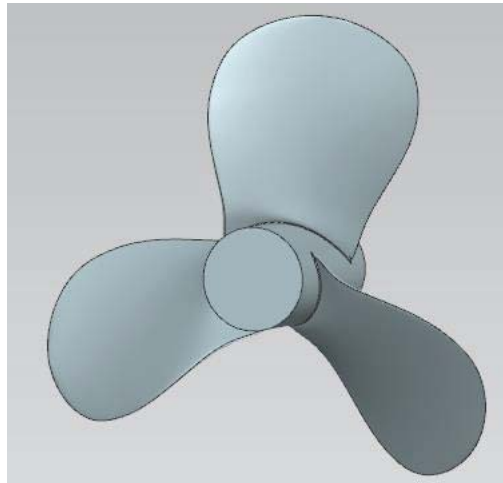
Figure 5.29. 3D Model of the Aft Propeller

The wake profile shown in Figure 5.24 is applied as an inlet profile in the performance analyses of the aft propeller. Therefore, periodicity is not used. In the CRP configuration, the length between the rotating domains of the propellers is 30 mm. Therefore, the upstream length is set to be 30 mm in Figure 5.30. Downstream and side lengths of the solution domain is kept the same as the whole model analysis of the designed forward propeller. Mesh is created based on the settings studied in Section 3.1. The created mesh has 8,005,320 cells. It is shown in Figure 5.31.

Figure 5.30. Solution Domain for the Aft Propeller
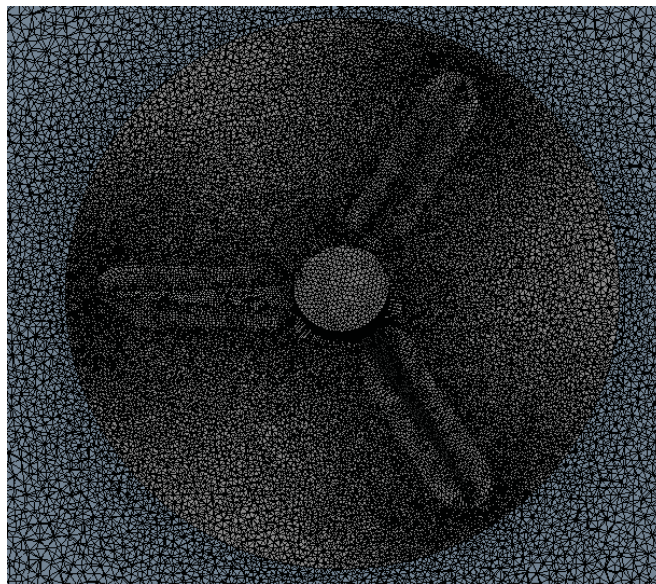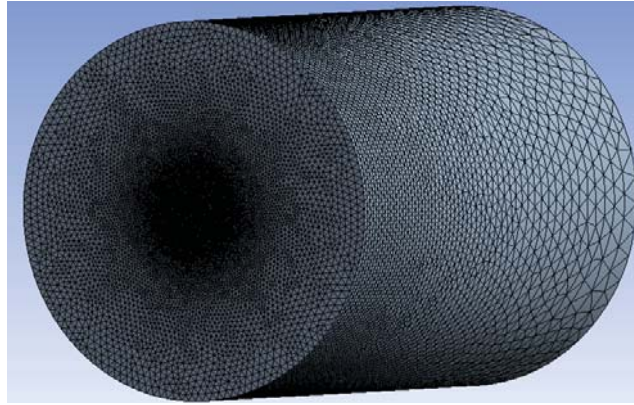
Figure 5.31. Mesh for the Aft Propeller

Boundary conditions and solution settings are kept the same as Section 3.1 except the inlet profile. The solution is obtained in 355 iterations. Convergence is obtained when the residual for continuity equation has reached 1e-4. Additionally, the thrust force created by the propeller is drawn throughout the solution to check whether the solution is converged or not. As it is presented in Figure 5.33, convergence is established.
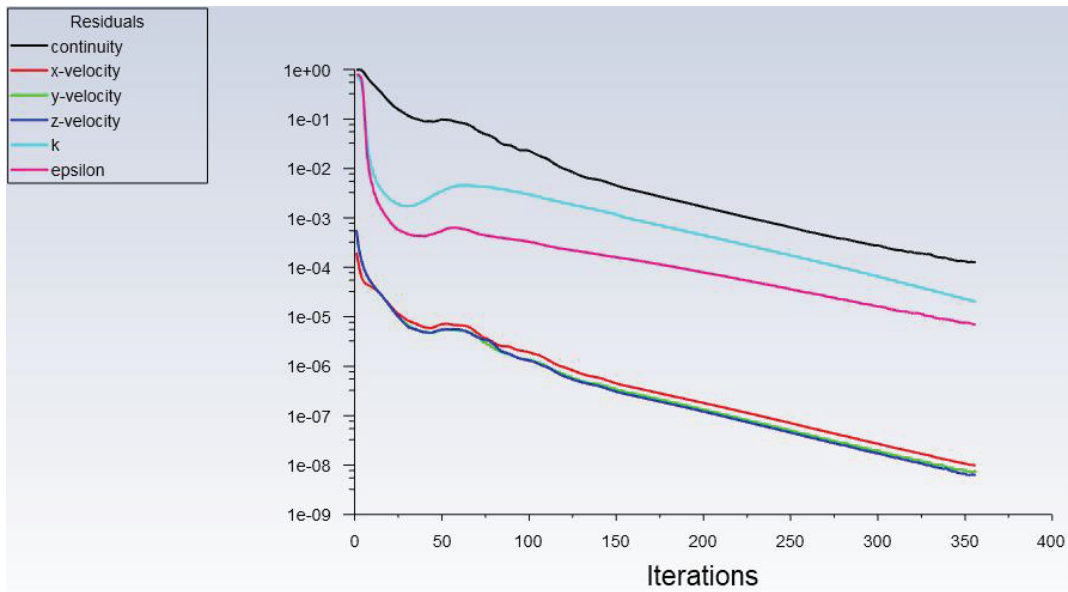
Figure 5.32. Residual Plot of the Numerical Analysis for the Aft Propeller
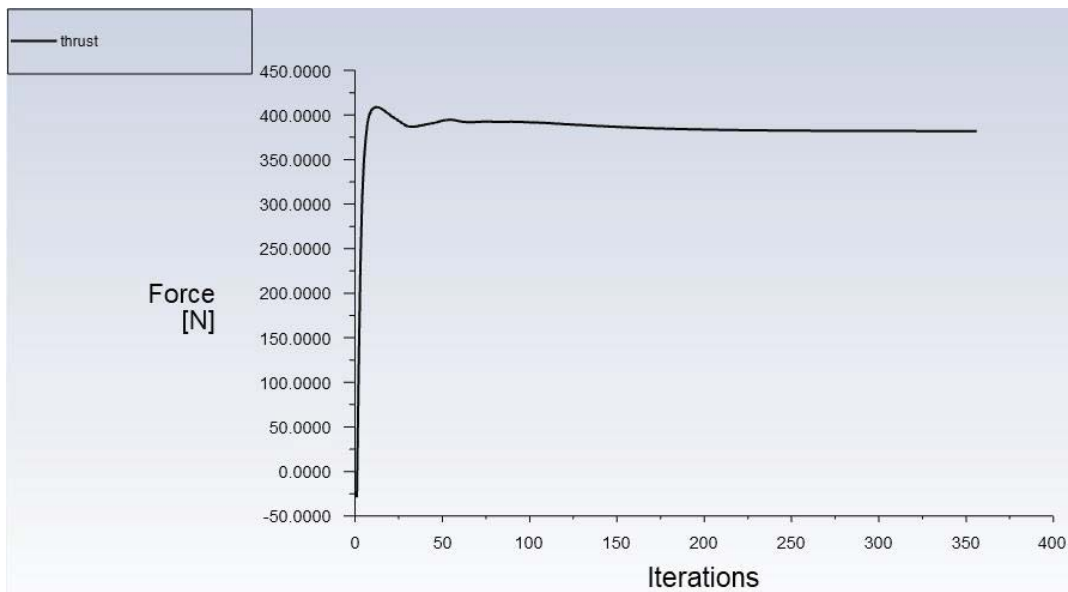
Figure 5.33. Convergence Plot of the Thrust Created by the Aft Propeller

Since the correct inputs for OpenProp are identified by CFD studies, it is possible to summarize the results of numerical analyses and OpenProp for the designed aft propeller as shown in Table 5.8.

Table 5.8. Comparison of Results for the Forward Propeller

Aft Prop	Numerical Analysis			OpenProp		
Revolution (rpm)	Thrust (N)	Torque (Nm)	Eff (%)	Thrust (N)	Torque (Nm)	Eff (%)
1145	369.84	40.16	0.710	360	38.39	0.723

The results of OpenProp for 1145 rpm are very close to the results obtained in the numerical analyses. The true error rate for the torque value is 4.41% for 1045 rpm. The error in torque directly influences the efficiency. Also, since OpenProp does not evaluate the thrust input, it shows the same input of 360 N in the results. This is also source of error for the efficiencies in the results of OpenProp.

To conclude, revolution speeds around 1145 rpm supply the required thrust of 360 N in the wake region of the forward propeller. Although the wake profile of the forward propeller is considered during design and performance analyses of aft propeller, existence of Suboff body in the upstream side is going to change the flow field. This change results in different thrust and torque outputs from the propeller which is investigated in the performance analyses of whole model including the DARPA Suboff and CRP in Section 5.6. However, performance analysis of propellers separately is advantageous for further whole model investigations to determine the starting point for the revolution speed.

5.5.3 Open Water Performance of the Aft Propeller

To compare the results for the aft propeller operating in the wake region of the forward propeller and uniform inlet, open water analysis of the aft propeller is carried out. The analysis is carried out on the final geometry obtained in the 11th iteration of Table 5.7, which is shown in Figure 5.28 and Figure 5.29. Solution domain is re-arranged so that the upstream length is kept enough. Solution domain is presented in Figure 5.34.
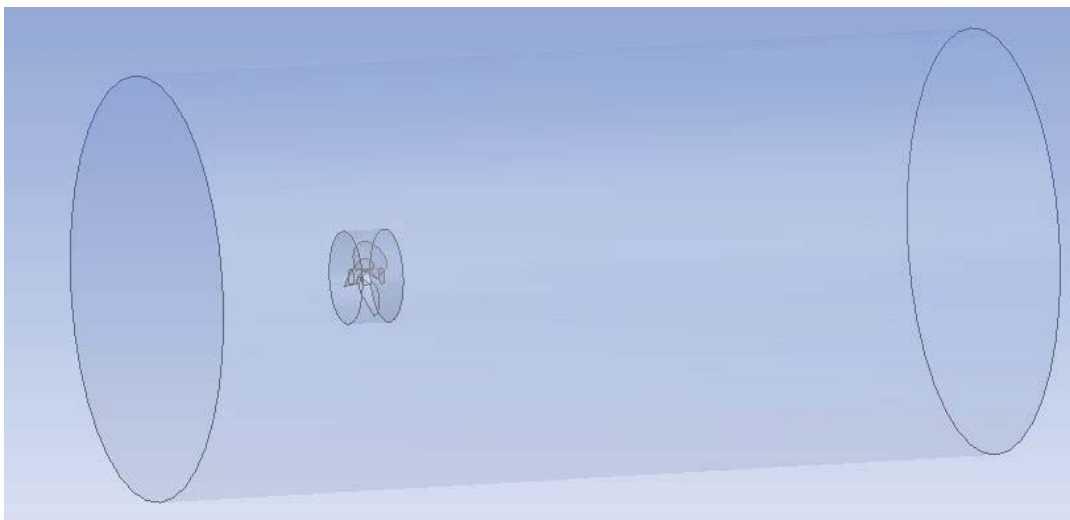
Figure 5.34. Solution Domain for Open Water Analysis of the Aft Propeller

Uniform inlet speed is set to 9.25 m/s. Other settings are kept the same as in Section 5.4.2. Convergence is established in 262 iterations. The plot showing the convergence of the thrust force created by the propeller is shown in Figure 5.35.
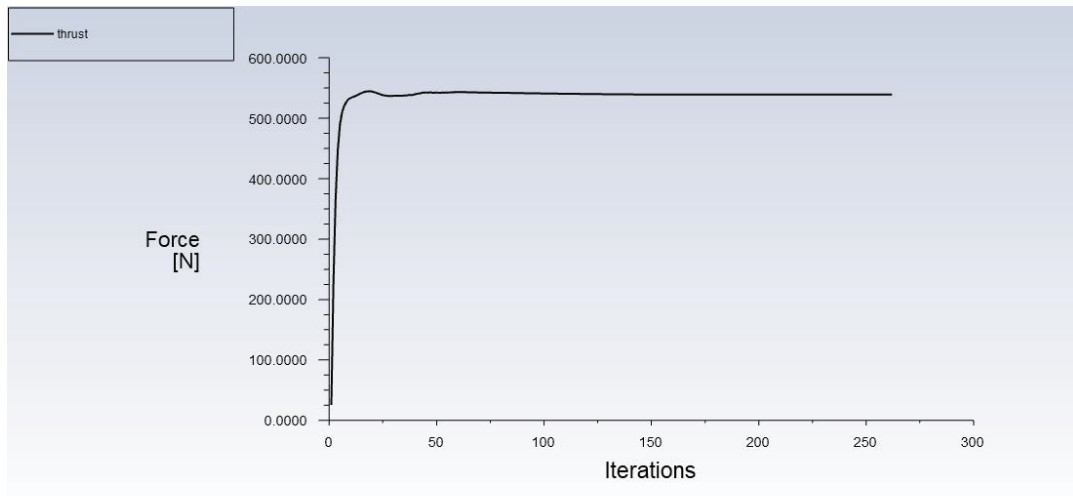
Figure 5.35. Thrust Created by the Aft Propeller in Open Water Analysis

The resultant torque and thrust values are compared in Table 5.9.

Table 5.9. Comparison of Results for Wake and Uniform Inlet Conditions

Aft Propeller	Thrust (N)	Torque (N.m)
Wake Inlet	369.84	40.16
Uniform Inlet	539.36	55.52

The propeller has higher thrust and torque outputs in open water conditions. There is an increase of 46% for the thrust and %38 increase for the torque. The flow has an axial speed of 9.25 m/s in the upstream of the aft propeller in uniform inlet condition whereas the flow has smaller speeds in the analysis started by the wake profile. For the wake profile, forward propeller leaves a non-uniform velocity profile for the aft propeller where velocity magnitude is smaller than the free-stream. For this reason, the flow energy is much higher for the case of uniform inlet. Therefore, aft propeller supplies 46% more thrust in uniform inlet condition. Also, the torque needed to rotate the propeller in this condition is higher.

89

5.6 Performance Analysis of CRP

According to the decided locations in Figure 5.10, forward and aft propellers are placed on the bare hull model of DARPA Suboff as shown in Figure 5.36.
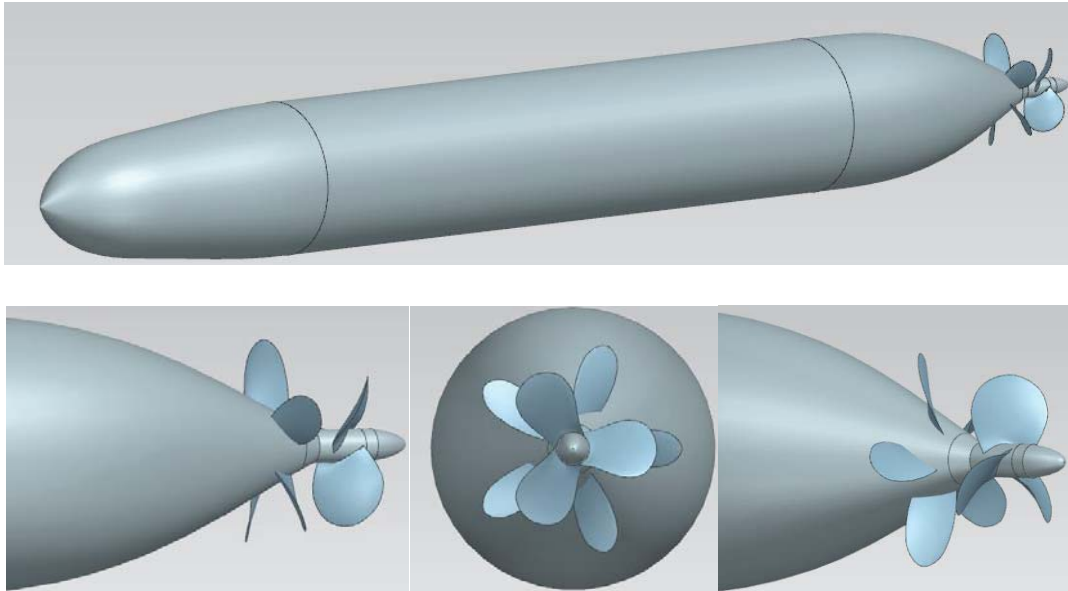
Figure 5.36. Suboff Geometry with CRP

As it is applied previous chapters and this chapter; Frozen Rotor approach, i.e. Multiple Reference Frame including stationary and rotational zones, is used in performance analyses. There are totally two rotational regions enclosing the forward and aft propellers.
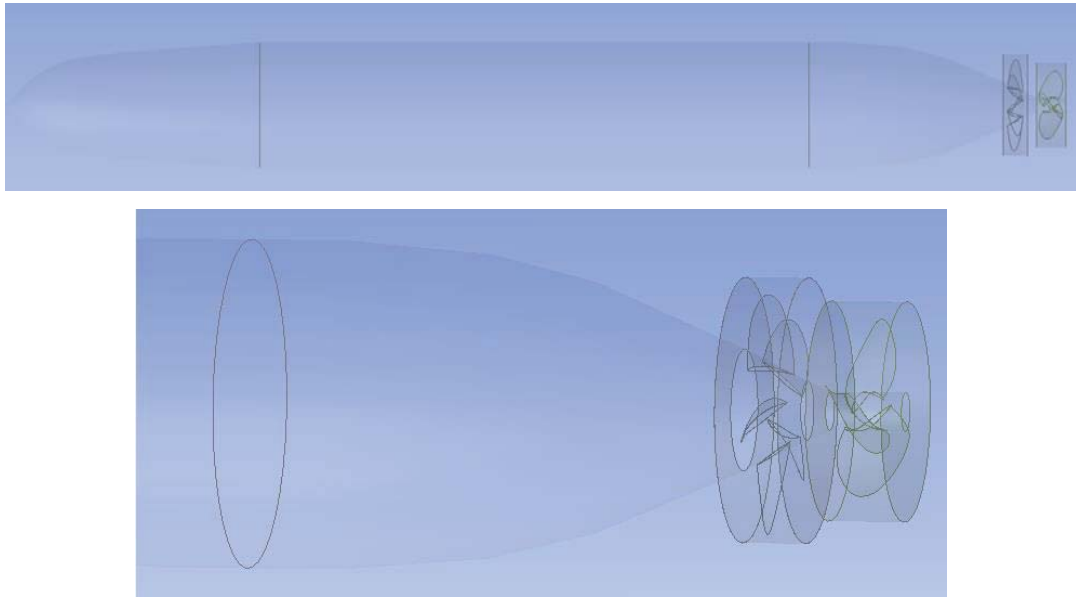
Figure 5.37. Rotational Domains Enclosing the Forward and Aft Propellers

Since the CRP mounts on the bare hull model of DARPA Suboff, the lengths specified in Figure 5.3 are used as upstream, downstream and side lengths.
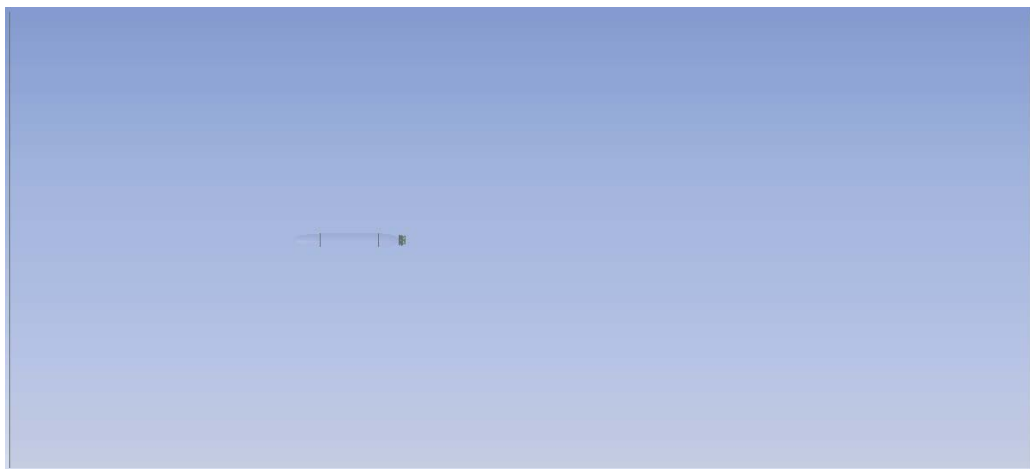
Figure 5.38. Solution Domain for the Whole Model

After the solution domain is defined, the model can be meshed. For this purpose; face sizing used for propellers in Section 5.4.2 and 5.5.2 and Suboff body in the beginning of this Chapter are combined to have a mesh with a fine boundary layer resolution for the complete model shown in Figure 5.39. The mesh consists of 18,216,589 cells.
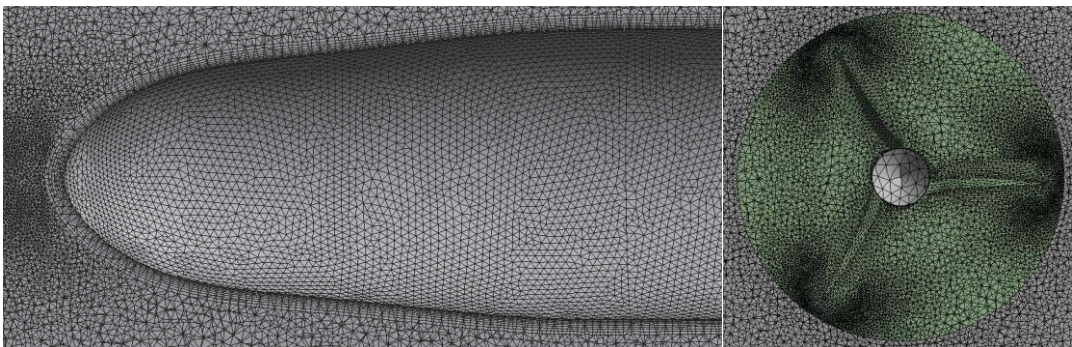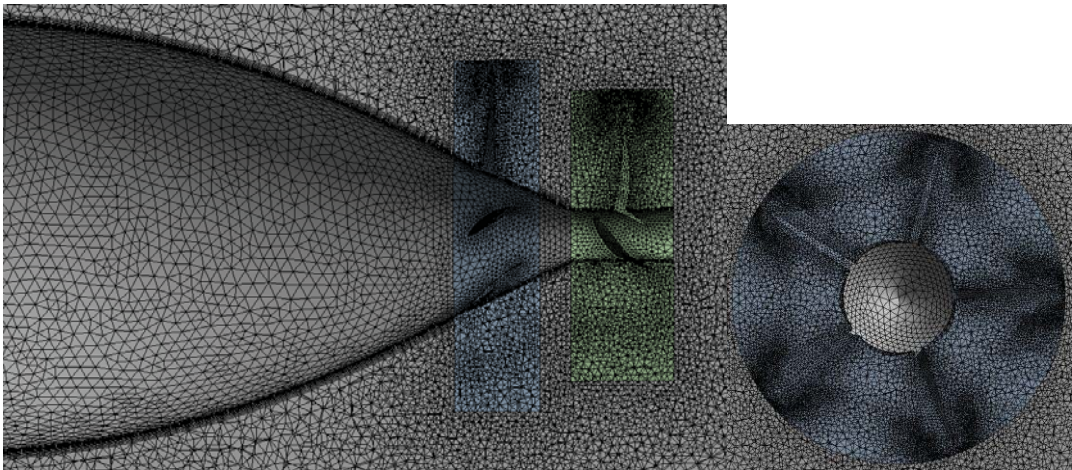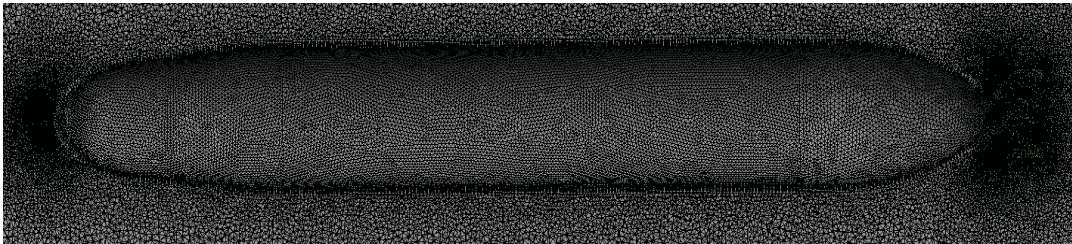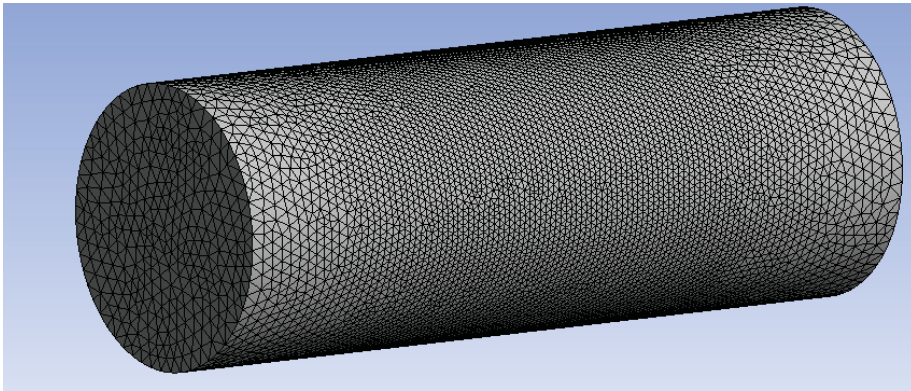
Figure 5.39. Mesh for Suboff Geometry with CRP

For the solution, the boundary conditions and solution settings are summarized in Table 5.10.

Table 5.10. Boundary Conditions and Solution Settings

Inlet	9.25 m/s
Cell Zone	Forward: +X with 1045 rpm Aft: -X with 1145 rpm
Outlet	Pressure outlet at a depth of 250 m
Solution Domain	One static domain One rotating domain for the forward propeller One rotating domain for the aft propeller
Time	Steady
Turbulence	Realizable $k\text{-}\epsilon$
Material	Sea water with $\varrho = 998$ kg/m^3 and $\mu = 0.001003$ kg/ms
Method	Frozen Rotor – MRF

With the boundary conditions and solution settings specified in Table 5.10, the residual for continuity equation dropped to 1e-6 in 437 iterations. Residual plot is presented in Figure 5.40.
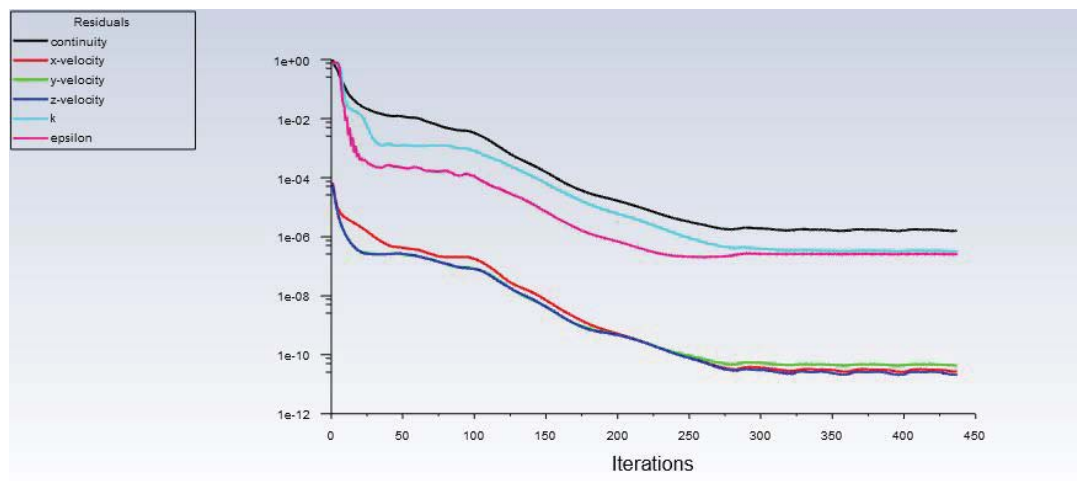
Figure 5.40. Residual plot for Suboff Geometry with CRP

Plots of net thrust and net torque are also obtained during the solution. Net thrust is obtained to be 136.3 N. Net torque is obtained by subtracting the torque outputs from the propellers. It has a value of 7.2 N.m.
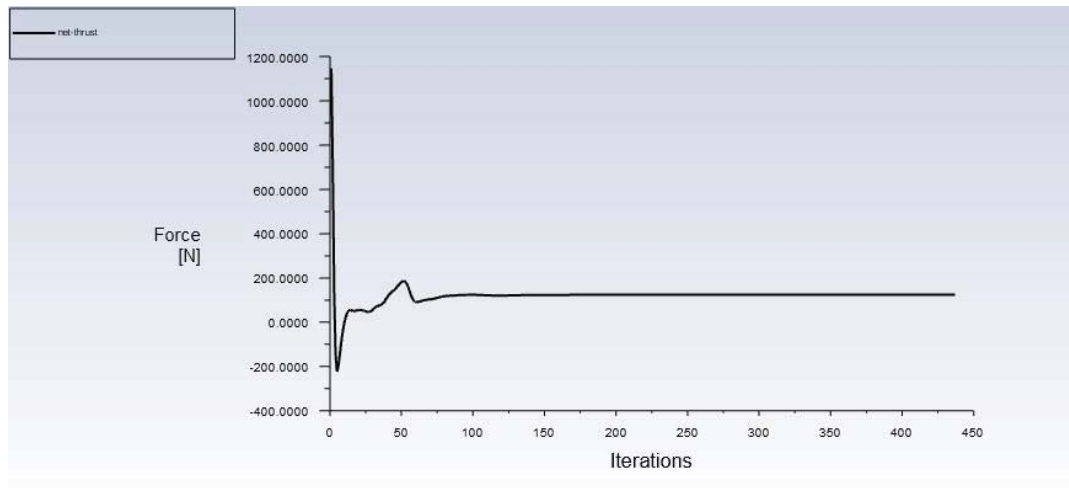
Figure 5.41. Plot of Net Thrust
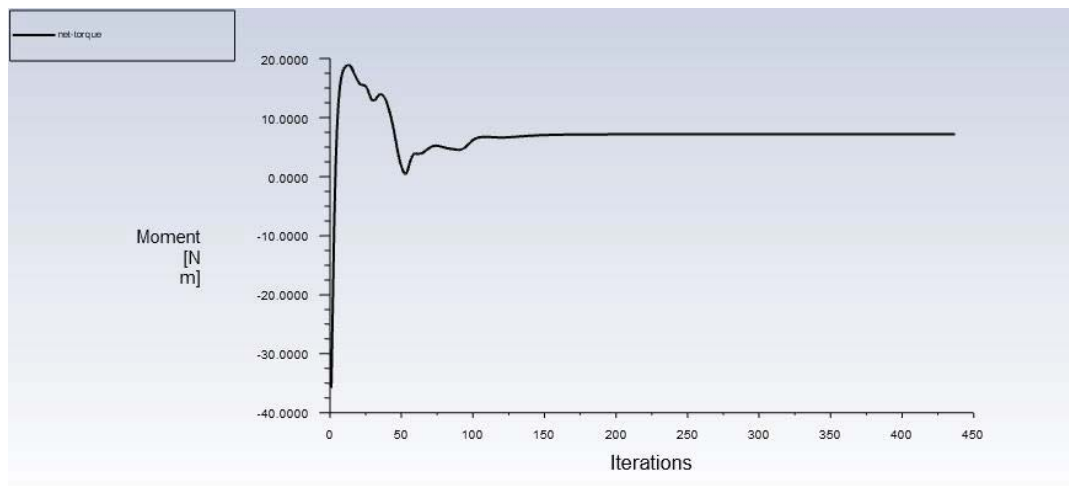
Figure 5.42. Plot of Net Torque

Absolute pressure and velocity contours of the solution are presented in Figure 5.43. Overall results are presented in Table 5.11.
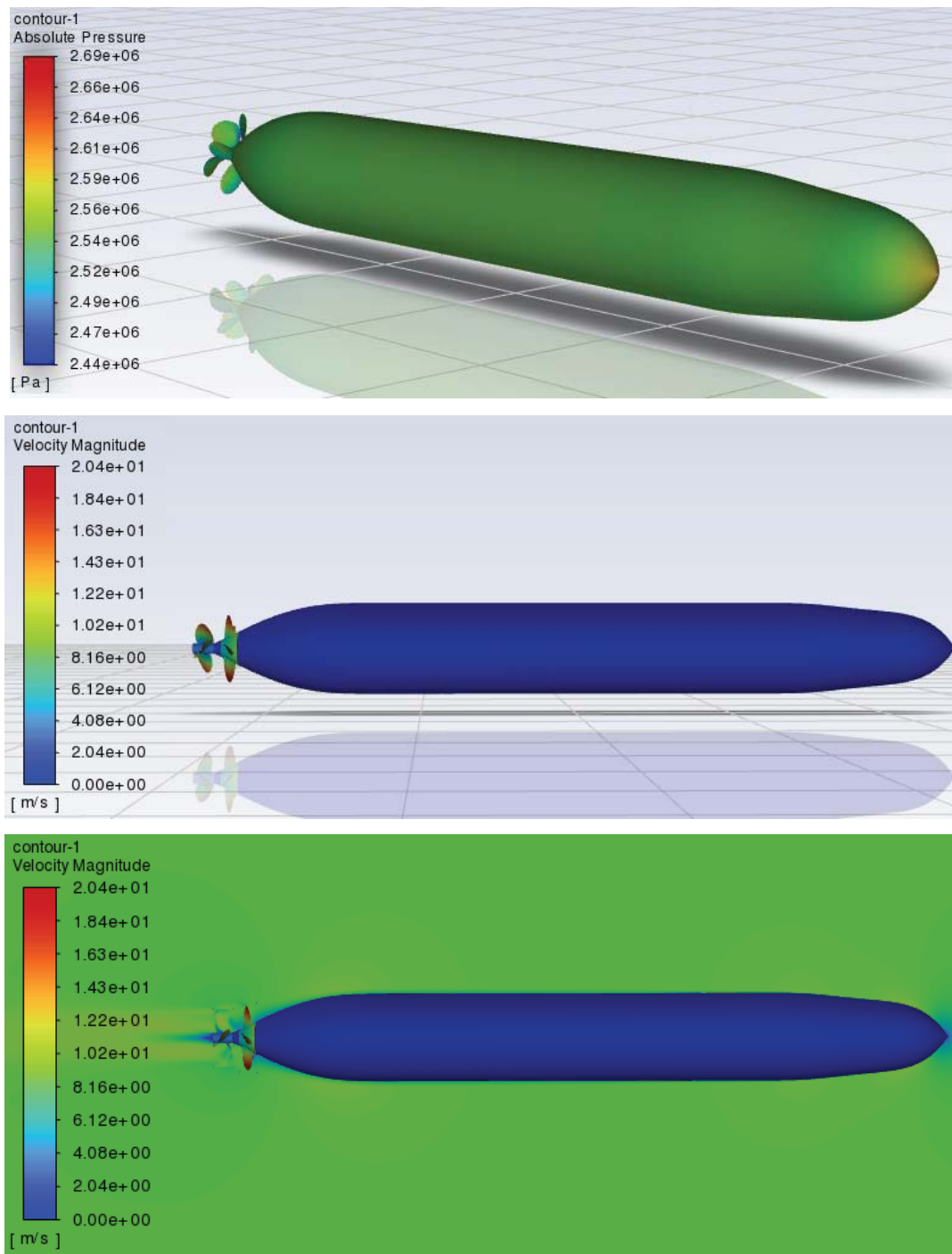
Figure 5.43. Absolute Pressure and Velocity Contours for Suboff with CRP

The contours show the same behavior in the nose section of the body as explained in Figure 5.8 and Figure 5.9. Due to suction effect of suction faces of the propellers, the local pressure of the flow decreases along the leading edge of the blades. This effect is more obvious for blade tips where the speed is maximum.

Table 5.11. Results for Performance Analysis of CRP

	Forward	Aft	CRP
Thrust (N)	493.4	431.8	925.2
Torque (N.m)	-55.4	48.2	-7.2
Rev. Speed. (rpm)	1045	1145	-

Before starting the design and analysis stages, the required thrust value was 800N including the drag contribution of the propellers. It is clear that the counter-rotating propeller produces the required thrust. The thrust loads of the propellers are 53.3% and 47.7% for the forward and aft propellers, respectively. Thrust loads are very close to the initial thrust distributions of 55% to 45%.

Due to the presence of a body ahead of the propellers, thrust and torque values are increased when compared with Table 5.6 and Table 5.8. The rate of increase is greater for the aft propeller both for thrust and torque. The propellers face with a lower velocity than a free-stream velocity, yielding a lower advance coefficient. In a typical open-water characteristic plot of a propeller such as Figure 1.5, lower advance coefficient results in greater thrust and torque at the same revolution speed. This seems to be the reason for the increases in thrust and torque values. A counter-acting torque appears by the aft propeller on the forward propeller which comes out to be a decreasing effect when compared with a single propeller. Since the placement and dimensions of the propellers differ due to geometric restrictions of the Suboff, outputs of the forward propeller are bigger than aft one, as expected.

Taylor wake fraction (w_T) and thrust deduction (t) are the terms arising when there is an interaction of propulsion device and hull. Since CRP is mounted on the stern of the submerged body in such a position that the flow into the CRP is affected by the presence of the hull [46]. Therefore, average speed of the flow ahead of CRP is (V_a) different from the advance speed of the body (V_s). It is usually less than the advancing speed. Dividing this difference by the advancing speed is called Taylor wake fraction.

$$w_T = \frac{V_s - V_a}{V_s} \tag{5.1}$$

Another term due to propeller-hull interaction is called thrust deduction, denoted as t. A propeller accelerates the flow ahead of itself in the stern of the body. This effect alters the drag force exerted by the fluid on the submerged body by increasing the rate of shear in the boundary layer. Therefore, the drag forces are different for bodies with and without a CRP. Dividing this difference by the drag with propellers is called thrust deduction.

$$t = \frac{T - R}{T} \tag{5.2}$$

To calculate w_T, average velocities are recorded on the opening faces of rotational domains in the direction of motion. For thrust deduction, viscous drag of the bare hull has already been calculated as 664.85 N in Section 5.1.

Table 5.12. Taylor Wake Fraction of CRP

	Average Speed Ahead (m/s)	Suboff Speed (m/s)	Taylor Wake Fraction
Forward Prop	8.37	9.25	0.095
Aft Prop	8.65	9.25	0.064

Table 5.13. Thrust Deduction of CRP

Drag of Suboff with CRP (N)	Drag of Suboff (N)	Thrust Deduction (*t*)
788.91	664.85	0.157

It is customary to define the required revolution speed for a submerged body to advance at constant velocity where net force acting on the body is equal to zero. This zero acceleration situation appears when the thrust created by CRP is equal to the drag exposed by the flow. When the propellers rotate at 1045 and 1145 rpm, the created thrust is slightly bigger than the exposed drag. Also, the forward propeller is dominant on the net torque. Therefore, the analysis is repeated for different revolution speeds to find the required revolution speed for zero acceleration point and minimize the net torque more. The analyses are tabulated in Table 5.14.

Table 5.14. Results for Performance Analyses of CRP for Constant Velocity

Trial	Revolution Speed (rpm)		Total Drag (N)	Total Thrust (N)	Net Thrust (N)	Net Torque (N.m)
	Forward	Aft				
1	1045	1145	788.9	925.2	136.3	-7.2
2	1040	1140	783.6	852.3	68.7	-5.0
3	1030	1140	780.1	791.5	11.4	-0.3
4	1025	1140	778.6	764.6	-18.1	1.9

In the second trial, revolution speeds are decreased to 1040 rpm for the forward propeller and 1140 rpm for the aft propeller. Net torque is decreased to 5.0 N.m from 7.2 N.m whereas the net thrust is still above the exposed drag. Another analysis is carried out for revolution speeds of 1030 rpm and 1140 rpm for the forward and aft propellers, respectively. The reason to decrease the revolution speed of the forward propeller alone is to decrease the net torque more. Since the torque output of the forward propeller is decreased, the net torque is obtained to be 0.3 N.m, which can be counted as a no-rolling condition. Net thrust is obtained to be slightly bigger than

the exposed drag. Another trial has been made to see the constant velocity point along with the point of zero net torque. For this purpose, revolution speed of the forward propeller is further decreased to 1025 rpm. The net thrust is in the direction of the exposed drag, which means that the CRP is not sufficient to drive the submerged body at constant velocity at this combination. Also, the net torque has changed its sign that the aft propeller is dominant on the net torque. Therefore, both constant velocity and zero torque points lie between the 3rd and 4th trials, especially around the revolution speeds of 1030 rpm for the forward propeller.

To conclude, in the investigated case, 17.9 knots of speed, 9.25 m/s, corresponds to the maximum speed of the DARPA Suboff as specified in Table 5.2. At this speed, revolution speeds of around 1030 rpm for the forward propeller and 1140 rpm for the aft propeller are found to be the required rotational speeds to advance at constant velocity. The generated thrust by CRP is adequate to maintain the maximum speed at the specified revolution speeds. This is relatively small revolution speeds when compared with propellers of torpedoes or AUVs at maximum speeds. In addition to that, the required revolution speed would be much more than a CRP in case of a single propeller. This benefit is due to the increased thrust by recovering part of the rotational kinetic energy shown in Figure 5.22 left by the forward propeller and turned out to an additional thrust by the aft propeller. Also, the other advancing speeds specified in Table 5.2 are going to require much smaller rotational speeds to advance with constant-velocity. Additionally, at the specified rotations, the net torque is almost zero, which is the other major advantage of CRP than a single propeller. Besides contributing in the total thrust, the aft propeller counter-acts the torque generated by the forward propeller in the opposite direction.

As a result, the designed CRP is suitable to drive the bare hull form of DARPA Suboff body at constant velocity with very low net torque by relatively small revolution speeds.

5.7 Velocity Diagrams of the Propellers

Velocities developed in 2D foil section of a blade can be drawn as depicted in Figure 5.44. In the wake region of the submerged body, the propellers face with a lower velocity than free-stream velocity as expressed in Table 5.12. There are two velocity components on a 2D blade section due to incoming flow which are tangential and axial velocities, shown as V_T and V_A. Due to the rotation of the blade, a velocity component in tangential direction develops whose magnitude is rotational speed multiplied by the radius where the section cut is taken along the blade. Additionally, there exist induced axial and tangential velocities which change the flow direction to the geometric pitch angle of β_i from hydrodynamic pitch angle of β. θ shows the developed blade angle which is sum of angle of attack, α, and geometric pitch angle, β_i.
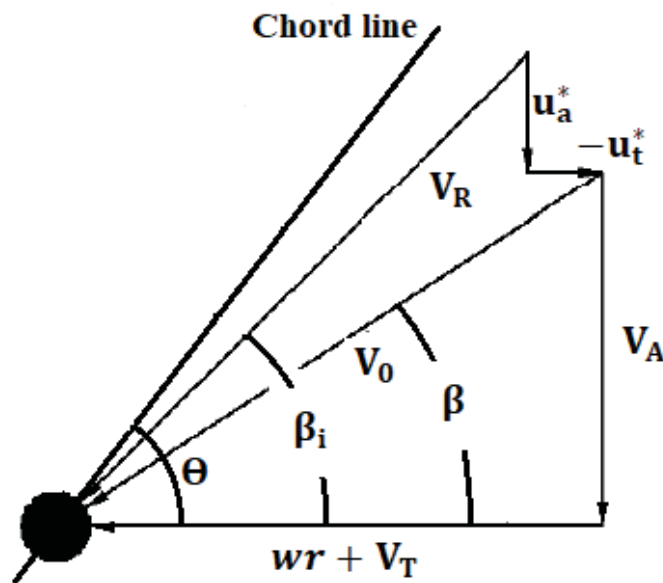
Figure 5.44. Velocity Diagram of a Propeller Blade

A section cut is taken at the mid-span of the forward propeller corresponding to a height of r=138.1mm. This height refers to the blade section of r/R=0.71 where R denotes the radius of the forward propeller. Geometric pitch angle and angle of attack are measured on the leading edge of the forward propeller at r/R=0.71.

$$\beta_{i,forward} = \tan^{-1}\left[\frac{V_A + u_a^*}{wr + V_T + u_t^*}\right] = 31.1°$$

$$\alpha_{forward} = \theta_{forward} - \beta_{i,forward} = 33.6° - 31.1° = 2.5°$$

Similarly, a section cut is taken at the mid-span of the aft propeller corresponding to a height of r=89.9mm. This height refers to the blade section of r/R=0.60 where R denotes the radius of the aft propeller. Geometric pitch angle and angle of attack are measured on the leading of the aft propeller at r/R=0.60.

$$\beta_{i,aft} = \tan^{-1}\left[\frac{V_A + u_a^*}{wr + V_T + u_t^*}\right] = 37.3°$$

$$\alpha_{aft} = \theta_{aft} - \beta_{i,aft} = 41.7° - 37.3° = 4.4°$$

5.8   Discussion

Before obtaining the results in the final performance analysis of the whole model, including the Suboff body and the CRP, each method used in the methodology is tested beforehand against an experimental measurement to validate the methods. The final model can be divided into two parts: propellers and the submerged body. The methodology for design and performance analyses of propellers is developed in Chapter 2 and Chapter 3 where verification of OpenProp, mesh independence study and comparison with experimental results for the DTMB4119 propeller are carried out. In addition to that, viscous flow analysis of the Suboff body alone is conducted to set the mesh and solution settings to be used in the whole model analysis by comparing the exposed drag with the experimental one. Therefore, the design and numerical analysis stages used in the design of CRP are already validated beforehand.

Parametric analysis of the forward propeller is studied first to decide on best combination of number of blades, propeller diameters and revolution speeds based on thrust distribution and geometric dimensioning of the propellers. Since the aft propeller operates in the wake region of the forward propeller, the wake region of the forward propeller is used as the input condition for the aft propeller both in geometric design and performance analyses. Iterative design methodology developed in Chapter 4 is used to achieve the desired thrust at the advance speed of 9.25 m/s for both propellers.

Once the propellers are chosen, performance analysis of the CRP is carried out. It is able to drive the bare hull form of DARPA Suboff at revolution speeds of 1030 rpm for the forward propeller and 1140 rpm for the aft propeller at constant velocity of 17.9 knots. The torque output of the forward propeller is counter-acted by the aft propeller which is one of the major advantages of a counter rotating propeller than a single propeller. Net torque is almost zero, which means there is not going to be any rolling motion which is a major problem for submerged vehicles. Obtained thrusts of propellers for combined configuration is larger than thrust levels in separate analyses of the propellers. This difference is explained by general open-water characteristics of a propeller and Taylor Wake Fraction. Since the propellers face with lower velocities than advance velocity of the submerged body, they operate with a lower advance coefficient in the wake of the body. This results in a higher thrust and torque coefficients. Therefore, the required revolution speed to advance at constant velocity is smaller than those in the characterization of the propellers separately.

CHAPTER 6

CONCLUSIONS AND SUGGESTIONS FOR FUTURE WORK

Counter-rotating propellers have gained more importance for developers in marine industry for the advantages of higher efficiency and torque-cancellation phenomena than a single propeller. Effect of torque-cancellation is more significant for small-volume underwater vehicles such as submarines, torpedoes and AUV's to prevent rolling. However, complex gearing requirements and non-standardized complicated flow region between the propellers prevent this concept to become a preferred choice. Therefore, it has been an extensive research area both in academia and marine industry.

In this thesis, a procedure is developed for the design and performance analyses of counter-rotating propellers. OpenProp is used as a design tool whereas ANSYS Fluent is used for performance evaluations. In Chapter 2, OpenProp is introduced and its design procedure is explained by using the DTMB4119 propeller. Verification of OpenProp is also carried out in Chapter 2 by comparing the performance results of OpenProp with the experimental ones. In Chapter 3, the designed propeller by the inputs of the DTMB4119 propeller is analyzed numerically to complete the verification of OpenProp, and also develop a methodology for performance analysis. In Chapter 4, the thrust and speed requirements of DTMB4119 propeller is copied to design a propeller from an unknown geometry. "Parametric Study" module of OpenProp is implemented to determine number of blades, geometric dimensioning and revolution speed by comparing the efficiencies for each configuration. By using the outputs of "Parametric Study", a tabulated propeller geometric data is used for blade design. An iterative methodology consisting of

geometric design in OpenProp and performance evaluations in Fluent has been developed in Chapter 4 to design the propeller for the specified speed and thrust requirements. By this conclusion, the procedure for design and performance analysis has been determined. In Chapter 5, bare hull model of DARPA Suboff is selected for the body on which a counter-rotating propeller is going to operate. Viscous flow analyses are conducted on the body to validate the numerical procedure with the experimental measurements. Thrust distribution between the forward and aft propellers is done to be able to start parametric analysis and design of the propellers. Based on the results of "Parametric Study" for the forward propeller, it is designed first based on the methodology developed in Chapter 4. After that, wake profile of the forward propeller is used in "Parametric Study" and "Single Design" modules of OpenProp, and also performance evaluations of the aft propeller. After that, the propellers are mounted on DARPA Suboff body for performance evaluations of the whole model. The CRP is able to drive the body at the specified speed. Wake fractions and thrust deduction are tabulated at that revolution speed. Also, required revolution speed for advancing at constant speed is calculated. Finally, velocity diagrams for each designed propeller are drawn.

To summarize, in this thesis study, a methodology for design and performance analyses of counter-rotating propellers is developed. Several verifications with experimental measurements are done to validate the used procedures in methodology.

As an extension of this thesis study, following topics can be recommended for future studies:

- Since OpenProp does not evaluate the final design in terms of the thrust output, an iterative methodology is developed in this thesis. The methodology includes several stages in different software such as OpenProp, Siemens NX and ANSYS Fluent. Also, several iterations shall be conducted in each stage to reach the target. Therefore, a master code can be developed to automate the procedure to save time and effort. In this code, the tabulated

data of blade design values and range for rotational speeds can be introduced so that the next iteration including the new blade design values and rotational speed can be determined.

- During the design and performance analyses of the CRP, cavitation analyses are not carried out. Therefore, cavitation analyses of the designed propellers can be investigated.

- It is better to have an experimental measurement behind any numerical analysis. Although the methodology for design and performance analysis is determined by comparing the results with experimental ones, CRP performance or open-water performance of separate propellers can be investigated by conducting experiments.

REFERENCES

[1]   Techet, A. H. (2004), "Propellers," *Hydrodynamics for Ocean Engineers.*

[2]   Khasnabis, S. (2022), "Different ways to reduce ship propeller vibrations and increase its efficiency," Marine Insight. https://www.marineinsight.com/naval-architecture/different-ways-to-reduce-ship-propeller-vibrations-and-increase-its-efficiency/

[3]   Corporation, J. M. U. (n.d.). *Energy saving devices: Hydrodynamic Engineering: Technology Development: Japan Marine United Corporation.* Energy saving devices | Hydrodynamic engineering | Technology development |Japan Marine United Corporation. https://www.jmuc.co.jp/en/rd/development/hydrodynamics/energy-saving/

[4]   Min, K.-S., Chang, B.-J., & Seo, H.-W. (2009), "Study on the Contra-Rotating Propeller system design and full-scale performance prediction method," *International Journal of Naval Architecture and Ocean Engineering*, pp. 29-38, doi: 10.2478/IJNAOE-2013-0004.

[5]   Liu X-L. (2009), "A potential based panel method for prediction of steady and unsteady performances of contra-rotating propellers," *Proceedings of the 1st International Symposium on Marine Propulsors*, Trondheim, Norway.

[6]   Gu, H., Kinnas, S.A. (2003), "Modelling of contra-rotating and ducted propellers via coupling of a vortex-lattice with a finite volume method," *Proceedings of Propellers/Shafting 2003 Symposium*, Society of Naval Architects and Marine Engineers, Virginia, USA.

[7]   Zhang, T., Yang, C. J., Song, B.W. (2010), "Investigations on the numerical simulation method for the open-water performance of contra-rotating propellers based on the MRF model," *Journal of Ship Mechanics*, 14(8).

[8]   Wang, Z. Z., Xiong, Y. (2013), "Effect of time step size and turbulence model on the open water hydrodynamic performance prediction of contra-rotating propellers," *China Ocean Eng.,* 27(2).

[9]   Brizzolara, S., Grassi, D., Tincani, E. P. (2012), "Design and analysis of counter-rotating propellers comparison of numerical and experimental results," *International Journal of Rotating Machinery.*

[10]   Grassi, D., Brizzolara S., Viviani, M., Savio, L., Caviglia, S. (2013), "Design and analysis of counter-rotating propellers comparison of numerical and experimental results," *Journal of Hydrodynamic, Ser. B*, 22(5).

[11]   Xin, G-Z., Ding, E-B., Tang, D-H. (2006), "A design method for contra-rotating propeller by lifting-surface method," *Journal of Ship Mechanics,* 10(2).

[12]   John Erricsson 1803-1899. RINA Affairs, October 2004.

[13]   Taggart, R. (1969), "Marine propeller principle and revaluation," *Gulf Publishing*.

[14]   Kravitz, E. (2011), "Analysis and experiments for contra-rotating propeller," *Master's Thesis, Massachusetts Institute of Technology.*

[15]   Carlton, J. (2008), "*Marine propeller and propulsion,"* Second edition.

[16]   Bernitsas, M. M., Ray, D., & Kinley, P. (1981), "KT, KQ and efficiency curves for the Wageningen b-series propellers,"

[17]   Windyandari, A., Haryadi, G. D., & Suharto, S. (2018), "Design and performance analysis of b-series propeller for traditional purse seine boat in the north coastal region of Central Java Indonesia," *Journal of Applied Engineering Science Vol. 16*, pp. 495-502, doi: 10.5937/jaes16-18506.

[18]   Yeo, K. B., Choong, W. H., & Hau, W. Y. (2014), "Wageningen b-marine propeller performance characterization through CFD," *Journal of Applied Sciences 14(11*), pp. 1215-1219, doi: 10.3923/jas.2014.1215.1219.

[19]   Troost, L. (1938), "Open water test series with modern propeller forms," *Trans. NECIES*, (54).

[20]   Troost, L. (1940), "Open water test series with modern propeller forms II, three bladed propellers," *Trans. NECIES.*

[21]   Troost, L. (1940), "Open water test series with modern propeller forms III, two bladed and five bladed propellers – extension of three and four bladed B-series," *Trans. NECIES,* (67).

[22]   Oosterveld, M. W.C., Van Ossannen, P. (1975), "Further computer-analyzed data of Wageningen B-screw series," *International Ship Building Progress*, 22(251).

[23]   Munson, B., Okiishi T., Huebsch, W., Rothmayer, A. (2013), "Fundamentals of fluid mechanics," Hoboken, Wiley&Sons.

[24]   Latt, A. K. (2017), "Numerical investigation of propulsion efficiency depending on propeller position," *Master's thesis, University of Rostock.*

[25]   Larsson, L., Raven, H. C. (2010), "The principles of naval architecture series: Ship resistance and flow," *The Society of NAME.*

[26]   Steen, S. (2014), "Experimental methods in marine hydrodynamics," NTNU Trondheim Norwegian.

[27] Jessup, S. D. (1989), "An experimental investigation of viscous aspects of propeller blade flow," *Doctoral dissertation, The Catholic University of America.*

[28] Kimball, R.W, Epps, B.P, M.J. Stanway, OpenProp MAT-LAB code, open-source at http://openprop.mit.edu.

[29] Kerwin, J.E. (2007), "Hydrofoils and Propellers," *MIT course 2.23 notes.*

[30] Chung, H.-L. (2007), "An enhanced propeller design program based on propeller vortex lattice lifting line theory*," Master's thesis, Massachusetts Institute of Technology.*

[31] D'epagnier, K.P. (2007), "A computational tool for the rapid design and prototyping of propellers for underwater vehicles," *Master's thesis, Massachusetts Institute of Technology.*

[32] Epps, B., Stanway, J., Kimball, R. (2009), "OpenProp: An open-source design tool for propellers and turbines," *SNAME Propeller and Shafting Conference.*

[33] Stubblefield, J.M. (2008), "Numerically based ducted propeller design using vortex lattice lattice lifting line theory," *Master's thesis, Massachusetts Institute of Technology.*

[34] Coney, W.B. (1989), "An enhanced propeller design program based on propeller vortex lattice lifting line theory," *Master's thesis, Massachusetts Institute of Technology.*

[35] Carlton, J. S. (1994), "Marine propellers and propulsion", Butterworth-Heinemann.

[36] Black, S.D. (1997), "Integrated lifting surface/Navier-Stokes design and analysis methods for marine propulsors," *Doctoral dissertation, Massachusetts Institute of Technology.*

[37] Saha, G. K., Maruf, H. I., & Hasan, R. (July 2019), "Marine propeller modelling and performance analysis using CFD tools", *AIP Conference Proceedings 2121*, doi: 10.1063/1.5115883.

[38] Röber, T., Kožulović, D., Kügeler, E., Nürnberger, D. (2006), "Appropriate turbulence modelling for turbomachinery flows using a two-equation turbulence model," *New Results in Numerical and Experimental Fluid Mechanics V. Notes on Numerical Fluid Mechanics and Multidisciplinary Design (NNFM), vol 92*, Springer, Berlin, Heidelberg, doi: 10.1007/978-3-540-33287-9_55.

[39] Duelley, R. S. (2010), "Autonomous underwater vehicle propulsion design," *Master's thesis, Virginia Polytechnic Institute and State University.* https://vtechworks.lib.vt.edu/bitstream/handle/10919/34789/Duelley_RS_T_2010.pdf?sequence=1https://vtechworks.lib.vt.edu/bitstream/handle/10919/34789/Duelley_RS_T_2010.pdf?sequence=1

[40] Liu, H.-L., & Huang, T. T. (June 1998), "Summary of DARPA Suboff experimental program data," *Report No: CRDKNSWC/HD-1298-11.*

[41] Esteves, F. R., Gomes, G. D., Katsuna, E. T., & Dantas, J. D. (2018), "Simulation of DARPA suboff model propeller-hull interaction," https://www.researchgate.net/publication/328542632.

[42] Gross, A., Kremheller, A., & Fassel, H. F. (2011), "Simulation of flow over suboff bare hull model," *49th AIAA Aerospace Sciences Meeting (AIAA 2011-290).*

[43] Toxopeus, S. (2008), "Viscous-flow calculations for bare hull DARPA SUBOFF submarine at incidence," *International Shipbuilding Progress 55*, pp. 227-251.

[44] Groves, N. C., Huang, T. T., & Chang, M. S. (March 1989), "Geometric characteristics of DARPA SUBOFF models (DTRC model Nos 5470 and 5471)," *Report No: DTRC/SHD-1298-01.*

[45] Min, K.-S., Chang, B.-J., & Seo, H.-W. (2009), "Study on the contra-rotating propeller system design and full-scale performance prediction method," *International Journal of Naval Architecture and Ocean Engineering*, pp. 29-38, doi: 10.2478/IJNAOE-2013.

[46] Molland, A. F., Turnock, S. R., & Hudson, D. A. (2017), "Ship resistance and propulsion practical estimation of ship propulsive power," *Cambridge University Press.*